

Multiple Spectrum Analysis for Food Quality and Safety

Lead Guest Editor: Haiyan Fu

Guest Editors: Hongyan Zou, Ying Hu, Yongjie Yu, Zi Xuan, and Hengye Chen





Multiple Spectrum Analysis for Food Quality and Safety

Journal of Food Quality

Multiple Spectrum Analysis for Food Quality and Safety

Lead Guest Editor: Haiyan Fu

Guest Editors: Hongyan Zou, Ying Hu, Yongjie Yu,
Zi Xuan, and Hengye Chen



Copyright © 2023 Hindawi Limited. All rights reserved.

This is a special issue published in "Journal of Food Quality." All articles are open access articles distributed under the Creative Commons Attribution License, which permits unrestricted use, distribution, and reproduction in any medium, provided the original work is properly cited.

Chief Editor

Anet Režek Jambrak , Croatia

Associate Editors

Ángel A. Carbonell-Barrachina , Spain
Ilija Djekić , Serbia
Alessandra Durazzo , Italy
Jasenka Gajdoš-Kljusurić, Croatia
Fuguo Liu , China
Giuseppe Zeppa, Italy
Yan Zhang , China

Academic Editors

Ammar AL-Farga , Saudi Arabia
Leila Abaza , Tunisia
Mohamed Abdallah , Belgium
Parise Adadi , New Zealand
Mohamed Addi , Morocco
Encarna Aguayo , Spain
Sayeed Ahmad, India
Ali Akbar, Pakistan
Pravej Alam , Saudi Arabia
Yousef Alhaj Hamoud , China
Constantin Apetrei , Romania
Muhammad Sajid Arshad, Pakistan
Md Latiful Bari BARI , Bangladesh
Rafik Balti , Tunisia
José A. Beltrán , Spain
Saurabh Bhatia , India
Saurabh Bhatia, Oman
Yunpeng Cao , China
ZhenZhen Cao , China
Marina Carcea , Italy
Marcio Carcho , Portugal
Rita Celano , Italy
Maria Rosaria Corbo , Italy
Daniel Cozzolino , Australia
Alessandra Del Caro , Italy
Engin Demiray , Turkey
Hari Prasad Devkota , Japan
Alessandro Di Cerbo , Italy
Antimo Di Maro , Italy
Rossella Di Monaco, Italy
Vita Di Stefano , Italy
Cüneyt Dinçer, Turkey
Hüseyin Erten , Turkey
Yuxia Fan, China

Umar Farooq , Pakistan
Susana Fiszman, Spain
Andrea Galimberti , Italy
Francesco Genovese , Italy
Seyed Mohammad Taghi Gharibzahedi ,
Germany
Fatemeh Ghiasi , Iran
Efsthios Giaouris , Greece
Vicente M. Gómez-López , Spain
Ankit Goyal, India
Christophe Hano , France
Hadi Hashemi Gahruei , Iran
Shudong He , China
Alejandro Hernández , Spain
Francisca Hernández , Spain
José Agustín Tapia Hernández , Mexico
Amjad Iqbal , Pakistan
Surangna Jain , USA
Peng Jin , China
Wenyi Kang , China
Azime Özkan Karabacak, Turkey
Pothiyappan Karthik, India
Rijwan Khan , India
Muhammad Babar Khawar, Pakistan
Sapna Langyan, India
Mohan Li, China
Yuan Liu , China
Jesús Lozano , Spain
Massimo Lucarini , Italy
Ivan Luzardo-Ocampo , Mexico
Nadica Maltar Strmečki , Croatia
Farid Mansouri , Morocco
Anand Mohan , USA
Leila Monjazebe Marvdashti, Iran
Jridi Mourad , Tunisia
Shaaban H. Moussa , Egypt
Reshma B Nambiar , China
Tatsadjieu Ngouné Léopold , Cameroon
Volkan Okatan , Turkey
Mozaniel Oliveira , Brazil
Timothy Omara , Austria
Ravi Pandiselvam , India
Sara Panseri , Italy
Sunil Pareek , India
Pankaj Pathare, Oman

María B. Pérez-Gago , Spain
Anand Babu Perumal , China
Gianfranco Picone , Italy
Witoon Prinyawiwatkul, USA
Eduardo Puértolas , Spain
Sneh Punia, USA
Sara Ragucci , Italy
Miguel Rebollo-Hernanz , Spain
Patricia Reboredo-Rodríguez , Spain
Jordi Rovira , Spain
Swarup Roy, India
Narashans Alok Sagar , India
Rameswar Sah, India
El Hassan Sakar , Morocco
Faouzi Sakouhi, Tunisia
Tanmay Sarkar , India
Cristina Anamaria Semeniuc, Romania
Hiba Shaghaleh , China
Akram Sharifi, Iran
Khetan Shevkani, India
Antonio J. Signes-Pastor , USA
Amarat (Amy) Simonne , USA
Anurag Singh, India
Ranjna Sirohi, Republic of Korea
Slim Smaoui , Tunisia
Mattia Spano, Italy
Barbara Speranza , Italy
Milan Stankovic , Serbia
Maria Concetta Strano , Italy
Antoni Szumny , Poland
Beenu Tanwar, India
Hongxun Tao , China
Ayon Tarafdar, India
Ahmed A. Tayel , Egypt
Meriam Tir, Tunisia
Fernanda Vanin , Brazil
Ajar Nath Yadav, India
Sultan Zahiruddin , USA
Dimitrios I. Zeugolis , Ireland
Chu Zhang , China
Teresa Zotta , Italy

Contents

Rapid and Nondestructive Identification of Origin and Index Component Contents of Tiegun Yam Based on Hyperspectral Imaging and Chemometric Method

Yue Zhang , Yuan Li , Cong Zhou , Junhui Zhou , Tiegui Nan , Jian Yang , and Luqi Huang 

Research Article (11 pages), Article ID 6104038, Volume 2023 (2023)

Determination of Vitamin B₁₂ in Milk and Dairy Products by Isotope-Dilution Liquid Chromatography Tandem Mass Spectrometry

Baifen Huang, Jingshun Zhang , Mengli Wang, and Zengxuan Cai 

Research Article (7 pages), Article ID 7649228, Volume 2022 (2022)

Determination of Mycotoxins and Veterinary Medicines in Duck Flesh and Viscera and Assessment of Their Exposure

Yi Zheng , Yuxin Wu, Huanxin Zhang, Xiaolan Chen , Zaixiang Lou , Huijuan Jing, and Chunpeng (Craig) Wan 

Research Article (7 pages), Article ID 2734839, Volume 2022 (2022)

Simultaneous Determination of Retinols and Tocols in Egg and Milk Products Based on RP-HPLC Linked with Fluorescent and Photodiode Array

Yingqi Chen , Chonggao Hu, Jiaojiao Xu , Xiaodong Pan, and Baifen Huang 

Research Article (9 pages), Article ID 8431662, Volume 2022 (2022)

Rapid Identification of Fupenzi (*Rubus chingii* Hu) and Its Adulteration by AuNP Visualization

Yuan Li , Yixin Suo , Liuna Wei , Yue Zhang, Youyou Wang , Jiabin Deng , Hengye Chen , Jian Yang , Tiegui Nan , Haiyan Fu , and Lanping Guo 

Research Article (10 pages), Article ID 6278549, Volume 2022 (2022)

Determining the Geographical Origin of Fuji Apple from China by Multivariate Analysis Based on Soluble Sugars, Organic Acids, and Stable Isotopes

Hui Zhang , Jiyun Nie , Zhaoguo Tong, Jing Li, An Li, Youming Shen, Jia Zhang, and Lixue Kuang

Research Article (12 pages), Article ID 5415257, Volume 2022 (2022)

A Study on the Volatile Compounds in *Elaeagnus angustifolia* L. Flowers during Flowering Season by Gas Chromatography-Mass Spectrometry Coupled with Advanced Chemometrics

Zhijing Liu, Degang Ding, Huapeng Cui , Chuanchuan Wang, Juntao Liu, Li Chen, Meijuan Fan, and Guangwei Geng 

Research Article (8 pages), Article ID 7111120, Volume 2021 (2021)

Research Article

Rapid and Nondestructive Identification of Origin and Index Component Contents of Tiegun Yam Based on Hyperspectral Imaging and Chemometric Method

Yue Zhang ^{1,2}, Yuan Li ¹, Cong Zhou ¹, Junhui Zhou ^{1,3}, Tiegui Nan ¹, Jian Yang ^{1,3} and Luqi Huang ¹

¹State Key Laboratory Breeding Base of Dao-di Herbs, National Resource Center for Chinese Materia Medica, China Academy of Chinese Medical Sciences, Beijing 100700, China

²School of Traditional Chinese Medicine, Yunnan University of Chinese Medicine, Kunming 650500, China

³Dexing Research and Training Center of Chinese Medical Sciences, Dexing 334220, China

Correspondence should be addressed to Jian Yang; yangchem2012@163.com and Luqi Huang; huangluqi01@126.com

Received 5 July 2022; Revised 7 September 2022; Accepted 24 November 2022; Published 22 February 2023

Academic Editor: Daniel Cozzolino

Copyright © 2023 Yue Zhang et al. This is an open access article distributed under the Creative Commons Attribution License, which permits unrestricted use, distribution, and reproduction in any medium, provided the original work is properly cited.

Tiegun yam is a typical food and medicine agricultural product, which has the effects of nourishing the kidney and benefitting the lungs. The quality and price of Tiegun yam are affected by its origin, and counterfeiting and adulteration are common. Therefore, it is necessary to establish a method to identify the origin and index component contents of Tiegun yam. Hyperspectral imaging combined with chemometrics was used, for the first time, to explore and implement the identification of origin and index component contents of Tiegun yam. The origin identification models were established by partial least squares-discriminant analysis (PLS-DA), support vector machine (SVM), and random forest (RF) using full wavelength and feature wavelength. Compared with other models, MSC-PLS-DA is the best model, and the accuracy of the training set and prediction set is 100% and 98.40%. Partial least squares regression (PLSR), random forest (RF), and support vector regression (SVR) models were used to predict the contents of starch, polysaccharide, and protein in Tiegun yam powder. The optimal residual predictive deviation (RPD) values of starch, polysaccharide, and protein prediction models selected in this study were 5.21, 3.21, and 2.94, respectively. The characteristic wavelength extracted by the successive projections algorithm (SPA) method can achieve similar results as the full-wavelength model. These results confirmed the application of hyperspectral imaging (HSI) in the identification of the origin and the rapid nondestructive prediction of starch, polysaccharide, and protein contents of Tiegun yam powder. Therefore, the HSI combined with the chemometric method was available for conveniently and accurately determining the origin and index component contents of Tiegun yam, which can expect to be an attractive alternative method for identifying the origin of other food.

1. Introduction

Yam is the fleshy underground tuber of *Dioscorea*. In China, yam is a typical food and medicine agricultural product. It is not only a common vegetable, often used for fresh eating, fresh stir-fry, steaming, making vermicelli, and potato chips, but also a traditional Chinese medicine which can invigorate the spleen and stomach, benefit the lung, generate saliva, and benefit the kidney [1]. Yam contains many nutrient metabolites which include starch, polysaccharide, and protein

[2]. Because of its nutritional content, it is widely used in traditional Chinese medicine to treat chronic diseases such as indigestion [3]. China is an important center of yam cultivation, with more than 90 varieties [4]. Tiegun yam (*D. opposite* Thunb.) is mainly produced in Wen County, Henan Province of China, has the best quality, and is considered to be the representative of Chinese yam (*Dioscorea opposite* Thunb.). In recent years, Tiegun yam has been planted in most areas of China, such as Inner Mongolia, Shaanxi, Jiangsu, Shandong, Hebei, and other places,

and there have been many problems with fake Tiegun yam from other origins in the market. The fake Tiegun yam not only damages the interests of consumers but also has a great difference from that of the Wen County Tiegun yam in nutrient substance. Starch is the most abundant ingredient, which also affects the taste of Tiegun yam, while polysaccharides and proteins are the main pharmacological components. The content of these three components has also become an important index to evaluate the quality of Tiegun Yam. Therefore, it is necessary to establish an analytical method to identify the origin and index component contents of Tiegun yam.

At present, the traditional nutrient content evaluation methods include enzymatic hydrolysis [5] and the underwater weight method [6] to determine the starch content. The content of polysaccharides was determined by inductively coupled plasma mass spectrometry (ICP-MS) [7], spectrophotometry [8], and liquid chromatography-tandem mass spectrometry (LC-MS) [9], and the content of protein was determined by the Kjeldner method [10], spectrophotometry, and combustion [11]. However, most of the traditional content determination methods are destructive, time consuming, and environment polluting with few other shortcomings and only applies to small samples and cannot meet the requirements of online monitoring [12]. In addition, the traditional methods of origin identification include liquid chromatography-mass spectrometry [13], gas chromatography-mass spectrometry [14], molecular biology techniques [15], stable isotope [16], and chemical fingerprinting [17]. However, traditional chemical methods have high accuracy but also have some disadvantages, such as high detection cost, difficult operation, and time consuming. Therefore, the establishment of a rapid and accurate detection method has an urgent market demand.

Hyperspectral imaging (HSI) technology is a non-destructive detection method that integrates image information and spectral information [18]. Compared with traditional spectral analysis technology, HSI can not only obtain two-dimensional spatial and one-dimensional spectral information that corresponds to internal and external features [5] but also collect data from multiple samples simultaneously. Compared to single-point measurement technologies, HSI is capable of performing spatial substance content analysis [19]. It has been widely used in the rapid identification of corn [20], sorghum [21], wolfberry [22], chrysanthemum [23], and other samples due to its characteristics of simultaneously obtaining spectral and spatial information. At the same time, HSI is also used for detecting the content of various substances, such as starch content in sorghum detection [19], corn grain oil content [24], total content of flavonoids in the cherry prediction [12], analysis of protein content in rice [11], and prediction of total flavonoids and polysaccharides in *Anoectochilus formosanus* [25]. All these studies have achieved satisfactory results. However, as far as we know, no studies have been published on using HSI to identify the origin and determine the contents of starch, polysaccharide, and protein in Tiegun yam.

In this study, we discussed the feasibility of the HSI method to identify the origin and determine the contents of starch, polysaccharide, and protein in Tiegun yam. An efficient and accurate method based on the graph segmentation algorithm was developed to achieve the rapid automatic identification and information extraction of the hyperspectral information of Tiegun yam powder samples. In addition, it combined with the chemometric method that can establish different models to realize the rapid identification of different regions of Tiegun yam and the accurate prediction index of its composition.

2. Materials and Methods

2.1. Sample Preparation. Tiegun yam samples were collected from late October to November 2019, from six producing areas, including Inner Mongolia (NM) ($n = 7$), Shaanxi (SX) ($n = 6$), Jiangsu (JS) ($n = 6$), Shandong (SD) ($n = 11$), Hebei (HB) ($n = 13$), and Henan (HN) ($n = 17$) provinces, and finally a total of 60 batches of Tiegun yam samples was collected. All batches of samples were purchased from the local medicinal herbs market, and each batch consisted of 10–20 Tiegun yam. The specific information of the sample is shown in Table 1. The collected Tiegun yam samples were cleaned, peeled, and cut into 10 cm sections and dried for approximately 36 hours in an oven at 50°C. Finally, all dried Tiegun yam samples were ground into powder and sifted through 50 mesh. The powder was sealed in a polyethylene bag and stored at 4°C.

2.2. Hyperspectral Imaging Systems. The HSI system consisted of an imaging spectrograph, a high-performance charged couple device (CCD) camera, a pair of 150 W halogen lamps (150 W/12 V, H-LAM Norsk Elektro Optikk, Norway), a mobile platform (Standa Translation Stage, Lithuania) driven by a stepper motor, and a computer with data acquisition and analysis software (HySpex Ground, Norsk Elektro Optikk, Norway). The imaging spectrograph consisted of SN0605 VNIR (H-V16, Norsk Elektro Optikk, Norway) and N3124 SWIR (H-S16, Norsk Elektro Optikk, Norway).

2.3. Hyperspectral Data Acquisition. First, 60 samples were randomly selected from different batches of Tiegun yam powder from each producing area, with a total of 360 samples. 15 g of each Tiegun yam samples powder sample was selected as a hyperspectral sample and loaded into a Petri dish with a diameter of 5 cm. The criterion is that the bottom of the Petri dish should not be seen when the powder is laid flat.

When the sample was collected, the distance between the spectrometer lens and the sample was 25 cm, the platform moving speed was 1.5 mm/s, the integration time of SN0605 VNIR lens was 3500 μ s, the frame time was 18000, and the spectral range was 410–990 nm. The integration time of the N3124 SWIR lens was 4500 μ s, the frame time was 46928, and the spectral range was 950–2500 nm. The spectral

TABLE 1: Detailed information of Tiegun yam.

Number	Origin	Quantity of sample
NM	Dengkou County, Bayanchuer city, Inner Mongolia, China	60
SX	Dali County, Weinan city, Shaanxi province, China	60
JS	Fengxian County, Xuzhou city, Jiangsu province, China	60
SD	Dingtao District, Heze city, Shandong province, China	60
HB	Li County, Baoding city, Hebei province, China	60
HN	Wen County, Jiaozuo city, Henan province, China	60

resolution of both VNIR and SWIR lenses was 6 nm. The samples were arranged on a black horizontal moving platform according to the matrix, and the Teflon whiteboard was placed at the end of the sample row to collect the hyperspectral images. In order to reduce the influence of natural light on the experiment, the whole experiment was conducted in a dark room. Finally, the average surface spectral data of the powder in each Petri dish were used as a region of interest (ROI).

2.4. Hyperspectral Image Processing. In order to eliminate the influence of instruments and environment on the sample data, the raw hyperspectral image data were corrected by software (HySpex RAD, Norsk Elektro Optikk, Norway), followed by black-and-white plate correction. Black-and-white plate correction is a common method in hyperspectral image data processing, which is used to eliminate the influence of air and surrounding environment on spectral images, so as to obtain the relative reflectance of the spectrum. This method is used to calculate the relative reflectivity of samples, whiteboards, and blackboards, and the calculation formula is as follows:

$$R = \frac{R_{raw} - R_d}{R_w - R_d}, \quad (1)$$

where R is the corrected reflectivity image, R_{raw} is the original reflectivity image, R_w is the whiteboard reference image, which is obtained by Teflon whiteboard (reflectivity is close to 1), and R_d is the blackboard reference image, which is obtained by covering the lens cap (reflectivity is close to 0).

2.5. Reference Measurement of Nutrient Substances Content

2.5.1. Evaluation of Starch Content. The soluble sugar and starch in the samples were separated by 80% ethanol, and the starch was hydrolyzed into glucose by acid hydrolysis. Glucose content was determined by anthrone colorimetry, and starch content was calculated [26]. Glucose standard solution of 1, 0.8, 0.4, 0.2, 0.1, and 0.05 mg/mL was prepared. The standard curve $Y = 2.9468x + 0.2768$ ($R^2 = 0.997$) was established with glucose concentration as abscissa and ΔA ($\Delta A = A - A_{blank}$) as abscissa. The 0.01 g Tiegun yam powder sample was weighed, and the test solution was configured. The absorbance value A was measured at 620 nm with a microplate reader. The abovementioned determination was completed with a total starch content

determination kit (BC0700, Solarbio, Beijing, China). The formula for calculating starch content is as follows:

$$M1 = \frac{x * V * F}{1.11 * W}, \quad (2)$$

where $M1$ stands for starch content (mg/g), x is the calculated concentration of starch based on the standard curve (mg/mL), W is the sample mass (g), F stands for sample dilution ratio, and V is the volume after extraction (ml).

2.5.2. Evaluation of Polysaccharide Content. Total polysaccharides were extracted by the water extraction and alcohol precipitation method, and the content of total polysaccharides was determined by the phenol-sulfuric acid method [27, 28]. Standard solution of 0.4, 0.2, 0.1, 0.05, 0.025, and 0.0125 mg/mL was prepared, and the standard curve $Y = 6.7386x + 0.2257$ ($R^2 = 0.998$) was established with concentration as abscissa and ΔA ($\Delta A = A - A_{blank}$). The 0.025 g Tiegun yam powder sample was weighed, and the test solution was configured. The absorbance value A was measured at 490 nm with a microplate tester. The abovementioned determination was completed with a total polysaccharide content determination kit (YX-W-ZDT, HEPENGBIO, Shanghai, China). The formula for calculating the polysaccharide content is as follows:

$$M2 = \frac{5 * Y}{W}, \quad (3)$$

where $M2$ stands for polysaccharide content (mg/g), Y is the calculated concentration of polysaccharide based on the standard curve (mg/mL), and W stands for sample mass (g).

2.5.3. Evaluation of Protein Content. Protein concentration was detected by the Bradford method. The standard protein solution of 0.0625, 0.125, 0.25, 0.5, 0.75, 1, and 1.5 mg/mL was configured to establish the standard curve $Y = 0.5676x + 1.4197$ ($R^2 = 0.994$). The 0.025 g Tiegun yam powder sample was weighed with the test solution, and the absorbance was measured at 595 nm. The Bradford protein Assay kit (P0006C, Beyotime Biotechnology, Shanghai, China) was used to detect protein concentration. The formula for calculating protein concentration is as follows:

$$M3 = \frac{Y}{W}, \quad (4)$$

where Y stands for protein concentration (mg/mL) and W stands for weight of the sample (g).

2.6. Statistical and Chemometrics Analysis

2.6.1. Statistical Analysis. The mean value and standard deviation of starch, polysaccharide, and protein contents of Tiegun yam from different origins were calculated. The contents of starch, polysaccharide, and protein of Tiegun yam from different producing areas were compared. One-way analysis of variance (ANOVA) ($P < 0.05$) was used to analyze whether there were significant differences in the contents of polysaccharides, starch, and proteins in Tiegun yam from different origins.

2.6.2. Data Preprocessing. A total of 360 hyperspectral data were obtained from the extraction of hyperspectral regions of interest. The pretreatment of spectral data can reduce errors caused by baseline changes such as background, noise, and other physical factors and can improve the prediction ability and stability of the model. In this study, five methods including multiple scattering corrections (MSCs), first derivative (D1), second derivative (D2), SG smoothing (SG), and standard normal variable transformation (SNV) were used to preprocess spectral data to improve the accuracy and stability of the discrimination model.

2.6.3. Chemometric Method. Three different classification models, including partial least squares discriminant analysis (PLS-DA), support vector machine (SVM), and random forest (RF), were established to identify the origin of Tiegun yam. Similarly, three different classification models including partial least square regression (PLSR), support vector regression (SVR), and random forest (RF) were established.

PLSR model, a classical linear regression algorithm, can consider both matrices x (spectral data) and y (chemical index), to find the maximal correlation between the new variables of X and Y [29, 30]. PLS-DA is a supervised classification algorithm adapted from PLSR. The optimal number of 10–12 important potential variables in different prediction groups was obtained by using the leave-one cross-validation method.

The SVM model, which aims to obtain the best hyperplane by selecting the hyperplane passing through the maximum possible gap between points of different categories, was used with a nonlinear radial basis function to reduce the training complexity. In this research, the SVM model was constructed based on the radial basis function, and the optimal combination of two important parameters, namely, the penalty factor ($C = 12000$) and the kernel parameter ($\gamma = 100$), was determined by a grid-search method [31]. Support vector regression (SVR) is an important application branch of the support vector machine (SVM).

RF is an integration algorithm based on a classified regression tree, which builds multiple regression trees by constructing multiple training sets with the putback samples. The number of trees in this study is 50.

The successive projections algorithm (SPA) was used to select the characteristic wavelength of the classification model. SPA is a forward variable selection algorithm that minimizes the space collinearity of vector quantity. Its advantage lies in extracting several characteristic wavelengths of the whole band and eliminating redundant information in the original spectral matrix. Finally, the characteristic variable modeling results are compared with the full-band modeling results.

2.6.4. Model Evaluation. The performance of the classification model was evaluated based on the classification discrimination accuracy and confusion matrix. The confusion matrix is a method to evaluate the prediction results of the classification model in data analysis. The specific evaluation indexes include accuracy, sensitivity, and specificity [32]. These precision indexes reflect the accuracy of model classification from different aspects.

$$\begin{aligned} \text{Accuracy} &= \frac{\text{TP} + \text{TN}}{\text{TP} + \text{FN} + \text{FP} + \text{TN}}, \\ \text{Sensitivity} &= \frac{\text{TP}}{\text{TP} + \text{FN}}, \\ \text{Specificity} &= \frac{\text{TN}}{\text{TN} + \text{FP}}, \end{aligned} \quad (5)$$

where TP is the number of true positive samples, TN is the number of true negative samples, FP is the number of false positive samples, and FN is the number of false negative samples.

The prediction effect of pretreatment methods combined with regression models was evaluated based on residual predictive deviation (RPD) and curve correlation coefficient R^2 values. Usually, the R^2 value from 0.61 to 0.80 and the RPD value ranging from 2.0 to 2.5 indicate that the model can be used for prediction. R^2 value between 0.81 and 0.90 and RPD value between 2.5 and 3.0 demonstrate high model performance. The model has an excellent prediction performance with an R^2 value higher than 0.90 and an RPD value higher than 3.0.

2.7. Data Division. The samples were randomly divided into training sets and prediction sets in a ratio of 7:3 for subsequent modeling and analysis. 240 (2/3 samples) and 120 (1/3 samples) samples were randomly assigned to establish prediction models for starch, polysaccharide, and protein. The predictive set content range should be included in the training set content range.

2.8. Software and Program. The image correction tool used in this study is RAD correction software. ROI was collected by ENVI 5.3 software (Harris Geospatial Solutions Inc., CO, USA). ANOVA was conducted on SPSS software (22.0 version, IBM Inc., Chicago, IL, USA). Data analysis, such as spectral data preprocessing and classification model construction, was realized by Matlab 2020a (MathWorks, USA) software, and scripts were written by our research group.

TABLE 2: Statistical values of starch, polysaccharide, and protein contents in Tiegun yam powder for both calibration and prediction sets (mg/g).

Content	Sets	Range	Mean	SD
Starch	Training	377.4–638.3	489.5	60.23
	Prediction	391.4–603.8	490.5	60.33
Polysaccharide	Training	8.06–36.01	22.41	8.13
	Prediction	8.06–35.20	23.57	11.04
Protein	Training	5.09–51.25	23.68	10.05
	Prediction	5.44–36.59	22.37	9.62

3. Results and Discussion

3.1. Statistical Analysis. The content ranges, mean, and standard deviation (SD) of starch, polysaccharide, and protein of Tiegun yam powder classified into a training set and prediction set are shown in Table 2. The contents of starch, polysaccharide, and protein training set ranged from (377.4 to 638.3) mg/g, (8.06 to 36.01) mg/g, and (5.09 to 51.25) mg/g and (391.4 to 603.8) mg/g, (8.06 to 35.20) mg/g, and (5.44 to 36.59) mg/g for the prediction set. The predictive set content range should be included in the training set content range. Meanwhile, at the same time, ANOVA showed that there were significant differences in starch, polysaccharide, and protein contents of Tiegun yam beans from 6 origins ($P < 0.05$). The starch content of Tiegun yam in JS was the highest, while that in SD was the lowest. The other four producing areas have little difference in starch content. The content of polysaccharide of Tiegun yam in NM, SX, and JS was lower than that in SD, HB, and HN. The protein content of Tiegun yam was very low in NM, and there was little difference in other producing areas. Wen County of Henan province, as an authentic production area of Tiegun yam, had a high content of all these three nutrients. In other words, starch, polysaccharide, and protein content was significantly affected by the origin. The place of origin can be used as a grouping basis for classification modeling of hyperspectral Tiegun yam.

3.2. Original Spectral Curve Analysis. The spectral curves of Tiegun yam powder samples from different origins (Figure 1) have similar variation trends in VNIR and SWIR bands, and the mean values of spectral data have obvious differences in visible near-infrared (VNIR) bands, which may be caused by the significant differences in chemical composition content of Tiegun yam powder samples from different origins as shown in Table 2. This is related to different plant base sources, environmental conditions, and planting methods. However, the overall spectral characteristics of the short wave near-infrared (SWIR) band are similar with little difference.

The absorption peaks near 980 nm, 1450 nm, and 1855 nm were mainly attributed to the moisture [33]. However, because 980 nm is where the VNIR band ends, the signature is not obvious. The absorption peak near 1210 nm corresponded to the second stretching overtone of C-H. This absorption peak was mainly attributed to carbohydrates and

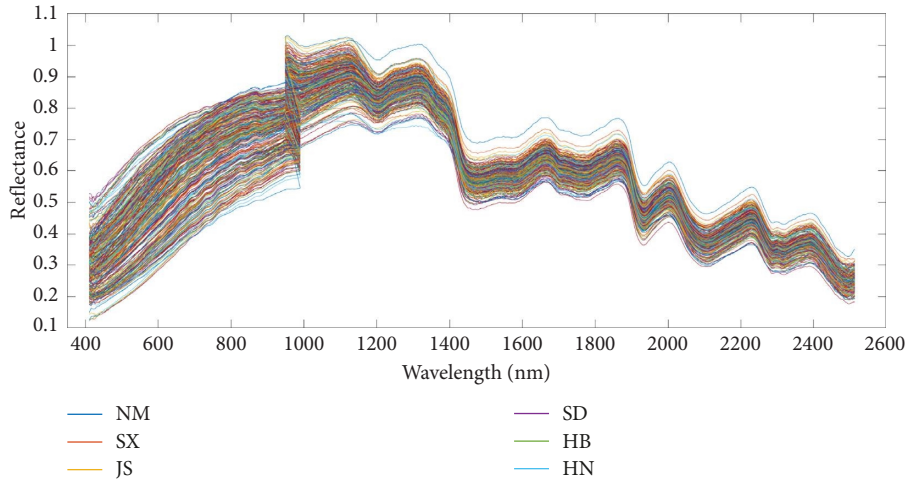
fats [34]. The absorption peak at 1290 nm and 1471 nm was formed by the in-plane bending of C-H. The absorption peak at 1648 nm was formed due to the effect of amide groups [35]. The absorption peak at 1792 nm indicated the anhydride group. The absorption peak at 2069 nm was formed due to the combined effect of stretching and bending of O-H. The absorption peak at 2101 and 2190 nm was the characteristic absorption peaks of the protein. The absorption peak at 2101 nm might be possibly associated with the carboxyl group. The absorption peak at 2190 nm indicated the combined absorption peak of C-H and C-O [11]. Compared to VNIR, the wavelengths in SWIR could fully reflect the vibration of molecular bonds in different compounds.

3.3. Results of the Origin Identification Model of Tiegun Yam.

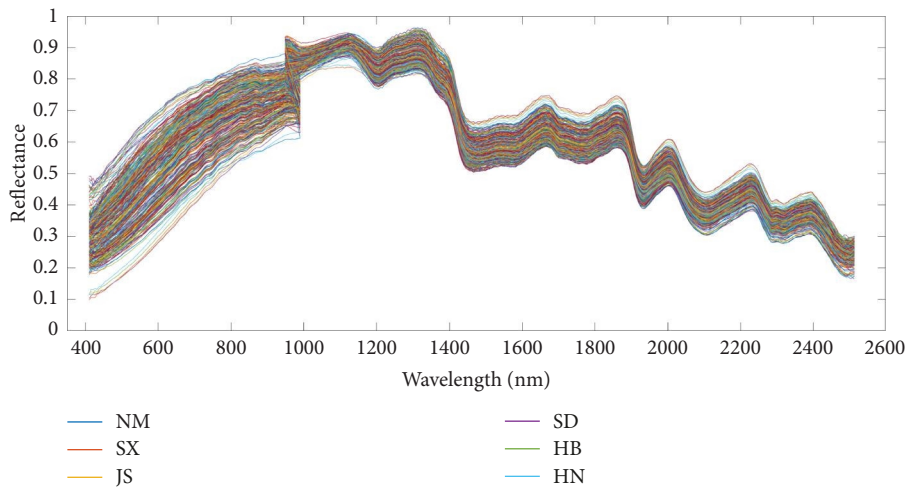
The original spectral data of Tiegun yam powder samples from different origins were preprocessed by MSC, D1, D2, SG, and SNV, and the training set/prediction set was divided into input variables to calculate the accuracy of PLS-DA, RF, and SVM classification and identification methods (Table 3). For the PLS-DA model, MSC preprocessing can improve the accuracy of the model training set and prediction set. The prediction set accuracy of raw data-PLS-DA was 96.00%, and that of MSC-PLS-DA was 98.40%, with an improvement of 2.40%. The SVM model has high precision in the training set and low precision in the prediction set, and there is a big gap between them. The SVM model may not be suitable for the origin identification data of Tiegun yam. The accuracy of the prediction set of the D2-RF model is 83.33%, which is 14.44% higher than the raw data, but lower than that of the MSC-PLS-DA model. Therefore, MSC-PLS-DA is the optimal model for the origin identification of Tiegun yam, and this model is used for spectral modeling after feature wavelength selection and model evaluation.

As shown in Figure 2, there are 55 feature wavelengths selected based on SPA. MSC preprocessing and PLS-DA algorithm are used for modeling, and the accuracy of the training set is 99.13% and the prediction set is 97.71%. The results show that the extraction of characteristic wavelength modeling can achieve almost the same results as full-wavelength modeling.

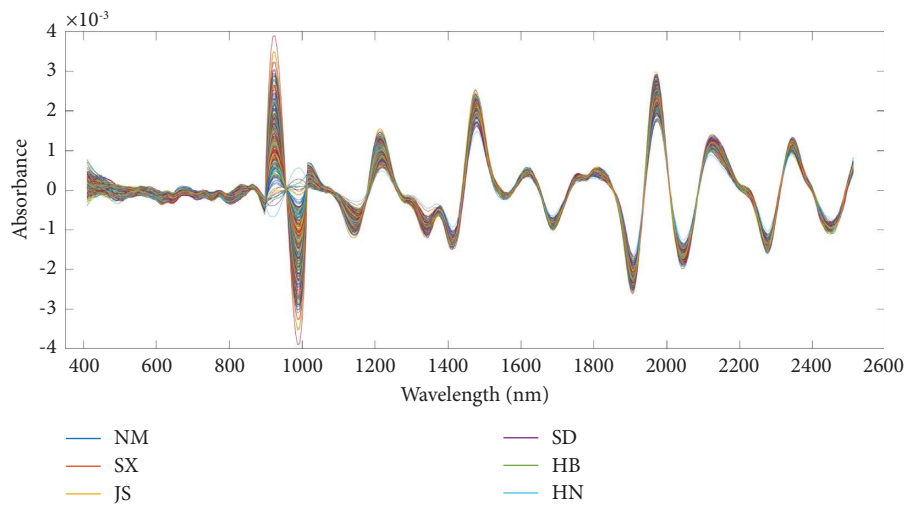
In classification problems, a confusion matrix is a visual evaluation criterion to describe the real category attributes of sample data and to predict the performance of algorithms. The behavior of the confounding matrix is a true label, listed as the predictive label. The bottom line shows the percentage of predicted correct or incorrect classification, that is, sensitivity and error rate. The right-most column shows the percentage of all examples that fall into each category that are correctly and incorrectly classified, that is, the precision and false negative rates. After MSC treatment of the full-band spectrum of Tiegun yam powder samples, the confusion matrix generated by the PLS-DA classification model prediction results of samples from different sources is shown in Figure 3(a), and the sensitivity and precision of the classification and identification models of each origin are all above 95. The confusion matrix generated by the PLS-DA classification model after SPA screening characteristic



(a)



(b)



(c)

FIGURE 1: Continued.

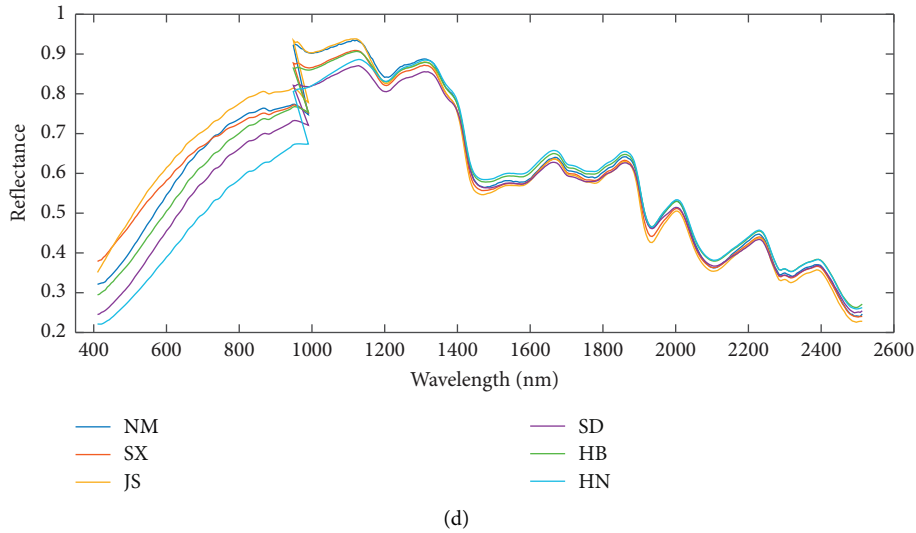


FIGURE 1: Raw spectra (a), spectra after pretreated by MSC (b), second derivative (c), and mean reflectance spectra (d) of Tiegun yam powder samples from different origins.

TABLE 3: Pairwise combination classification accuracy of the preprocessing method and classification model of Tiegun yam powder samples from different origins.

Models	Preprocessing	Accuracy (%)	
		Training set	Prediction set
PLS-DA	Raw data	99.57	96.00
	MSC	100.00	98.40
	D1	100.00	96.00
	D2	97.82	95.42
	SG	98.72	95.20
	SNV	99.15	96.80
SVM	Raw data	98.81	61.11
	MSC	97.22	61.11
	D1	98.81	25.93
	D2	34.52	27.78
	SG	98.41	59.26
	SNV	100.00	24.07
RF	Raw data	97.14	68.89
	MSC	99.05	76.67
	D1	99.05	52.22
	D2	100.00	83.33
	SG	98.09	77.78
	SNV	97.14	68.89

variables of spectral data is shown in Figure 3(b). The precision and sensitivity of different producing areas are both above 92%, which is not different from full-wavelength identification, thus showing a good performance.

3.4. Starch, Polysaccharide, and Protein Content Prediction. The prediction results of Tiegun yam powder showed that the three models had better prediction ability for starch content but worse prediction ability for polysaccharide and protein content than starch. Spectral data preprocessing is an important step in chemometrics modeling. Its purpose is to reduce the error caused by background, noise, and other

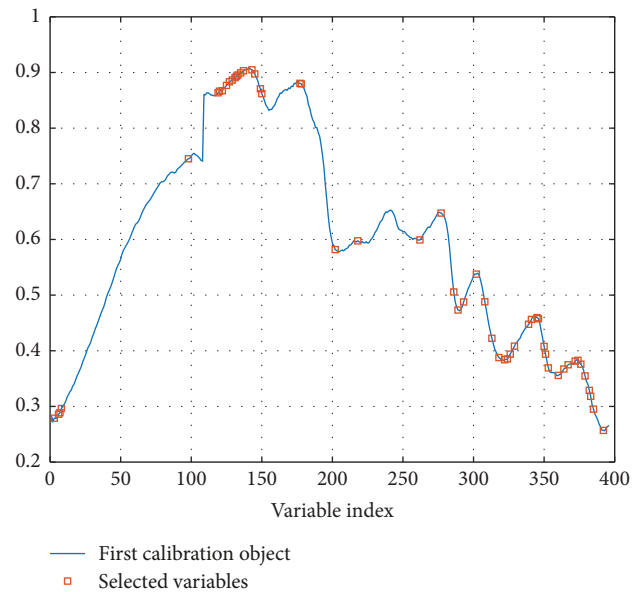


FIGURE 2: Screening results of SPA characteristic variables.

physical factors so as to improve the prediction ability and stability of the model. Tamburini et al. [36] have also reported that MSC, SNV, D1, and D2 can improve the accuracy of PLSR models. In contrast, the Caporaso study [37] showed that the accuracy of the model was not improved when the MSC, SNV, and D1 or D2 were applied. The prediction results of different pretreatment combined with three models for starch, polysaccharide and protein are shown in Tables S1, S2, and S3. MSC, D2, SG smooth, and SNV pretreatment methods can all improve the accuracy of the model, but the improved accuracy varies significantly according to different components and models. The first derivative does not apply to the prediction model. As shown in Table 4, R^2 values of the training set and the prediction set

Output Class	Target Class						
	NM	SX	JS	SD	HB	HN	Total
NM	19 15.2%	0 0.0%	0 0.0%	0 0.0%	0 0.0%	0 0.0%	100% 0.0%
SX	0 0.0%	21 16.8%	0 0.0%	0 0.0%	0 0.0%	0 0.0%	100% 0.0%
JS	0 0.0%	0 0.0%	16 12.8%	0 0.0%	0 0.0%	0 0.0%	100% 0.0%
SD	0 0.0%	0 0.0%	0 0.0%	22 17.6%	0 0.0%	0 0.0%	100% 0.0%
HB	0 0.0%	0 0.0%	0 0.0%	0 0.0%	22 17.6%	1 0.8%	95.7% 4.3%
HN	0 0.0%	0 0.0%	0 0.0%	0 0.0%	0 0.0%	1 0.8%	95.8% 4.2%
	100% 0.0%	100% 0.0%	100% 0.0%	100% 0.0%	95.7% 4.3%	95.8% 4.2%	98.4% 1.6%

(a)

Output Class	Target Class						
	NM	SX	JS	SD	HB	HN	Total
NM	27 20.6%	0 0.0%	0 0.0%	0 0.0%	0 0.0%	0 0.0%	100% 0.0%
SX	0 0.0%	15 11.5%	0 0.0%	0 0.0%	0 0.0%	1 0.8%	93.8% 6.3%
JS	0 0.0%	0 0.0%	16 12.2%	0 0.0%	0 0.0%	0 0.0%	100% 0.0%
SD	0 0.0%	0 0.0%	0 0.0%	22 16.8%	0 0.0%	1 0.8%	95.7% 4.3%
HB	0 0.0%	0 0.0%	0 0.0%	0 0.0%	1 0.8%	24 18.3%	96.0% 4.0%
HN	0 0.0%	0 0.0%	0 0.0%	0 0.0%	0 0.0%	24 18.3%	100% 0.0%
	100% 0.0%	100% 0.0%	100% 0.0%	95.7% 4.3%	100% 0.0%	92.3% 7.7%	97.7% 2.3%

(b)

FIGURE 3: The hyperspectral raw data (a) and hyperspectral data after characteristic wavelength selection (b) results of origin identification prediction set of Tiegun yam powder samples.

TABLE 4: Prediction results of spectral data of Tiegun yam powder samples after different pretreatments.

Content	Models	Training set		Prediction set		
		R^2	RMSEC (mg/g)	R^2	RMSEP (mg/g)	RPD
Starch	PLSR	0.9598	11.0908	0.9270	13.6931	3.22
	SVR	0.9948	3.8399	0.9636	10.7103	5.21
	RF	0.9896	8.4654	0.9677	14.4532	3.45
Polysaccharide	PLSR	0.8684	2.6837	0.8425	2.9637	2.52
	SVR	0.9996	0.1397	0.9275	2.0717	3.21
	RF	0.9818	1.6933	0.9012	3.5702	1.45
Protein	PLSR	0.8933	2.4077	0.8610	2.6676	2.61
	SVR	0.9943	0.5219	0.8939	2.6464	2.94
	RF	0.9770	1.7388	0.9292	3.5203	1.63

should be significantly different, and the optimal pretreatment method should be selected for different models based on the size of the prediction model of starch RPD value. The optimal prediction model of starch, polysaccharide, and protein was D2-SVR. Among the three models, SVR has the best prediction result, followed by PLSR, and RF has the lowest prediction result. The D2-SVR prediction model of starch had a higher R^2 value (0.9636) and RPD value (5.21) and lower RMSE value (RMSEC = 3.8399 mg/g; RMSEP = 10.7103 mg/g). For the polysaccharide prediction model, the parameters of the optimal model were R^2 = 0.9275, RPD = 3.21, RMSEC = 0.1397 mg/g, and RMSEP = 2.0717 mg/g. For the protein prediction model, the parameters of the optimal model were R^2 = 0.8939, RPD = 2.94, RMSEC = 0.5219 mg/g, and RMSEP = 2.6464 mg/g, indicating that the prediction models have good accuracy and stability. Therefore, appropriate spectral pretreatment is needed in the starch prediction model to improve the regression model. The D2-

SVR prediction model results of the three components are shown in Figure 4.

The characteristic variables were selected based on the SPA method. 39 characteristic wavelengths were selected for the starch regression model, 23 characteristic variables for the polysaccharide regression model, and 48 characteristic variables for the protein model. The modeling results of the model selected above are shown in Table 5. D2-SVM was used to model hyperspectral data selected by characteristic wavelength. RPD values of starch, polysaccharide, and protein models were 4.45, 2.05, and 2.18, respectively. The results show that the characteristic wavelength modeling of protein extraction can obtain almost the same results as that of the full-wavelength modeling. The selection of SPA characteristic wavelengths revealed the important spectral regions for predicting the index components of Tiegun yam powder. In addition, modeling results similar to those of full-wavelength can be obtained, which greatly reduces the difficulty of model data processing and reduces the time of model operation.

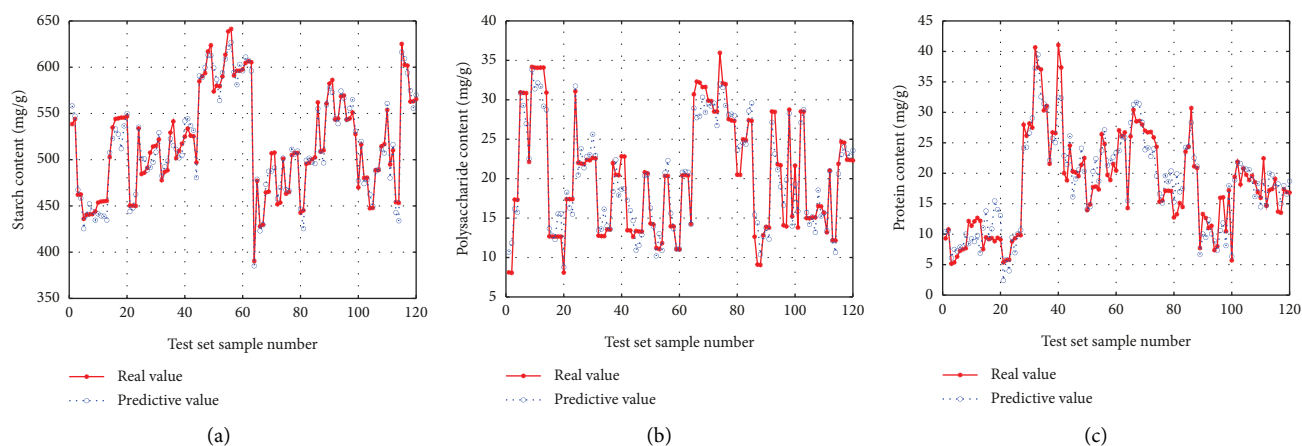


FIGURE 4: D2-SVR prediction model results for starch (a), polysaccharide (b), and protein (c).

TABLE 5: Prediction results of selected data by SPA of Tiegun yam powder samples.

Content	Number	Training set		Prediction set		
		R^2	RMSEC (mg/g)	R^2	RMSEP (mg/g)	RPD
Starch	39	0.9943	4.0396	0.9521	12.0895	4.45
Polysaccharide	23	0.9992	0.2161	0.8145	3.5468	2.05
Protein	48	0.9608	1.4008	0.8259	3.3886	2.18

4. Conclusions

This study indicated that it was feasible to use hyperspectral technology combined with chemometric pretreatment and modeling to fast and nondestructive identification of the origin and nondestructive detection of starch, polysaccharide, and protein contents of the Tiegun yam powder samples. Some spectral pretreatment methods (MSC and SNV) can improve the accuracy of hyperspectral data, while others (first-order derivation) are not suitable for the content regression model. MSC combined with PLS-DA is the best combination for the discriminant model, and the accuracy of the training set and the prediction set is over 98%. D2-SVR was the best pretreatment method for starch, polysaccharide, and protein prediction models with relatively high R^2P and RPD values. The characteristic wavelength extracted by the SPA method can achieve similar results to the full-wavelength model, which can greatly reduce the complexity of the model and can reduce the operation time of the model. This study demonstrates the great potential of using hyperspectral images to quickly and nondestructively determine the indicator components of samples, which will be helpful for further prediction of other chemical components in Tiegun yam or applied to other materials with the homology of medicine and food.

Data Availability

The data used to support the findings of this study are included in the article.

Conflicts of Interest

The authors declare that they have no conflicts of interest.

Authors' Contributions

Yue Zhang conceptualised the study, curated the data, wrote of the manuscript, and reviewed and edited the data. Yuan Li performed the investigation. Cong Zhou curated and investigated the data. Junhui Zhou provided the resources and supervised the study. Tiegui Nan supervised the study. Jian Yang provided the resources, developed the methodology, conceptualised and supervised the study, and acquired the funding. Luqi Huang provided the resources, conceptualised and supervised the study, and acquired the funding.

Acknowledgments

This work was supported by the National Key R&D Program of China (Grant no. 2020YFC1712700), the scientific and technological innovation project of the China Academy of

Chinese Medical Sciences (Grant nos. CI2021A04005 and CI2021A01809), the China Agriculture Research System of MOF and MARA (Grant no. CARS-21), and the Shandong Provincial Key Research and Development Program (a Major Technological Innovation Project) (Grant no. 2021CXGC010508).

Supplementary Materials

The supplementary materials included prediction results of Starch, polysaccharide, and protein from different pretreatment spectral data of Tiegun yam powder samples in Result 3.4, which are shown in table S1, S2, and S3. (*Supplementary Materials*)

References

- [1] C. G. Lyu, J. Yang, T. L. Wang et al., "A field trials-based authentication study of conventionally and organically grown Chinese yams using light stable isotopes and multi-elemental analysis combined with machine learning algorithms," *Food Chemistry*, vol. 343, Article ID 128506, 2021.
- [2] L. An, Y. L. Yuan, J. W. Ma et al., "NMR-based metabolomics approach to investigate the distribution characteristics of metabolites in *Dioscorea opposita* Thunb. cv. Tiegun," *Food Chemistry*, vol. 298, Article ID 125063, 2019.
- [3] S. Guo, X. Y. Zhao, Y. Ma, Y. B. Wang, and D. Wang, "Fingerprints and changes analysis of volatile compounds in fresh-cut yam during yellowing process by using HS-GC-IMS," *Food Chemistry*, vol. 369, Article ID 130939, 2022.
- [4] S. Y. Zhou, G. L. Huang, and G. Y. Chen, "Extraction, structural analysis, derivatization and antioxidant activity of polysaccharide from Chinese yam," *Food Chemistry*, vol. 361, Article ID 130089, 2021.
- [5] F. X. Wang, C. G. Wang, S. Y. Song, S. S. Xie, and F. L. Kang, "Study on starch content detection and visualization of potato based on hyperspectral imaging," *Food Sciences and Nutrition*, vol. 9, no. 8, pp. 4420–4430, 2021.
- [6] P. Meise, S. Seddig, R. Uptmoor, F. Ordon, and A. Schum, "Assessment of yield and yield components of starch potato cultivars (*Solanum tuberosum* L.) under nitrogen deficiency and drought stress conditions," *Potato Research*, vol. 62, no. 2, pp. 193–220, 2019.
- [7] D. D. Xu, W. Zheng, Y. Q. Zhang, Q. P. Gao, M. X. Wang, and Y. Gao, "A method for determining polysaccharide content in biological samples," *International Journal of Biological Macromolecules*, vol. 107, pp. 843–847, 2018.
- [8] M. A. Galvão, M. R. Ferreira, B. M. Nunes, A. S. Santana, K. P. Randau, and L. A. Soares, "Validation of a spectrophotometric methodology for the quantification of polysaccharides from roots of *Operculina macrocarpa* (jalapa)," *Revista Brasileira de Farmacognosia*, vol. 24, no. 6, pp. 683–690, 2014.
- [9] K. Raymond, J. M. Lacey, G. Dimitar et al., "Mucopolysaccharides quantitation in serum by liquid chromatography-tandem mass spectrometry," *Molecular Genetics and Metabolism*, vol. 123, p. S123, 2018.
- [10] S. Pakfetrat, S. Amiri, M. Radi, E. Abedi, and L. Torri, "The influence of green tea extract as the steeping solution on nutritional and microbial characteristics of germinated wheat," *Food Chemistry*, vol. 332, Article ID 127288, 2020.
- [11] C. Y. Ma, Z. S. Ren, Z. H. Zhang, J. Du, C. Q. Jin, and X. Yin, "Development of simplified models for nondestructive testing of rice (with husk) protein content using hyperspectral imaging technology," *Vibrational Spectroscopy*, vol. 114, Article ID 103230, 2021.
- [12] B. Wang, J. L. He, S. J. Zhang, and L. L. Li, "Nondestructive prediction and visualization of total flavonoids content in *Cerasus Humilis* fruit during storage periods based on hyperspectral imaging technique," *Journal of Food Process Engineering*, vol. 44, no. 10, 2021.
- [13] G. Y. Deng, S. W. Guo, F. Zaman, T. Y. Li, and Y. Q. Huang, "Recent advances in animal origin identification of gelatin-based products using liquid chromatography-mass spectrometry methods: a mini review," *Reviews in Analytical Chemistry*, vol. 39, no. 1, pp. 260–271, 2020.
- [14] A. M. Li, S. L. Duan, Y. T. Dang et al., "Origin identification of Chinese Maca using electronic nose coupled with GC-MS," *Scientific Reports*, vol. 9, no. 1, Article ID 12216, 2019.
- [15] H. Nakanishi, K. Yoneyama, M. Hara, A. Takada, and K. Saito, "The origin identification method for crude drugs derived from arthropods and annelids using molecular biological techniques," *Journal of Natural Medicines*, vol. 74, no. 1, pp. 275–281, 2020.
- [16] J. Zhang, Z. Q. Tian, Y. Q. Ma et al., "Origin identification of the sauce-flavor Chinese baijiu by organic acids, trace elements, and the stable carbon isotope ratio," *Journal of Food Quality*, vol. 2019, pp. 1–7, 2019.
- [17] H. W. Gu, X. L. Yin, T. Q. Peng et al., "Geographical origin identification and chemical markers screening of Chinese green tea using two-dimensional fingerprints technique coupled with multivariate chemometric methods," *Food Control*, vol. 135, Article ID 108795, 2022.
- [18] G. Elmasry, M. Kamruzzaman, D. W. Sun, and P. Allen, "Principles and applications of hyperspectral imaging in quality evaluation of agro-food products: a review," *Critical Reviews in Food Science and Nutrition*, vol. 52, no. 11, pp. 999–1023, 2012.
- [19] H. P. Huang, X. J. Hu, J. P. Tian et al., "Rapid and non-destructive prediction of amylose and amylopectin contents in sorghum based on hyperspectral imaging," *Food Chemistry*, vol. 359, Article ID 129954, 2021.
- [20] X. L. Bai, C. Zhang, Q. L. Xiao, Y. He, and Y. D. Bao, "Application of near-infrared hyperspectral imaging to identify a variety of silage maize seeds and common maize seeds," *RSC Advances*, vol. 10, no. 20, pp. 11707–11715, 2020.
- [21] Z. Z. Bai, X. J. Hu, J. P. Tian, P. Chen, H. B. Luo, and D. Huang, "Rapid and nondestructive detection of sorghum adulteration using optimization algorithms and hyperspectral imaging," *Food Chemistry*, vol. 331, Article ID 127290, 2020.
- [22] C. Zhang, W. Y. Wu, L. Zhou, H. Cheng, X. Q. Ye, and Y. He, "Developing deep learning based regression approaches for determination of chemical compositions in dry black goji berries (*Lycium ruthenicum* Murr.) using near-infrared hyperspectral imaging," *Food Chemistry*, vol. 319, Article ID 126536, 2020.
- [23] J. He, L. D. Chen, B. Q. Chu, and C. Zhang, "Determination of total polysaccharides and total flavonoids in *Chrysanthemum morifolium* using near-infrared hyperspectral imaging and multivariate analysis," *Molecules*, vol. 23, no. 9, p. 2395, 2018.
- [24] L. Zhang, Y. Q. Wang, Y. G. Wei, and D. An, "Near-infrared hyperspectral imaging technology combined with deep convolutional generative adversarial network to predict oil content of single maize kernel," *Food Chemistry*, vol. 370, Article ID 131047, 2022.
- [25] X. Chu, R. Li, H. Y. Wei et al., "Determination of total flavonoid and polysaccharide content in *Anoectochilus*

- formosanus in response to different light qualities using hyperspectral imaging,” *Infrared Physics & Technology*, vol. 122, Article ID 104098, 2022.
- [26] I. da Silva Lindemann, C. Lambrecht Dittgen, C. de Souza Batista et al., “Rice and common bean blends: effect of cooking on in vitro starch digestibility and phenolics profile,” *Food Chemistry*, vol. 340, Article ID 127908, 2021.
- [27] H. Q. Zhao, Z. B. Wang, Y. P. Sun, C. J. Yang, B. Y. Yang, and H. X. Kuang, “Advances in isolation, identification and bioactivity of Fritillaria polysaccharides,” *Chinese Traditional Patent Medicine*, vol. 44, pp. 505–510, 2020.
- [28] H. Lin, S. H. Gui, B. B. Yu, X. H. Que, and J. Q. Zhu, “Analysis of polysaccharides and monosaccharides from *Rehmannia glutinosa* by different processing technology and effects on ovarian granulosa cells,” *Chinese Traditional Patent Medicine*, vol. 41, pp. 2958–2963, 2019.
- [29] I. Baek, H. Lee, B. K. Cho, C. Mo, D. E. Chan, and M. S. Kim, “Shortwave infrared hyperspectral imaging system coupled with multivariable method for TVB-N measurement in pork,” *Food Control*, vol. 124, Article ID 107854, 2021.
- [30] W. D. Zhang, A. L. Cao, P. Y. Shi, and L. Y. Cai, “Rapid evaluation of freshness of largemouth bass under different thawing methods using hyperspectral imaging,” *Food Control*, vol. 125, Article ID 108023, 2021.
- [31] A. Borin, M. F. Ferrão, C. Mello, D. A. Maretto, and R. J. Poppi, “Least-squares support vector machines and near infrared spectroscopy for quantification of common adulterants in powdered milk,” *Analytica Chimica Acta*, vol. 579, no. 1, pp. 25–32, 2006.
- [32] W. Lan, S. Wang, Y. Wu et al., “A novel fluorescence sensing strategy based on nanoparticles combined with spectral splicing and chemometrics for the recognition of *Citrus reticulata* ‘Chachi’ and its storage year,” *Journal of the Science of Food and Agriculture*, vol. 100, no. 11, pp. 4199–4207, 2020.
- [33] J. Ma and D. W. Sun, “Prediction of monounsaturated and polyunsaturated fatty acids of various processed pork meats using improved hyperspectral imaging technique,” *Food Chemistry*, vol. 321, Article ID 126695, 2020.
- [34] L. Yang, H. Q. Gao, L. W. Meng et al., “Nondestructive measurement of pectin polysaccharides using hyperspectral imaging in mulberry fruit,” *Food Chemistry*, vol. 334, Article ID 127614, 2021.
- [35] X. Li, F. Feng, R. Z. Gao et al., “Application of near infrared reflectance (NIR) spectroscopy to identify potential PSE meat,” *Journal of the Science of Food and Agriculture*, vol. 96, no. 9, pp. 3148–3156, 2016.
- [36] E. Tamburini, E. Mamolini, M. De Bastiani, M. G. Marchetti, and W. R. Seitz, “Quantitative determination of *Fusarium proliferatum* concentration in intact garlic cloves using near-infrared spectroscopy,” *Sensors*, vol. 16, p. 1099, 2016.
- [37] N. Caporaso, M. B. Whitworth, and I. D. Fisk, “Total lipid prediction in single intact cocoa beans by hyperspectral chemical imaging,” *Food Chemistry*, vol. 344, Article ID 128663, 2021.

Research Article

Determination of Vitamin B₁₂ in Milk and Dairy Products by Isotope-Dilution Liquid Chromatography Tandem Mass Spectrometry

Baifen Huang, Jingshun Zhang , Mengli Wang, and Zengxuan Cai 

Zhejiang Provincial Center for Disease Control and Prevention, Hangzhou, China

Correspondence should be addressed to Zengxuan Cai; caizx_cdc@163.com

Received 13 April 2022; Accepted 23 July 2022; Published 12 August 2022

Academic Editor: Ying Hu

Copyright © 2022 Baifen Huang et al. This is an open access article distributed under the Creative Commons Attribution License, which permits unrestricted use, distribution, and reproduction in any medium, provided the original work is properly cited.

An isotope-dilution liquid chromatography tandem mass spectrometry method was established for the determination of vitamin B₁₂ in milk and dairy products. The samples were spiked with stable isotope-labeled vitamin B₁₂ and digested by pepsin and amylase. The various forms of cobalamin were transformed to cyanocobalamin by potassium cyanide after they were released from the enzymatically digested samples. Cyanocobalamin was extracted and purified by an immunoaffinity SPE cartridge and then measured in multiple reaction monitoring mode (MRM). The linear correlation coefficient (R^2) of this method was greater than 0.999 in the range of 2–100 ng/mL. The detection limit and the quantification limit were 0.5 $\mu\text{g}/\text{kg}$ and 1.0 $\mu\text{g}/\text{kg}$, respectively. The spiked recoveries ranged from 92.0% to 99.4% at the three spiked levels with the relative standard deviation (RSD) between 1.89% and 4.51%. The measured results of NIST SRM1849a and NIST SRM1869a by the current method are all within the reference value range. The Z value was 0.8 during participating in the FAPAS proficiency test using the developed method in 2021. The method is simple, rapid, accurate, and sensitive, and it is suitable for the determination of vitamin B₁₂ in different types of milk and dairy products such as whey powder, whole milk powder, pure milk, fermented milk, infant formula, and prescription food for special medical purposes.

1. Introduction

Vitamin B₁₂ (VB₁₂) is also known as cobalamin or cobamide, and it has at least five chemical variants with similar molecular structure [1] (Figure 1). The naturally occurring forms of VB₁₂ in food are hydroxocobalamin, 5'-deoxyadenosylcobalamin, methylcobalamin, sulphitocobalamin, and a small amount of cyanocobalamin. Among them, cyanocobalamin has the most stable chemical structure, and other chemical variants of VB₁₂ are photolabile [2, 3]. The amount of VB₁₂ required by the human body is very small. However, VB₁₂ is an essential nutrient for humans, which plays an important role in the formation of normal red blood cells and the maintenance of the normal function of myelinated nerve cells in the human body. VB₁₂ deficiency can cause anemia, nervous system disorders, and other symptoms [4–6]. The recommended intake for adults is 2 $\mu\text{g}/\text{d}$ and

the adequate intake (AI) for infants at 0–6 months and 6–12 months is 0.6 $\mu\text{g}/\text{d}$ [7]. VB₁₂ cannot be synthesized by humans *de novo* and it must be acquired through dietary intake of animal-based foods rich in VB₁₂ such as milk and dairy products [8]. VB₁₂ is usually presented as a protein-bound form in milk and dairy products, whereas cyanocobalamin is the main form of VB₁₂ used in human dietary supplements. The low content of VB₁₂ in food usually has various photolabile forms, which make it difficult for quantitative detection. It is urgent to establish an effective detection method for the determination of VB₁₂ in various foods including milk and dairy products.

The existing reported methods for determination of VB₁₂ in infant formula mainly include microbiological assays [9, 10], high-performance liquid chromatography (HPLC) [11–19], liquid chromatography-tandem mass spectrometry (LC-MS/MS) [20–26], and liquid chromatography and

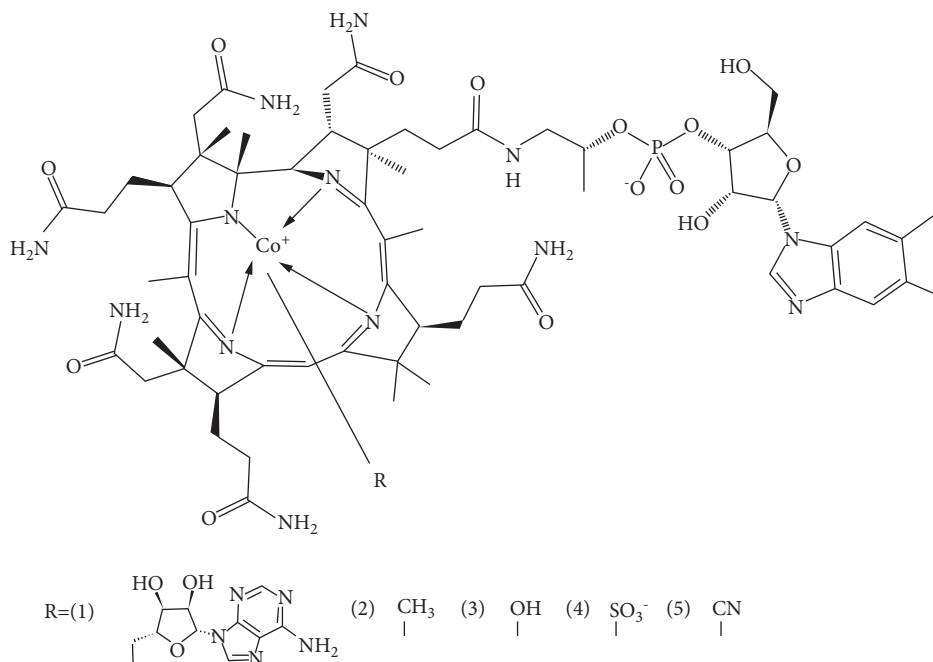


FIGURE 1: Structure of vitamin B₁₂: (1) 5'-deoxyadenosylcobalamin; (2) methylcobalamin; (3) hydroxocobalamin; (4) sulphitocobalamin; (5) cyanocobalamin.

inductively coupled plasma-mass spectrometry (LC-ICP-MS) [27–29]. The microbiological assays usually have a long measurement time and complicated operation. The strains need to be frequently resurrected and stored until analysis. Multiple dilutions need to be prepared to optimize a suitable linear range for the determination of samples with unknown contents. It is difficult for unskilled inspectors to carry out the inspection tests. HPLC methods for determination VB₁₂ usually employ immunoaffinity purification and online solid phase extraction (SPE) followed by column switching techniques. Although HPLC methods have the advantages of simple operation, efficient separation, and high degree of automation, the methods based on UV detectors are not sensitive enough to detect VB₁₂ in non-fortified food. It takes a long time to transform VB₁₂ to fluorescent compounds by derivatization reaction using a fluorescence detector as VB₁₂ itself does not emit fluorescence. In recent years, LC-MS/MS has been used to detect the content of VB₁₂ in food. The trace level VB₁₂ content in food can be detected by LC-MS/MS due to its high selectivity and sensitivity. However, the sample preparation using pepsin and potassium cyanide has not been comprehensively optimized in the existing reports. Based on our research of vitamins [30–32], in this study, an isotope-dilution ultra-performance liquid chromatography tandem mass spectrometry (UPLC-MS/MS) method was established to detect VB₁₂ content in milk and dairy products. This study focused on the effects of pepsin and potassium cyanide solution during sample preparation on the determination results of VB₁₂ in milk and dairy products. The sample preparation procedure, quality control, and chromatographic and mass spectrometry conditions were systematically optimized for the first time. The immunoaffinity SPE cartridge and stable isotope-labeled VB₁₂

were applied for sample pretreatment and MS analysis to ensure high specificity and good accuracy of the developed method. The method has the characteristics of high sensitivity, good repeatability, and high accuracy, and it can be applied and popularized in food testing laboratories.

2. Materials and Methods

2.1. Chemical Reagents. HPLC grades of acetonitrile (ACN), ethanol (EOH), acetic acid, and ammonium acetate were purchased from Fisher Chemical (Canada). Analytical grade sodium acetate and sodium hydroxide were purchased from Shanghai Lingfeng Chemical Reagent Co. Ltd. (China). Ultrapure water was obtained from a Milli-Q water purification system (Millipore, USA). Vitamin B₁₂ (cyanocobalamin, 1.000 ± 0.006 mg/mL) was purchased from SIGMA (USA). [¹³C₇]-vitamin B₁₂ (0.995 ± 0.030 μg/mL) was purchased from Beijing Manhage Biotechnology Co. Ltd. (China). Immunoaffinity SPE cartridge was purchased from R-Biopharm (Germany). Pepsin from porcine gastric mucosa (250 U/mg, 400 U/mg, 600–1800 U/mg, 2500 U/mg) and Takadiastase (100 U/mg) were purchased from SIGMA (USA). Milk and dairy products were purchased from local supermarkets in Hangzhou, China.

2.2. Analytical Instrumentation. The analyte chromatographic separation was performed on an Waters BEH C₁₈ column (10 cm × 2.1 mm i. d.; 1.7 μm), and the mobile phase consisted of water containing 2.5 mmol/L ammonium acetate (A) and water/acetonitrile (10:90 V/V) (B), for a total run time of 7 min and column temperature of 40°C, with a sample injection volume of 2 μL. The chromatographic

TABLE 1: LC/MS/MS parameters.

Compound (m/z)	Precursor ion (m/z)	Daughter ion	Cone voltage (V)	Collision energy (eV)
Vitamin B ₁₂	678.6	147.1*	32	37
		359.2		23
[¹³ C ₇]-vitamin B ₁₂	681.5	153.9*	32	37
		365.8		23

*means qualifier ion.

gradient was operated at a flow rate of 0.4 mL/min starting from 0 min: 2% B; 0–1 min: 2% B; 1–4 min: 2%–90% B; 4–5 min: 90% B; 5–7 min: 2% B.

The mass spectrometer was XEVO TQ-S, a triple quadrupole instrument equipped with an ESI ionization source (Waters Corp.). All analyses were conducted in positive ESI mode using multiple reaction monitoring on the 2 main product ions; the optimized mass spectrometer conditions for both analytes are reported in Table 1. The capillary voltage was 3.0 kV, source temperature was 150°C, and desolvation temperature was 650°C. Nitrogen was used as desolvation gas (1000 L/h) and cone gas (50 L/h), whereas the collision gas was argon (flow rate of 0.25 mL/min). Data acquisition processing was performed using MassLynx 4.1 software (Waters Corp.).

2.3. Preparation of Standard Solutions. Vitamin B₁₂ intermediate standard (20.0 µg/mL) was prepared by diluting 1 mL of vitamin B₁₂ stock standard solution (cyanobalamine, 1.000 ± 0.006 mg/mL) to 50 mL with water. Vitamin B₁₂ working standard (200 ng/mL) was prepared by diluting 1 mL of vitamin B₁₂ intermediate standard (20.0 µg/mL) to 100 mL with water. [¹³C₇]-vitamin B₁₂ working standard (50 ng/mL) was prepared by diluting 2.5 mL of [¹³C₇]-vitamin B₁₂ stock standard solution (0.995 ± 0.030 µg/mL) to 50 mL with water. A set of standard solutions containing vitamin B₁₂ in the concentration range of 2–100 ng/mL was prepared, containing 5 ng/mL of [¹³C₇]-vitamin B₁₂.

2.4. Sample Preparation-Extraction and Purification. Weigh, to the nearest 0.01 g, about 30 g of solid milk and dairy products into a 500 mL flask, dissolve the sample in 180 g of warm water (40°C to 45°C) and mix until homogeneous. The liquid milk can be weighed directly after shaking. Reconstituted milk or liquid milk was accurately weighed into a 50 mL centrifuge tube to withstand high temperatures of 100°C. 100 µL of [¹³C₇]-vitamin B₁₂ working standard solution (50 ng/mL), 25 mL of sodium acetate solution, 10 mg of Takadiastase, and 1 mL of potassium cyanide (1%) were added, respectively, under agitation and the solution was incubated at 37°C for 30 min in thermostatic oscillator. The hydrolysates were transferred to a water bath at 100°C for 30 min. Cooling down to room temperature, the solution was shaken fully and centrifuged at 8000 r/min for 10 min. The supernatant was filtered through a 1.6 µm glass fiber filter paper before purification.

All filtrate was loaded onto an immunoaffinity column, using a suitable glass adapter. The column was washed with 10 mL of water and then completely dried by passing

through at least 10 mL of air. Vitamin B₁₂ was eluted into a 10 mL glass tube with 1 mL of methanol for 3 times by complete denaturation of the antibody. The eluate was concentrated to dryness at 60°C under slow nitrogen gas flow and reconstituted in 1 mL of mobile phase and filtered through a 0.22 µm membrane filter before HPLC analysis.

3. Results and Discussion

3.1. Optimization of the MS/MS Conditions. Structural information to confirm the identity of analytes and the optimization of the instrumental sensitivity were obtained by performing a preliminary fragmentation study and MS/MS experiments. Full scans under the positive ESI mode for vitamin B₁₂ and [¹³C₇]-vitamin B₁₂ were acquired for the selection of the precursor ions according to the relative intensities of multiple charged ions. [M + 2H]²⁺ at m/z 678.1 and 681.8 were the precursor ions selected for vitamin B₁₂ and [¹³C₇]-vitamin B₁₂ as it gave the most intense peak in the mass spectrum. Product ion scan mass spectra are shown in Figure 2. Collision-induced dissociation (CID) of vitamin B₁₂ produced two product ions at m/z 147 and 359, and [¹³C₇]-vitamin B₁₂ produced two product ions at m/z 154 and 366, also shown by the fragmentation pattern in Figure 2. For each analyte, two among all available MRM transitions were chosen on the basis of the best chromatographic signal-to-noise (S/N) ratio, to perform quantitative and confirmative analysis on the selected food matrices.

3.2. Optimization of the LC Separation Conditions. Acetonitrile was selected as an organic modifier for its chromatographic selectivity, and ammonium acetate was added to the mobile phase, it could provide the best ionization conditions. The best compromise in terms of sensitivity and analyte separation was afforded by the 2.5 mmol/L concentration of ammonium acetate as mobile phase A and water/acetonitrile (10:90 V/V) as mobile phase B.

3.3. Optimization of Extraction Solvent. Vitamin B₁₂ can dissolve in strong polar solvents, such as water, methanol, and ethanol, but not in organic solvents with medium polarity, such as acetone, chloroform, and ether. Thus, strong polar solvent was suitable for extraction in the sample process. There are other kinds of naturally occurring cobalamin in infant formula, prepared milk powder, and instant grain food including fortified cyanocobalamin. These cobalamins coordinated with the protein to form stable large molecular compounds. The cobalamin must dissociate from

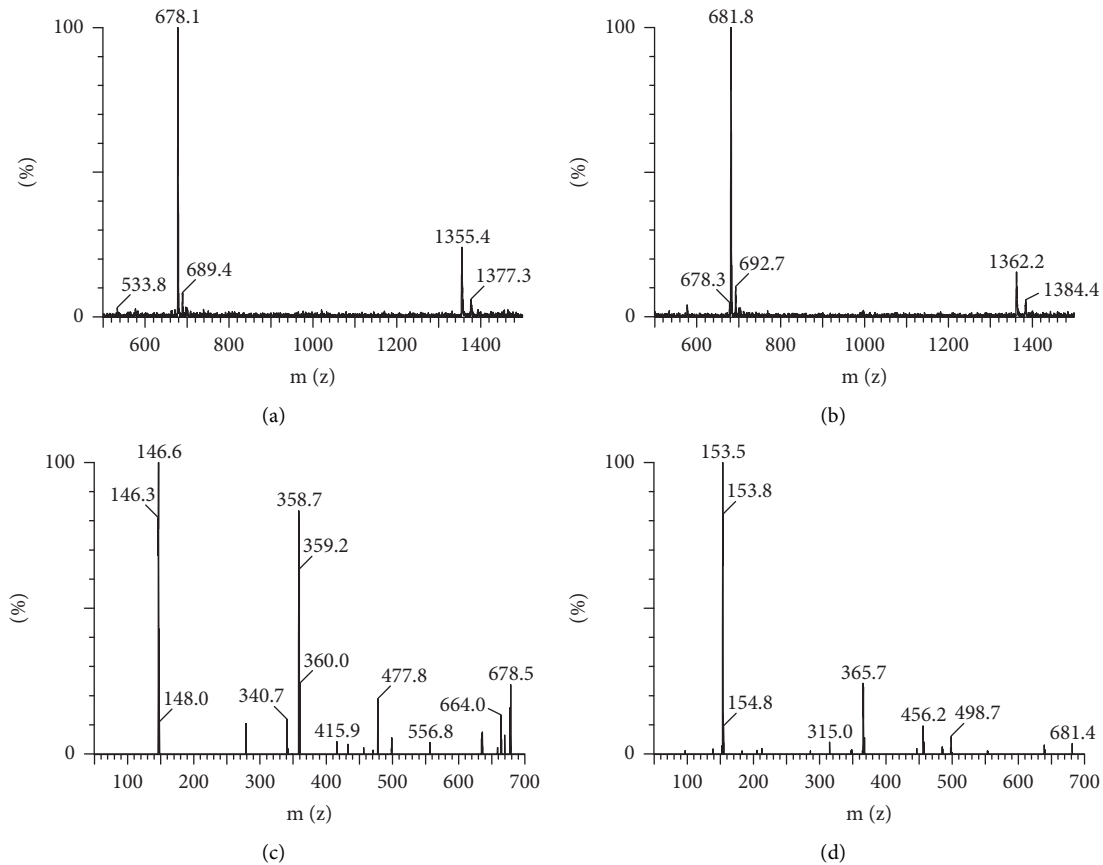


FIGURE 2: Mass spectrum of full scan and daughter scan of VB₁₂ and isotope-labeled VB₁₂. (a) MS scan of VB₁₂ (b) Full MS scan of ¹³C₇-VB₁₂ (c) Daughter scan of VB₁₂ (d) Daughter scan of ¹³C₇-VB₁₂.

TABLE 2: Comparison of results by adding potassium cyanide or not.

Samples	Adding potassium cyanide		Not adding potassium cyanide		<i>t</i> -Test <i>P</i> value
	Value (μg/kg)	SD (μg/kg)	Value (μg/kg)	SD (μg/kg)	
FAPAS-1	19.90	2.13	8.75	0.65	<0.05
FAPAS-2	16.49	3.12	9.97	0.48	<0.05
NIST SRM 1849a	47.17	4.06	42.12	0.51	0.814 > 0.05
Infant formula-1	39.88	2.76	10.09	1.4	<0.05
Infant formula-2	32.76	0.57	23.08	0.94	<0.05
Non-fat milk powder	28.82	2.79	5.54	0.38	<0.05
Demineralized whey	23.81	2.06	15.83	0.6	<0.05
Whole milk powder	16.73	1.81	3.23	0.17	<0.05
Pure milk	4.44	0.53	1.14	0.23	<0.05

combined compounds and transform into cyanobalamin prior to determination, and the reaction was proceeded in the condition of aqueous solution. Enzymatic hydrolysis of diastase can also react in aqueous solution. Therefore, water was chosen as the extraction solvent.

3.4. Necessity of Potassium Cyanide. There are many speciations of vitamin B₁₂ with physiological activity, such as cyanocobalamin, aquacobalamin, adenosylcobalamin, and mecobalamin in natural food. Cyanocobalamin was the most stable speciation among them, and other

speciation of vitamin B₁₂ must be transformed into cyanobalamin prior to determination. In this study, measured results of 9 milk and dairy products were compared by adding potassium cyanide or not. As shown in Table 2, there was a significant difference between the two groups, most of the *p* values were less than 0.05, excepting sample of NIST SRM 1849a, which was 0.814. The measured values adding potassium cyanide are 1.1–14.9 times more than the results without potassium cyanide. Measured values would significantly lower if potassium cyanide was not used in the determination of vitamin B₁₂ in milk and dairy products and would cause determination deviation.

3.5. Optimization of Enzymatic Hydrolysis Conditions.

Pepsin is often used coupled with diastase in the determination of vitamin B₁₂ [11–14]; in the meanwhile, there are background values of vitamin B₁₂ in pepsin. To further evaluate the influence of background value, several pepsins were purchased with different activities of 250 U/mg, 400 U/mg, 600 U/mg, and 2500 U/mg, respectively. The concentration of vitamin B₁₂ was determined following the optimization method in 1 g sample with 0.2 g pepsin and 0.05 g diastase added. As shown in Figure 3, the background value of vitamin B₁₂ in pepsin increased with the activity of pepsin. The background value of vitamin B₁₂ in pepsin cannot be neglected.

3.6. Choice of Internal Standard. In most cases, the concentrations of vitamin B₁₂ are not very high in foods, although it widely exists in dairy products. It is necessary to purify and concentrate in the determination to achieve ideal detection sensitivity. Two studies [21, 22] reviewed vitamin B₁₂ loss during cooking treatment with contradictory results. The absolute recovery of immunoaffinity SPE cartridge for vitamin B₁₂ is not very well; meanwhile, quality differences between batches would influence the accuracy of determination. Luo [24] developed an analytical method for the determination of vitamin B₁₂ in food products and multivitamin multimineral tablets by HPLC-ESI-MS, and ginsenoside Re was used as an internal standard (I.S.). Ginsenoside Re is not a perfect internal standard of vitamin B₁₂ for the obvious contrast between the molecular structure of ginsenoside Re and vitamin B₁₂. In this study, to achieve the purpose of accurate quantification, [¹³C₇]-vitamin B₁₂ isotope-labeled vitamin B₁₂ was used as an internal standard in the whole analysis.

3.7. Matrix Effect. Liquid chromatography coupled with tandem mass spectrometry (LC-MS/MS) has become a “gold standard” in many fields of analytical chemistry. One of the most common interference types in the case of LC-MS/MS analyses is the alteration of ionization efficiency (usually ionization suppression) due to co-eluting compounds, called matrix effect (ME). Matrix effect results in differing analyte peak areas while comparing the sample and standard with the same analyte concentration. There are many fats, proteins, and sugars naturally present in milk, which would produce interfering substances after enzymatic hydrolysis and heating process. These interfering substances would cause certain matrix effects in the LC-MS/MS analyses if purification process was less efficient. In common, matrix effect was calculated as a ratio of the slope of the matrix matching the standard curve and the slope of the solvent standard curve. There is no obvious matrix effect if the ratio is between 85% and 115%. It is difficult to find a blank matrix of vitamin B₁₂ for vitamin B₁₂ is widespread in milk and dairy products, so the isotope of vitamin B₁₂ was used to evaluate the matrix effect of infant formula, non-fat milk powder, fermented milk, and cheese samples instead of

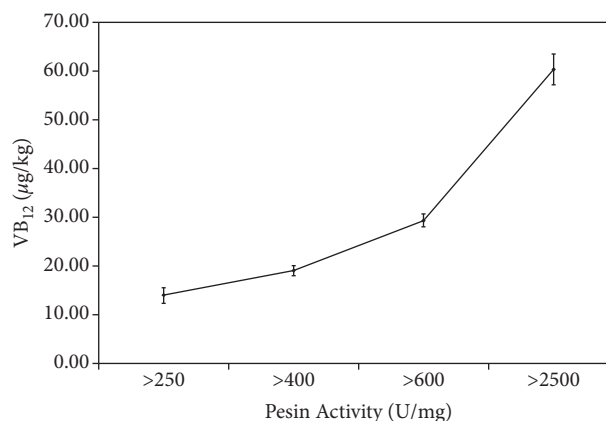


FIGURE 3: Relationship of background value of vitamin B₁₂ and pepsin activity.

vitamin B₁₂ in this study. The matrix effect (ME%) can be quantitatively expressed by (1), where A_{matrix} and A_{standard} are the peak areas of the equal amount of [¹³C₇]-vitamin B₁₂, respectively, in presence and in the absence of possibly interfering compounds.

$$\text{ME\%} = \frac{A_{\text{matrix}}}{A_{\text{standard}}} \times 100\%. \quad (1)$$

This technique is also called post-extraction spiking; the analytical signal of a blank sample extract spiked with [¹³C₇]-vitamin B₁₂ (A_{matrix}) is compared with the signal of the equal amount of [¹³C₇]-vitamin B₁₂ in pure solvent (A_{standard}).

ME% ($n=6$) of infant formula, non-fat milk powder, fermented milk, and cheese was $99.51\% \pm 1.71$, $102.51\% \pm 6.12$, $102.15\% \pm 4.65$, and $102.18\% \pm 1.66$, respectively. The results have shown that the purification effect of immunoaffinity SPE cartridge was efficient, and the interfering substance almost can be removed after purification treatment with immunoaffinity SPE cartridge.

3.8. Method Validation. The standard series solutions with the concentration of 2, 5, 10, 25, 50, and 100 ng/mL were prepared, and the standard curves were drawn according to the corresponding peak areas. The correlation coefficients were all greater than 0.999, and the standard curves had good linearity. The limit of quantitation (LOQ) and the limit of detection (LOD) were investigated according to 10 times and 3 times of signal-to-noise ratio, respectively. When 1 g of infant formula was taken for determination, the limit of quantitation and the limit of detection were 1.0 µg/kg and 0.5 µg/kg, respectively.

The whole milk powder (the background value was $16.7 \mu\text{g/kg} \pm 1.8 \mu\text{g/kg}$) was selected as the sample. Each standard addition concentration was determined 6 times in parallel. The recoveries of vitamin B₁₂ were 92.0%~99.4%. The RSD of six repeated determination was 3.03%~5.76%.

For further confirmation of the accuracy of the established method, two standard reference materials (SRMs),

TABLE 3: Results of vitamin B₁₂ in NIST SRM1849a and NIST SRM1869 (*n* = 6).

SRM	Measured value ($\mu\text{g}/\text{kg}$)	RSD%	Reference value ($\mu\text{g}/\text{kg}$)
NIST SRM1849a	47.2	4.82	48.2 \pm 8.5
NIST SRM1869	44.8	4.69	43.5 \pm 6.5

NIST SRM1849a and NIST SRM1869 infant formula, were selected as verified objects. The results are shown in Table 3.

The present method was also applied to determine vitamin B₁₂ in the infant formula of FAPAS Proficiency Test in 2021. The measured value was 19.9 \pm 1.0 $\mu\text{g}/\text{kg}$, and *Z* value was 0.8, and the result is satisfied.

4. Concluding Remarks

An isotope-dilution liquid chromatography tandem mass spectrometry method was established for the determination of vitamin B₁₂ in milk and dairy products. The sample preparation procedure using pepsin and potassium cyanide, quality control, and chromatographic and mass spectrometry conditions were systematically optimized for the first time. The various forms of cobalamin were transformed to cyanocobalamin by potassium cyanide after they were released from the enzymatically digested samples. Cyanocobalamin was extracted and purified by immunoaffinity SPE cartridge before UPLC-MS/MS. The measured results of NIST SRM1849a and NIST SRM1869a by the current method are all within the reference value range. The *Z* value was 0.8 during participating in the FAPAS proficiency test using the developed method in 2021. All validation results showed that the method is simple, accurate, and sensitive, and it is suitable for the determination of vitamin B₁₂ in different types of milk and dairy products.

Data Availability

The data used to support the findings of this study are included within the article.

Conflicts of Interest

The authors declare that they have no conflicts of interest.

References

- [1] F. Watanabe and T. Bito, "Determination of cobalamin and related compounds in foods," *Journal of AOAC International*, vol. 101, no. 5, pp. 1308–1313, 2018.
- [2] T. Bito and F. Watanabe, "Biochemistry, function, and deficiency of vitamin B₁₂ in *Caenorhabditis elegans*," *Experimental Biology and Medicine*, vol. 241, no. 15, pp. 1663–1668, 2016.
- [3] S. S. Kumar, R. S. Chouhan, and M. S. Thakur, "Trends in analysis of vitamin B₁₂," *Analytical Biochemistry*, vol. 398, no. 2, pp. 139–149, 2010.
- [4] F. O'Leary and S. Samman, "Vitamin B₁₂ in health and disease," *Nutrients*, vol. 2, no. 3, pp. 299–316, 2010.
- [5] Z. Schneider and A. Stroinski, *Comprehensive B₁₂: Chemistry, Biochemistry, Nutrition, Ecology, Medicine*, De Gruyter, Berlin, Germany, 1987.
- [6] I. Ortigues-Marty, D. Micol, S. Prache, D. Dozias, and C. L. Girard, "Nutritional value of meat: the influence of nutrition and physical activity on vitamin B₁₂ concentrations in ruminant tissues," *Reproduction, Nutrition, Development*, vol. 45, no. 4, pp. 453–467, 2005.
- [7] C. Nutrition Society, *Chinese Dietary Reference Intakes*, Science Press, Beijing, China, 2013.
- [8] E. M. Brouwer-Brolsma, R. A. M. Dhonukshe-Rutten, J. P. Van Wijngaarden, N. Zwaluw, N. Velde, and L. de Groot, "Dietary sources of vitamin B-12 and their association with vitamin B-12 status markers in healthy older adults in the B-PROOF study," *Nutrients*, vol. 7, no. 9, pp. 7781–7797, 2015.
- [9] L. H. Zhang, K. X. Wang, and M. Wang, "Application and discussion of microbiological method for assay of vitamin B₁₂ in milk powder," *China Dairy Industry*, vol. 36, no. 10, pp. 58–60, 2008.
- [10] M. Berth, C. Bonroy, K. Guerti, W. Uyttenbroeck, and M. Uytterhoeven, "Comparison of five commercially available ELISA kits for the determination of intrinsic factor antibodies in a vitamin B12 deficient adult population," *The International Journal of Literary Humanities*, vol. 38, no. 1, pp. e12–e14, 2016.
- [11] D. Y. Fan, Y. Z. Zhang, and H. P. Wu, "Development of a simple and sensitive HPLC-DAD method for quantification of vitamin B12 fortified in infant food," *Analytical Methods*, vol. 13, no. 41, pp. 4920–4925, 2021.
- [12] E. C. Marley, E. Mackay, and G. Young, "Characterisation of vitamin B12 immunoaffinity columns and method development for determination of vitamin B12 in a range of foods, juices and pharmaceutical products using immunoaffinity clean-up and high performance liquid chromatography with UV detection," *Food Additives & Contaminants: Part A*, vol. 26, no. 3, pp. 282–288, 2009.
- [13] K. Schimpf, R. Spiegel, L. Thompson, and D. Dowell, "Determination of vitamin B₁₂ in infant formula and adult nutritional by HPLC: first Action 2011.10," *Journal of AOAC International*, vol. 95, no. 2, pp. 313–318, 2012.
- [14] X. Qiu, H. S. Zhang, Y. H. Yin et al., "Determination of active vitamin B12 (cobalamin) in dietary supplements and ingredients by reversed-phase liquid chromatography: single-laboratory validation," *Food Chemistry*, vol. 298, Article ID 125010, 2019.
- [15] B. Nshime, J. Koedam, B. Stanton, Q. Tran, and P. Chen, "Liquid chromatography method for the simultaneous quantification of biotin and vitamin B12 in vitamin B supplements," *Journal of AOAC International*, vol. 102, no. 2, pp. 445–450, 2019.
- [16] International Organization for Standardization, *ISO 20634: 2015(E) Infant formula and adult nutritional-Determination of vitamin B12 by reversed phase high performance liquid chromatography*, Vernier, Geneva, Switzerland, 2015.
- [17] L. D. Butler-Thompson, W. A. Jacobs, K. J. Schimpf et al., "Determination of Vitamin B₁₂ in infant, adult, and pediatric formulas by HPLC-UV and column switching: collaborative study, final action 2011.10," *Journal of AOAC International*, vol. 98, no. 6, pp. 1655–1665, 2015.

- [18] A. S. Fayed, M. A. M. Hegazy, and N. S. A. Wahab, "Chromatographic analysis of a multicomponent mixture of B1, B6, B12, benfotiamine, and diclofenac; Part I: HPLC and UPLC methods for the simultaneous quantification of these five components in tablets and capsules," *Journal of AOAC International*, vol. 99, no. 6, pp. 1513–1521, 2016.
- [19] W. J. Lee, Y. B. Lee, M. H. Huh, and J. K. Choi, "Determination of the chemical stability of cyanocobalamin in medical food by a validated immunoaffinity column-linked HPLC method," *Journal of Food Quality*, vol. 2022, Article ID 1619936, 8 page, 2022.
- [20] A. Repossi, E. Zironi, T. Gazzotti, A. Serraino, and G. Pagliuca, "Vitamin B12 determination in milk, whey and different by-products of ricotta cheese production by ultra performance liquid chromatography coupled with tandem mass spectrometry," *Italian Journal of Food Safety*, vol. 6, no. 4, pp. 6795–7155, 2017.
- [21] M. L. Wang, S. Asam, J. Q. Chen, and M. Rychlik, "Development of stable isotope dilution assays for the analysis of natural forms of vitamin B12 in meat," *Journal of Agricultural and Food Chemistry*, vol. 69, no. 36, pp. 10722–10730, 2021.
- [22] E. Zironi, T. Gazzotti, A. Barbarossa, C. Devicienti, M. Scardilli, and G. Pagliuca, "Technical note: development and validation of a method using ultra performance liquid chromatography coupled with tandem mass spectrometry for determination of vitamin B₁₂ concentrations in milk and dairy products," *Journal of Dairy Science*, vol. 96, no. 5, pp. 2832–2836, 2013.
- [23] E. Zironi, T. Gazzotti, A. Barbarossa, F. Farabegoli, A. Serraino, and G. Pagliuca, "Determination of vitamin B₁₂ in dairy products by ultra performance liquid chromatography-tandem mass spectrometry," *Italian Journal of Food Safety*, vol. 3, no. 4, pp. 4513–5255, 2014.
- [24] J. H. Lee, J. H. Shin, J. M. Park et al., "Analytical determination of vitamin B₁₂ content in infant and toddler milk formulas by liquid chromatography tandem mass spectrometry (LC-MS/MS)," *Korean Journal for Food Science of Animal Resources*, vol. 35, no. 6, pp. 765–771, 2015.
- [25] J. Li, W. J. Lin, and Q. W. Cao, "Determination of total vitamin B₁₂ in milk powder by ultra-performance liquid chromatography-tandem mass spectrometry after purification on an immunoaffinity cartridge," *Acta Nutrimenta Sinica*, vol. 42, no. 1, pp. 72–77, 2020.
- [26] L. D'Ulivo, L. Yang, J. F. Ding et al., "Determination of cyanocobalamin by isotope dilution LC-MS/MS," *Analytica Chimica Acta*, vol. 990, pp. 103–109, 2017.
- [27] S. Dubascoux, J. Richoz Payot, P. Sylvain, M. Nicolas, and E. Campos Gimenez, "Vitamin B12 quantification in human milk-Beyond current limitations using liquid chromatography and inductively coupled plasma-Mass spectrometry," *Food Chemistry*, vol. 362, Article ID 130197, 2021.
- [28] A. Knoop, P. Planitz, B. Wust, and M. Thevis, "Analysis of cobalt for human sports drug testing purposes using ICP-and LC-ICP-MS," *Drug Testing and Analysis*, vol. 12, no. 11-12, pp. 1666–1672, 2020.
- [29] R. Wenzel, D. Major, and K. Harly, "Determination of vitamin B₁₂ in equine urine by liquid chromatography-inductively coupled-plasma mass spectrometry," *Journal of Trace Elements in Medicine & Biology*, vol. 50, pp. 634–639, 2018.
- [30] B. F. Huang, X. D. Pan, J. S. Zhang, J. J. Xu, and Z. X. Cai, "Determination of vitamins D₂ and D₃ in edible fungus by reversed-phase two-dimensional liquid chromatography," *Journal of Food Quality*, vol. 2020, Article ID 8869279, 6 page, 2020.
- [31] B. F. Huang, Z. X. Cai, J. S. Zhang, and J. Xu, "An efficient solid-phase extraction-based liquid chromatography method to simultaneously determine diastereomers α -tocopherol, other tocots, and retinol isomers in infant formula," *Journal of Food Quality*, vol. 2021, pp. 1–8, Article ID 5591620, 2021.
- [32] B. Y. Lu, Y. P. Ren, B. F. Huang, W. Liao, Z. Cai, and X. Tie, "Simultaneous determination of four water-soluble vitamins in fortified infant foods by ultra-performance liquid chromatography coupled with triple quadrupole mass spectrometry," *Journal of Chromatographic Science*, vol. 46, no. 3, pp. 225–232, 2008.

Research Article

Determination of Mycotoxins and Veterinary Medicines in Duck Flesh and Viscera and Assessment of Their Exposure

Yi Zheng ¹, Yuxin Wu,¹ Huanxin Zhang,¹ Xiaolan Chen ¹, Zaixiang Lou ²,
Huijuan Jing,² and Chunpeng (Craig) Wan ³

¹Jiangsu Provincial Key Laboratory of Veterinary Bio-pharmaceutical High Tech Research,
Jiangsu Agri-animal Husbandry Vocational College, Taizhou 225300, China

²State Key Laboratory of Food Science and Technology, School of Food Science and Technology, Jiangnan University,
Wuxi 214122, China

³Jiangxi Key Laboratory for Postharvest Technology and Nondestructive Testing of Fruits and Vegetables, College of Agronomy,
Jiangxi Agricultural University, Nanchang 330045, China

Correspondence should be addressed to Zaixiang Lou; louzaixiang@126.com and Chunpeng (Craig) Wan;
chunpengwan@jxau.edu.cn

Received 22 April 2022; Revised 13 June 2022; Accepted 30 June 2022; Published 8 August 2022

Academic Editor: Yong-Jie Yu

Copyright © 2022 Yi Zheng et al. This is an open access article distributed under the Creative Commons Attribution License, which permits unrestricted use, distribution, and reproduction in any medium, provided the original work is properly cited.

Mycotoxins can accumulate in various feeds and thus may get in duck meat, which may have severe food safety and public health implications. This study examined mycotoxins and veterinary medications in duck meat marketed in eight marketplaces around China. For the determination of mycotoxins, including the mycotoxins aflatoxin B1 (AFB1), aflatoxin B2 (AFB2), aflatoxin M1 (AFM1), T-2 toxin, zearalenone (ZEN), and ochratoxin A (OTA), a liquid-chromatography tandem mass spectrometry (LC-MS/MS) method was validated. Overall, 13 out of 48 samples (27%) presented AFB1, and AFB2 was present in 14 out of 48 samples with positive levels ranging from 0.5 µg/kg (gizzard) to 4.1 µg/kg (lung). Eleven samples were contaminated with AFM1. T-2 was also found in three parts of duck samples (duck gizzard, neck, and lung), and the 5th and 48th samples were contaminated with T-2. ZEN was found in 5 of 48 analyzed samples (10%), and OTA was present in 21 out of 48 samples. The maximum kinds of mycotoxins found simultaneously in duck samples were six in duck lungs. High co-occurrence of mycotoxins was verified in several samples. The detection rate of various veterinary drugs was 0–12.5% in duck meat samples, and the over standard rate was 2.1%. Co-occurrence of veterinary drugs was verified in several samples.

1. Introduction

Mycotoxins are, in general, stable molecules, which are challenging to remove from foods once they have been produced [1, 2]. Aflatoxins, metabolites of *Aspergillus flavus* and *Aspergillus parasiticus*, are highly toxic substances [3, 4]. Its harmfulness lies in its damaging effect on human and animal liver tissues, and it can cause liver cancer or even death in severe cases [5, 6]. They are present in soil and plants and various nuts, especially grain and oil products such as peanuts, corn, rice, soybeans, and wheat. [7–10]. Ochratoxin A (OTA) is another mycotoxin [7], and it mainly contaminates agricultural grain products such as oats,

barley, wheat, corn, feed, and animal food (such as pig kidney and liver) [10, 11]. A variety of other mycotoxins (including various aflatoxins, deoxynivalenol, and zearalenone) also may contaminate foods [12–14].

Ducks are one of the most sensitive animals to mycotoxin contamination. In recent years, the global production amount of duck meat and duck eggs has been increasing year by year, so it is necessary to study the harmful effects of mycotoxins on ducks, especially ducklings [15]. The feed contaminated with multiple mycotoxins is particularly harmful to ducks [16]. Certain mycotoxins frequently cause harm to the muscle, stomach, and intestines of broilers, while such damage is uncommon in meat ducks. The

immune system, liver, and heart are the essential target organs of mycotoxin in ducks. After ducks eat mouldy feed, mycotoxins may damage the liver and kidneys of the animals. These mycotoxins may remain in the liver, lungs, heart, and other parts of animals [17]. Therefore, this study aims to investigate the residual mycotoxins in various tissues and organs of ducks purchased from the market, providing a reference for the occurrence of mycotoxins in various tissues of duck meat.

Veterinary drugs play an essential role in ensuring animal health and improving the quality of animal products, but they also have many adverse effects, such as the problem of veterinary drug residues in animal products. Although the maximum limits of veterinary drug residues in food and the management regulations for veterinary drugs have been issued successively, the abuse of veterinary drugs is still severe. Therefore, we studied the veterinary drug residues in duck meat samples.

2. Materials and Methods

2.1. Reagents and Standard Solutions. The standards of aflatoxin-B1 (AFB1), aflatoxin-B2 (AFB2), aflatoxin-M1 (AFM1), T-2 toxin (T-2), ochratoxin A (OTA), and zearalenone (ZEN) all with purity >98% were purchased from Yuanye (Yuanye, Shanghai, China). EURO-DIAG-NOSTICA and BIOO SCIENTIFIC CO provided the enzyme-linked immunosorbent assay kits. The standard veterinary medicines were all purchased from Dr. Ehrenstorfer (Augsburg, Germany). Each mycotoxin's standard stock solution at 10 mg/L was prepared in MeOH. From this, a mix of working solutions at 100 µg/L each was prepared in MeOH. All solutions and standards were stored at -18°C.

2.2. Sampling. Forty-eight duck meat samples were purchased from 8 different local markets in Taizhou. The samples were vacuum-packed (portions of 50 g) and stored at -18°C until the analysis.

2.3. Mycotoxin Analysis. Instrument and analytical conditions: The assays were performed using a Waters HPLC (Waters, Milford) with a QqQ mass spectrometer (Waters, Manchester, U.K.). A C18 column (150 × 4.6 mm) maintained at 30°C was used for analytical separation. The method was similar to those previously applied in food by Peromingo et. al [18]. The mobile phase A was water/acetic acid 99:1 (v/v). The mobile phase B was methanol/acetic acid 99:1 (v/v). The solvent gradient in volume ratios was as follows: 0–0.5 min, 95% A; 0.5–7 min, 95% A-35% A; 7–11 min, 35% A-25% A; 11–13 min, 25% A-0% A; 13–20 min, 0% A. The flow rate was 0.8 mL/min.

Mass spectrometry conditions were as follows: positive ion scanning, the capillary voltage of 3.0 KV; cone hole gas flow rate of 50 L/h; ion source temperature of 100°C; the dissolvent temperature of 400°C; collision energy of 20 eV; and dissolvent gas flow rate of 700 L/h.

Sample preparation: The extraction of mycotoxins in meat samples was performed according to the method

optimized by Zou et al. [19] and Sulyok et al. [4]. Firstly, all samples were thawed. Briefly, 20 mL extraction solvent acetonitrile/water/acetic acid (79/20/1, v/v/v) were added with 2 g of each sample and the samples were extracted for 90 min at room temperature (200 rpm). After extraction, it was centrifuged. The supernatant was taken, and then the same volume of the same solvent was added and diluted to half of the original concentration. Five microliter was used for LC-MS/MS analysis.

2.4. Method Validation and Quality Control. The chromatographic peak area of mycotoxins was taken as the ordinate (Y), the corresponding content was taken as the abscissa (X), and a linear regression equation was obtained as a standard curve [20]. The limit of detection (LOD) and the limit of quantification (LOQ) of each mycotoxin was taken as the corresponding concentrations when the signal-to-noise ratio was 3 (signal-to-noise ratio = 3), and the signal-to-noise ratio was 10, respectively. Precision for inter- and intraday was expressed as relative standard deviation (% RSD). These parameters were determined by analysis of triplicate spiked samples on the same day (intraday) and three subsequent days (interday) at three concentration levels: 5 µg/kg, 40 µg/kg, and 100 µg/kg for mycotoxins (AFB1, AFB2, AFM1, OTA, ZEN, and T-2).

2.5. Veterinary Drug Analysis. The veterinary drugs in the samples were extracted according to the recommended method of each kit. Then, each veterinary drug in samples was determined according to the recommended procedure of the respective kit.

2.6. Statistical Analyses. Calibration curves were submitted to regression analysis by the least square method and analysis of variance (ANOVA), where the lack of fit was assessed. It was found that all curves were statistically significant ($p < 0.05$), and no lack of fit was found ($p < 0.05$). All statistical analyses were performed in Statistica 10.0 (StatSoft®).

3. Results and Discussion

3.1. Method Validation for the Determination of Mycotoxins. As shown in Table 1, good linearity was observed for six mycotoxins, with determination coefficients (R^2) higher than 0.979. LODs ranged from 0.01 to 0.02 µg/kg. LOQs ranged from 0.1 to 0.2 µg/kg. The results here obtained are similar to several other chromatographic methods reported in a literature review conducted by Zhang [21]. For multi-mycotoxin analysis, it is difficult to obtain identical optimization conditions because of the differences in physico-chemical properties of these mycotoxins.

The percentage of recovery (%) was higher than 87% (Table 2). The relative standard deviation (% RSD) values for interday and intraday precision were lower than 11%. The results obtained are within the control limits recommended by Chinese Regulation (GB 5009.22–2016).

TABLE 1: Performance parameters: limit of detection (LOD), linear range, and coefficient of determination (R^2) obtained with developed LC-MS/MS method.

Mycotoxin	LOD ($\mu\text{g}/\text{kg}$)	Linear range ($\mu\text{g}/\text{kg}$)	Linearity (R^2)
AFB1	0.01	0.1–100	0.998
AFB2	0.01	0.1–100	0.997
AFM1	0.01	0.1–100	0.983
T-2	0.01	0.1–100	0.979
OTA	0.02	0.2–100	0.989
ZEN	0.01	0.1–200	0.996

TABLE 2: Results for the recovery and precision arising from the validation of the analytical method.

Analyte	Medium			High			Low		
	Recovery (%) ($n=6$)	Intraday precision (%) ($n=6$)	Interday precision (%) ($n=6$)	Recovery (%) ($n=6$)	Intraday precision (%) ($n=6$)	Interday precision (%) ($n=6$)	Recovery (%) ($n=6$)	Intraday precision (%) ($n=6$)	Interday precision (%) ($n=6$)
AFB1	91.3	5.82	6.38	105.9	8.90	7.83	95.6	3.61	8.91
AFB2	87.2	8.61	9.60	103.8	6.37	8.67	90.8	5.87	7.34
AFM1	103.7	7.31	6.83	93.7	6.96	9.18	87.3	9.18	9.66
T-2	87.6	5.86	10.61	92.6	7.82	9.60	87.5	10.60	5.87
OTA	90.5	7.90	9.61	89.1	9.10	8.17	91.3	9.24	8.20
ZEN	106.9	9.66	7.90	88.6	7.91	6.15	106.1	9.61	8.93

Levels used for precisions and recovery assays were level 1 = 5 $\mu\text{g}/\text{kg}$, level 2 = 40 $\mu\text{g}/\text{kg}$, and level 3 = 100 $\mu\text{g}/\text{kg}$ for AFB1, AFB2, AFM1, OTA, T-2, and ZEN.

3.2. *Mycotoxins in Real Samples.* Overall, 13 out of 48 samples (27%) presented AFB1, as shown in Table 3. The duck heart is the part where AFB1 appears most, and 50% of heart samples contained AFB1, followed by the neck and lung. AFB1 was not detected (<LOD) in any sample. Thirteen samples were contaminated with AFB1 with levels ranging from 0.1 to 1.3 $\mu\text{g}/\text{kg}$.

Among the emerging mycotoxins studied, AFB2 was one of the most usual mycotoxins, present in 15 out of 48 samples with positive levels ranging from 0.5 $\mu\text{g}/\text{kg}$ (gizzard) to 4.1 $\mu\text{g}/\text{kg}$ (lung). AFB2 was present in five parts of duck samples, from which the duck neck showed the highest level, followed by the duck heart (Table 4). For duck leg samples, AFB2 was not detected in any sample. Duck lung is the part where AFB2 appears most, present in 63% of samples.

AFM1 was also found in six parts of duck samples (Duck gizzard, breast, neck, heart, leg, and lung). Overall, 11 samples were contaminated with AFM1 (Table 5). The positive samples contaminated with AFM1 ranged from 0.1 to 4.0 $\mu\text{g}/\text{kg}$. Several positive samples showed total AFM1 higher than those laid down for milk and other products by the Chinese State standard (0.5 $\mu\text{g}/\text{kg}$, GB2761-2011). There is a specific correlation between AFM1 and AFB1 because the primary phase biotransformation of AFB1 is AFM1.

Not detected. T-2 was also found in three parts of duck samples (Duck gizzard, neck, and lung), with levels ranging from 0.2 to 1.1 $\mu\text{g}/\text{kg}$ (Table 6). Overall, five samples were contaminated with T-2. Duck lung is the part where T-2 appears most, present in 25% of samples, followed by neck and gizzard. In duck heart, leg, and breast samples, T-2 was not detected in any sample.

Regarding ZEN, it was found in 5 of 48 analyzed samples (10%), with the positive levels ranging from 12.8 to 17.2 $\mu\text{g}/\text{kg}$ (Table 7). ZEN was present in three parts of duck samples, from which, duck lung showed the highest level (17.2 $\mu\text{g}/\text{kg}$),

followed by duck breast and gizzard. For duck neck, heart, and leg samples, ZEN was not detected in any sample. Duck gizzard and breast are the parts where ZEN appears most, present in 25 percent of total samples.

In general, the results obtained for the AFB1 regulated are lower than those reported in the literature: around 7 $\mu\text{g}/\text{kg}$ for AFB1 in fresh and processed meat in Egypt [1]. In another report [22], an analysis of 22 retail products showed one Parma meat with a very high level of OTA contamination (56–158 $\mu\text{g}/\text{kg}$) that exceeded the Italian regulatory limit of 1 $\mu\text{g}/\text{kg}$, and their results were higher than the OTA contents of our study. In some other studies [23, 24], lower contents of mycotoxin were detected in meat samples.

3.3. *Veterinary Drug Residue in Actual Samples.* As shown in Table 9, in the duck meat samples collected, the detection rate of various veterinary drugs was 0–12.5%, and veterinary drug residues were detected in various parts of duck meat and various duck viscera, and the overall detection rate was not high. There was only 1 sample with veterinary drug residue exceeding regulatory limits. Among the 48 samples of duck meat and duck viscera, three veterinary drugs, oxytetracycline, clenbuterol hydrochloride, and streptomycin, were all detected in 4 groups of duck meat or viscera samples, and the detection rates of other veterinary drugs were lower. Five veterinary drugs were detected simultaneously in the Duck gizzard and duck neck samples. Few kinds of veterinary drugs were detected in the duck meat and duck viscera samples from other parts. Chloramphenicol, which the state prohibits from being used in animal food, is detected in the samples. Once detected, it will be judged to exceed the standard. For chloramphenicol residues, the total detection rate was 2.1%.

TABLE 3: Levels of AFB1 in duck meats ($\mu\text{g}/\text{kg}$).

Source of samples	Number of samples	Average ($\mu\text{g}/\text{kg}$)					
		Duck breast	Duck gizzard	Duck neck	Duck heart	Duck leg	Duck lung
Market 1	3	1.3	—	0.5	0.5	—	LOQ
Market 2	3	<LOQ	—	LOQ	—	—	—
Market 3	3	—	—	—	—	0.1	LOQ
Market 4	3	—	—	—	—	—	—
Market 5	3	—	—	LOQ	LOQ	—	—
Market 6	3	—	—	—	0.3	—	—
Market 7	3	—	—	—	LOQ	—	—
Market 8	3	—	—	—	—	—	0.1

Not detected. When the content of mycotoxin found in infusion was < LOQ, it was considered the arithmetic mean between the limit of detection (LOD) and the limit of quantification (LOQ).

TABLE 4: Levels of AFB2 in duck meats ($\mu\text{g}/\text{kg}$).

Source of samples	Number of samples	Average ($\mu\text{g}/\text{kg}$)					
		Duck breast	Duck gizzard	Duck neck	Duck heart	Duck leg	Duck lung
Market 1	3	3.1	0.5	0.5	0.5	—	3.6
Market 2	3	—	—	4.1	3.9	—	3.1
Market 3	3	—	—	—	—	—	3.8
Market 4	3	—	—	1	—	—	—
Market 5	3	—	—	—	0.9	—	—
Market 6	3	—	<LOQ	—	—	—	—
Market 7	3	—	—	—	2	—	1.1
Market 8	3	—	—	—	—	—	<LOQ

Not detected. When the content of mycotoxin found in infusion was < LOQ, it was considered the arithmetic mean between the limit of detection (LOD) and the limit of quantification (LOQ).

TABLE 5: Levels of AFM1 in duck meats ($\mu\text{g}/\text{kg}$).

Source of samples	Number of samples	Average ($\mu\text{g}/\text{kg}$)					
		Duck breast	Duck gizzard	Duck neck	Duck heart	Duck leg	Duck lung
Market 1	3	—	2.3	—	—	—	1.5
Market 2	3	—	—	—	—	—	1.8
Market 3	3	—	—	—	—	2.1	4.0
Market 4	3	—	—	—	0.6	—	—
Market 5	3	—	—	—	0.5	—	—
Market 6	3	—	—	0.3	—	—	—
Market 7	3	—	—	—	—	—	0.1
Market 8	3	—	—	0.4	0.1	—	—

TABLE 6: Levels of T-2 in duck meats ($\mu\text{g}/\text{kg}$).

Source of samples	Number of samples	Average ($\mu\text{g}/\text{kg}$)					
		Duck breast	Duck gizzard	Duck neck	Duck heart	Duck leg	Duck lung
Market 1	3	—	0.2	<LOQ	—	—	—
Market 2	3	—	—	—	—	—	—
Market 3	3	—	—	—	—	—	1.1
Market 4	3	—	—	—	—	—	0.5
Market 5	3	—	—	—	—	—	—
Market 6	3	—	—	—	—	—	—
Market 7	3	—	—	<LOQ	—	—	—
Market 8	3	—	—	—	—	—	—

Not detected. When the content of mycotoxin found in infusion was < LOQ, it was considered the arithmetic mean between the limit of detection (LOD) and the limit of quantification (LOQ).

TABLE 7: Levels of ZEN in duck meats ($\mu\text{g}/\text{kg}$).

Source of samples	Number of samples	Average ($\mu\text{g}/\text{kg}$)					
		Duck breast	Duck gizzard	Duck neck	Duck heart	Duck leg	Duck lung
Market 1	3	—	14.4	—	—	—	0
Market 2	3	—	12.8	—	—	—	—
Market 3	3	—	—	—	—	—	17.2
Market 4	3	16.9	—	—	—	—	—
Market 5	3	13.6	—	—	—	—	—
Market 6	3	—	—	—	—	—	—
Market 7	3	—	—	—	—	—	—
Market 8	3	—	—	—	—	—	—

Not detected. Among the mycotoxins studied, OTA was most often found and was present in 21 out of 48 samples (Table 8), with positive levels ranging from 0.72 $\mu\text{g}/\text{kg}$ (gizzard) to 1.02 $\mu\text{g}/\text{kg}$ (lung). OTA was present in six parts of duck samples, from which duck lung showed the highest level, followed by duck breast, neck, heart, gizzard, and leg. OTA has been detected in all the duck parts studied. Duck gizzard and lung are the part where OTA appears most, present in 63% of samples.

TABLE 8: Levels of OTA in duck meats ($\mu\text{g}/\text{kg}$).

Source of samples	Number of samples	Average ($\mu\text{g}/\text{kg}$)					
		Duck breast	Duck gizzard	Duck neck	Duck heart	Duck leg	Duck lung
Market 1	3	0.96	0.94	0.95	0.95	—	0.93
Market 2	3	0.93	0.94	—	0.92	0.92	0.94
Market 3	3	0.93	—	—	0.94	0.92	1.02
Market 4	3	—	—	—	—	—	0.94
Market 5	3	—	0.93	0.95	—	—	0.92
Market 6	3	—	0.93	—	—	—	—
Market 7	3	0.86	—	—	—	—	—
Market 8	3	—	0.72	—	—	—	—

Not detected. The maximum number of mycotoxins found simultaneously in duck samples was six in duck lung, followed by neck and gizzard with five mycotoxins, and heart and breast with four mycotoxins each. There were three types of mycotoxins detected in duck leg samples, which was the least. Thus, high co-occurrence of mycotoxins was verified in these samples.

TABLE 9: Detection of veterinary drug residues in duck meat and viscera samples.

Duck	Oxytetracycline	Chlortetracycline	Tetracycline	Clenbuterol hydrochloride	Chloramphenicol	Gentamicin	Streptomycin	Furans
Breast	Relevance amount (samples)	0	0	1	0	0	0	1
	Over standard rate (%)	0	0	0	0	0	0	0
Gizzard	Relevance amount (samples)	1	0	1	1	0	1	1
	Over standard rate (%)	0	0	0	0	0	0	0
Neck	Relevance amount (samples)	0	1	1	1	1	0	1
	Over standard rate (%)	0	0	0	0	12.5	0	0
Heart	Relevance amount (samples)	1	1	0	0	0	1	1
	Over standard rate (%)	0	0	0	0	0	0	0
Leg	Relevance amount (samples)	1	1	1	0	0	0	0
	Over standard rate (%)	0	0	0	0	0	0	0
Lung	Relevance amount (samples)	1	0	0	0	0	0	1
	Over standard rate (%)	0	0	0	0	0	0	0

In the test, it was found that some duck meat samples contained multiple veterinary drugs simultaneously. Although this can synergize the drugs and improve the drug effect, it also increases the veterinary drug residues. In the samples with veterinary drug residues detected, there were six samples with two or more veterinary drug residues. The potential harm to human health caused by veterinary drug residues in animal food has been recognized by more and more people. The detection rate of veterinary drug residues in duck meat samples was 0–12.5%, and the exceeding rate was 2.1%. Only one sample had chloramphenicol residues exceeding the standard. Chloramphenicol can cause bone marrow hematopoietic disorders, leading to severe aplastic anemia, agranulocytosis, and other diseases.

For this reason, countries around the world and China have banned its use in animal breeding. In addition, samples containing chloramphenicol, gentamicin, streptomycin were also found simultaneously. The combined use of such a variety of veterinary drugs enhances disease resistance and increases the residues of veterinary drugs, which is worthy of attention.

4. Conclusions

Six mycotoxins were simultaneously determined in 48 duck meat samples using an LC-MS/MS method, and the analytical performance (such as linearity, reproducibility, and sensitivity) of the method showed that it was accurate and sensitive for all the mycotoxins analyzed. The analysis indicated the presence of mycotoxins in 43% of the samples. AFB1 was present in 27% of the samples, with levels ranging from 0.1 to 1.3 $\mu\text{g}/\text{kg}$. The maximum number of mycotoxins found simultaneously in duck samples was six in duck lung, followed by neck and gizzard with five mycotoxins, and heart and breast with four mycotoxins each. There were three types of mycotoxins detected in duck leg samples, which was the least. Thus, high co-occurrence of mycotoxins was verified in these samples. The detection rate of 8 veterinary drugs in duck meat and viscera samples was 0–12.5%, and the exceeding rate was 2.1%. Co-occurrence of several veterinary drug residues was found in some duck meat and viscera samples.

Data Availability

All the data used to support the findings of this study are included in the paper.

Conflicts of Interest

The authors declare no conflicts of interest.

Acknowledgments

The authors gratefully acknowledge the financial support provided by Project NSFKF201905 of Jiangsu Provincial Key Laboratory of Veterinary Bio-pharmaceutical High Tech Research, Jiangsu Agricultural Science and Technology Innovation Fund (CX(21)3005), and academic leader of Jiangsu Province Blue Project (su[2019]3).

References

- [1] N. H. Aziz and Y. A. Youssef, "Occurrence of aflatoxins and aflatoxin-producing moulds in fresh and processed meat in Egypt," *Food Additives & Contaminants*, vol. 8, no. 3, pp. 321–331, 1991.
- [2] Z. Ye, X. Wang, R. Fu et al., "Determination of six groups of mycotoxins in Chinese dark tea and the associated risk assessment," *Environmental Pollution*, vol. 261, Article ID 114180, 2020.
- [3] M. E. Smela, S. S. Currier, E. A. Bailey, and J. M. Essigmann, "The chemistry and biology of aflatoxin B1: from mutational spectrometry to carcinogenesis," *Carcinogenesis*, vol. 22, no. 4, pp. 535–545, 2001.
- [4] M. Sulyok, F. Berthiller, R. Krska, and R. Schuhmacher, "Development and validation of a liquid chromatography/tandem mass spectrometric method for the determination of 39 mycotoxins in wheat and maize," *Rapid Communications in Mass Spectrometry*, vol. 20, no. 18, pp. 2649–2659, 2006.
- [5] N. Bousbia, M. A. Vian, M. A. Ferhat, B. Y. Meklati, and F. Chemat, "A new process for extraction of essential oil from Citrus peels: microwave hydrodiffusion and gravity," *Journal of Food Engineering*, vol. 90, no. 3, pp. 409–413, 2009.
- [6] A. Nbk, B. Cjfa, C. Dmsm, and A. Rf, "Occurrence of aflatoxins in edible vegetable oils in Sri Lanka," *Food Control*, vol. 101, pp. 97–103, 2019.
- [7] S. Casal, T. Vieira, R. Cruz, and S. C. Cunha, "Ochratoxin A in commercial soluble coffee and coffee substitutes," *Food Research International*, vol. 61, pp. 56–60, 2014.
- [8] D. L. Eaton and J. D. Groopman, "The toxicology of aflatoxins: human health, veterinary, and agricultural," *Animal Feed Science & Technology*, vol. 68, pp. 368–369, 1997.
- [9] H. N. Mishra and C. Das, "A review on biological control and metabolism of aflatoxin," *Critical Reviews in Food Science and Nutrition*, vol. 43, no. 3, pp. 245–264, 2003.
- [10] J. Tolosa, Y. Rodríguez-Carrasco, M. J. Ruiz, and P. Vila-Donat, "Multi-mycotoxin occurrence in feed, metabolism and carry-over to animal-derived food products: a review," *Food and Chemical Toxicology*, vol. 158, Article ID 112661, 2021.
- [11] M. Leite, A. Freitas, A. S. Silva, J. Barbosa, and F. Ramos, "Maize food chain and mycotoxins: a review on occurrence studies," *Trends in Food Science & Technology*, vol. 115, pp. 307–331, 2021.
- [12] E. González-Peñas, "Mycotoxins: classification, occurrence and determination," *Encyclopedia of Dairy Sciences*, Academic Press, Cambridge, MA, USA, 2022.
- [13] S. Z. Iqbal, "Mycotoxins in food, recent development in food analysis and future challenges; a review," *Current Opinion in Food Science*, vol. 42, pp. 237–247, 2021.
- [14] B. H. Zainudin, M. I. Iskandar, S. Sharif, A. A. Ahmad, and M. F. Safian, "Validation of quick and highly specific quantitation method of mycotoxin in cocoa beans by high resolution multiple reaction monitoring technique for reference materials analysis," *Journal of Food Composition and Analysis*, vol. 106, Article ID 104289, 2021.
- [15] M. Buszewska-Forajta, "Mycotoxins, invisible danger of feedstuff with toxic effect on animals," *Toxicon*, vol. 182, pp. 34–53, 2020.
- [16] M. J. Adegbeye, P. R. K. Reddy, C. A. Chilaka et al., "Mycotoxin toxicity and residue in animal products: prevalence, consumer exposure and reduction strategies—a review," *Toxicon*, vol. 177, pp. 96–108, 2020.
- [17] E. Chiavaro, C. Cacchioli, E. Berni, and E. Spotti, "Immunoaffinity clean-up and direct fluorescence measurement of

- afatoxins B1 and M1 in pig liver: comparison with high-performance liquid chromatography determination,” *Food Additives & Contaminants*, vol. 22, no. 11, pp. 1154–1161, 2005.
- [18] B. Peromingo, M. Sulyok, M. Lemmens, A. Rodríguez, and M. Rodríguez, “Diffusion of mycotoxins and secondary metabolites in dry-cured meat products,” *Food Control*, vol. 101, pp. 144–150, 2019.
- [19] Z. Zou, Z. He, H. Li et al., “Development and application of a method for the analysis of two trichothecenes: deoxynivalenol and T-2 toxin in meat in China by HPLC–MS/MS,” *Meat Science*, vol. 90, no. 3, pp. 613–617, 2012.
- [20] L. Caldeiro, J. Sousa, L. Nunes, H. T. Godoy, and S. C. Cunha, “Herbs and herbal infusions: determination of natural contaminants (mycotoxins and trace elements) and evaluation of their exposure,” *Food Research International*, vol. 144, Article ID 110322, 2021.
- [21] L. Zhang, X. W. Dou, C. Zhang, L. Antonio, and M. H. Yang, “A review of current methods for analysis of mycotoxins in herbal medicines,” *Toxins*, vol. 10, no. 2, Article ID 65, 2018.
- [22] L. M. Sørensen, J. Mogensen, and K. F. Nielsen, “Simultaneous determination of ochratoxin A, mycophenolic acid and fumonisin B2 in meat products,” *Analytical and Bioanalytical Chemistry*, vol. 398, no. 3, pp. 1535–1542, 2010.
- [23] V. Bernáldez, J. J. Córdoba, M. Rodríguez, M. Cordero, L. Polo, and A. Rodríguez, “Effect of *Penicillium nalgioense* as protective culture in processing of dry-fermented sausage “salchichón,”” *Food Control*, vol. 32, no. 1, pp. 69–76, 2013.
- [24] A. Rodríguez, V. Bernáldez, M. Rodríguez, M. J. Andrade, F. Núñez, and J. J. Córdoba, “Effect of selected protective cultures on ochratoxin A accumulation in dry-cured Iberian ham during its ripening process,” *LWT—Food Science and Technology*, vol. 60, pp. 923–928, 2015.

Research Article

Simultaneous Determination of Retinols and Tocols in Egg and Milk Products Based on RP-HPLC Linked with Fluorescent and Photodiode Array

Yingqi Chen ², Chonggao Hu,¹ Jiaojiao Xu ¹, Xiaodong Pan,¹ and Baifen Huang ¹

¹Zhejiang Provincial Center for Disease Control and Prevention, Hangzhou 310051, China

²Zhejiang Chinese Medical University, Hangzhou 310053, China

Correspondence should be addressed to Baifen Huang; bhuang@cdc.zj.cn

Yingqi Chen and Chonggao Hu contributed equally to this work.

Received 31 March 2022; Accepted 14 June 2022; Published 2 August 2022

Academic Editor: Hong Yan Zou

Copyright © 2022 Yingqi Chen et al. This is an open access article distributed under the Creative Commons Attribution License, which permits unrestricted use, distribution, and reproduction in any medium, provided the original work is properly cited.

In this paper, we built a method of verifying the 4 retinols of vitamin A and 8 tocopherol isomers of vitamin E in the food industry based on RP-HPLC-PDA-FLR. The effect of laboratory light conditions on the target components was considered for the first time, and it was found that the loss rate of the target components was the smallest in the case of a white laboratory bench with red or LED light in the dark room. There was no finding of extraction recoveries of the target components with a significant difference under different saponification conditions. Meanwhile, it was found that using ethyl acetate/n-hexane mixed solvent as the extraction solvent could ensure the effective extraction of the target components. Finally, baseline separation of 12 components was achieved within 45 min using the C₃₀ column. With the help of methodological verification, we found that the recovery rate ranged from 76.45% to 93.52%, and RSD was between 0.19% and 12.99%; the Limit of Detection minimum value was 0.01 mg/100 g and the Limit of Quantitation minimum value was 0.03 mg/100 g. The detection method was successfully applied to the distribution detection of 4 kinds of retinols and 8 kinds of vitamin E in egg and dairy products and provided technical support for the accurate nutritional evaluation of vitamin A and vitamin E.

1. Introduction

Vitamin A, also known as retinol, refers to all isoprene-like compounds with full *trans*-retinol biological activity, because it has four conjugated double bonds on the side chain; theoretically, there are 16 kinds of *cis*- and *trans*-isomers; due to the stereoteric hindrance effect, the geometric isomers that exist in nature mainly include all-*trans* retinol, 9-*cis* retinol, 13-*cis* retinol, and 11-*cis* retinol. Among the isomers, the biovalence of the all-*trans* formula is the highest (measured at 100%), followed by that of the 13-*cis* (75%), that of the 9-*cis* is 23%, and that of the 11-*cis* is 24% [1–3]. Vitamin A is one of the 13 essential vitamins in the human body; as a fat-soluble antioxidant, it can maintain vision and promote bone growth in the human body; it is mainly distributed in animal-derived foods like animal livers, egg

yolk, and cream, and the main form in food is retinol and its esters [4, 5]. Vitamin E is mainly derived from various plant seeds, and it mainly has 8 kinds of forms: 4 kinds of tocopherols (α -, β -, γ -, and δ -tocopherol) and 4 kinds of tocotrienols (α -, β -, γ -, and δ -tocotrienol). Studies had shown that all forms of tocopherols had similar antioxidant activities, which was essential for the optimal functioning of reproductive, muscular, neurological, and immune systems in various animals [4, 5]. The biological activities of β -, γ -, and δ -tocopherol and α - and β -tocotrienol are 50%, 10%, 3%, 50%, and 5% of α -tocopherol [1], respectively; there is no relevant research data on the α -tocopherol activity equivalent of γ -tocotrienol and δ -tocotrienol, but studies had shown that γ - and δ -tocotrienol had a preventive effect on the prevention of colorectal cancer, gastric cancer, prostate cancer, breast cancer, and other diseases [6–9]; they also

could reduce cholesterol, alleviate cardiovascular disease, and improve nonalcoholic fatty liver and other diseases [10–12].

At present, the methods of isolating and detecting vitamin A or E in food mainly include the liquid chromatography (HPLC) method [13, 14], liquid chromatography-mass spectrometry (HPLC-MS) method [15, 16], and gas chromatography (GC) method [17, 18]. When determining vitamin E, the GC method often requires the introduction of chemical groups suitable for determining the type of detection to convert analytes through the derivatization process, and cholesterol in animal-derived foods will interfere with the determination of tocopherols. Compared with the GC method, the pretreatment process of the LC method is relatively simple and is more suitable for the simultaneous detection of retinols and tocopherols. Normal-phase liquid chromatography (NP-HPLC) method [19] and reversed-phase liquid chromatography (RP-HPLC) method [13, 15] can both be used for the analysis of vitamin E; NP-HPLC is separated by polar adsorption of compounds; it is very suitable for the separation of retinol isomers and tocopherol subtypes, but it uses n-hexane or other volatile solvents as mobile phases; the system equilibrium time is long and the reproducibility is poor. The RP-HPLC method often uses MeOH or ACN as the mobile phase, when using the traditional ODS (C₁₈) column to separate tocopherols; it is difficult to effectively separate β -tocopherol and γ -tocopherol and β -tocotrienol and γ -tocotrienol [20–22]. Separation of these two isomers requires pentafluorophenyl columns (PFP), chiral chemical columns, or long-chain alkyl-bonded silica columns (C₃₀) [23–25]. At present, most of the separation and detection of retinol *cis*- and *trans*-isomers in food focus on all-*trans* retinol and 13-*cis* retinol, and the simultaneous separation of 4 retinol *cis*- and *trans*-isomers has not been reported.

The isolation and determination of 4 retinols and 8 tocopherols in food can be better used for food nutrition evaluation, which is of great significance for the implementation of accurate nutrition assessment of residents. In this study, we established a quantitative method for the simultaneous determination of 4 retinol *cis*- and *trans*-isomers and 8 tocopherol isoforms in food by RP-HPLC. The chromatographic separation conditions and the sample pretreatment methods were optimized for better performance.

2. Materials and Methods

2.1. Chemicals and Materials. All-*trans* retinol (CAS no. 68-26-8), 9-*cis* retinol (CAS no. 68-26-8), 11-*cis* retinol (CAS no. 68-26-8), and 13-*cis* retinol (CAS no. 68-26-8) were purchased from TRC Company; α -tocopherol (CAS no. 10191-41-0), β -tocopherol (CAS no. 148-03-8), γ -tocopherol (CAS no. 54-28-4), δ -tocopherol (CAS no. 119-13-1), α -tocotrienol (CAS no. 1721-51-3), β -tocotrienol (CAS no. 490-23-3), γ -tocotrienol (CAS no. 14101-61-2), and δ -tocotrienol (CAS no. 25612-59-3) were purchased from Chromadex, USA, with purity more than 96%. Absolute ethanol (EtOH), methanol (MeOH), ethyl acetate, and

n-hexane (HPLC grade) were purchased from Fisher Company of the United States; ascorbic acid, 2,6-di-tert-butyl-p-cresol (BHT), and potassium hydroxide (KOH) (analytical purity) were purchased from Aladdin company; food products were purchased from a supermarket in Hangzhou.

2.2. Instrument Conditions. High-performance liquid chromatography (Waters Company, USA) was used (equipped with PDA and FLR).

Consider the following: column: C₃₀ column (150 × 4.6 mm, 3 μ m); column temperature: 28°C; mobile phase: phase A, water; phase B, MeOH, gradient elution (see Table 1); flow rate: 0.8 mL/min; detection wavelength: PDA = 325 nm (retinol); FLR: Ex = 294 nm, Em = 328 nm (vitamin E); sample volume: 20 μ L.

2.3. Experimental Methods

2.3.1. Standard Solution Preparation. After the standard stock solution is prepared by dissolving in absolute ethanol, the absorbance of each component is determined according to the wavelength of Table 2, and the corrected concentration of each standard stock solution is calculated according to the specific absorbance coefficient $E_{1\text{cm}}^{1\%}$. A certain amount of standard stock solution was pipetted separately to prepare the intermediate solution, of which 4 retinol concentrations were 10.0 μ g/mL, and 8 tocopherol concentrations were 50 μ g/mL for subsequent use.

2.3.2. Sample Preparation

Experimental Environment. The pretreatment process of this study was carried out under the white experimental table of red light (illuminance 20LUX) or white LED lamp (illuminance 70LUX) in the dark room to reduce the loss of the target compound from the influence of light factors.

Saponification. After a certain number of samples had been reduced, crushed, and homogenized as required, a homogenized sample was weighed at 0.5 g and mixed in a 50 mL centrifuge tube, 0.4 g of ascorbic acid was added, 6 mL of 0.1% BHT EtOH solution was vortexed and mixed for 30 s, and then 3 mL of KOH solution was added in it, vortexed, mixed well, and shaken at 80°C \pm 2°C for 30 min (or vortexed for 16 h \pm 2 h at 25°C \pm 5°C).

Extraction. 6 mL of 40% ethanol aqueous solution and 5 mL of water were added to the saponification solution described above, and then 20 mL of ethyl acetate/n-hexane mixture (1/1 = v/v) was added and extracted for 10 min, and the upper layer of solution was transferred to another 50 mL centrifuge tube after high-speed centrifugation. Another 10 mL of ethyl acetate/n-hexane mixture (1/1 = v/v) was added to the original centrifuge tube and extracted for 10 min, and then the upper organic phase was merged. Water was added to 50 mL in a centrifuge tube incorporating the upper organic

TABLE 1: Mobile phase gradient elution conditions.

T (min)	A (%)	B (%)
0.0	17	83
15.0	17	83
15.5	7	93
22.0	7	93
32.0	5	95
37.0	5	95
37.5	17	83
45.0	17	83

phase, followed by centrifugation after slight shaking, and the upper organic phase was transferred and blow-dried with nitrogen. Finally, made up to 5 mL by MeOH/Water(4/1,v/v) and passed through the microporous filter membrane, and took the filtrate to be determined.

2.3.3. Methodological Verification. The established HPLC-PDA-FLR method is verified in terms of specificity, linear range, the Limit of Detection, the Limit of Quantitation, precision, and accuracy. The linearity of each analyte is assessed by calculating the slope, intercept, and correlation coefficients of each component within a certain concentration range; the Limit of Detection and the Limit of Quantitation are determined by low concentration level standardization experiments and determined as the lowest concentrations that produce chromatographic peaks, with a signal-to-noise ratio (S/N) of 3 times and 10 times as Limit of Detection and Limit of Quantitation, respectively; and the accuracy and precision of this research method are tested by three levels of different concentration standardization experiments in infant formula. In addition, it is validated using infant/adult nutrition formulas SRM 1849a and SRM 1869 reference standards provided by the National Institute of Standards and Technology (NIST).

3. Results and Discussion

3.1. Chromatographic Conditions

3.1.1. Selection of Column and Mobile Phase. To separate and detect 4 kinds of retinols and 8 kinds of tocopherols at the same time, it is necessary to select a suitable column and optimize the mobile phase at the same time. As far as the separation of retinol is concerned, the RP-LC separation method of the *trans*- and the *cis*-isomers was less documented, and the authors had used polysaccharide derivatives to modify chiral silicone columns (OD-5H column) to separate α -tocopherol and other tocopherols and retinol isomers in infant formula [22] and obtained an ideal analysis result, but its defect was that it was impossible to separate 11-*cis* retinol and 9-*cis* retinol at the same time; what is more, the C₁₈ column cannot be used for the separation of *cis*- and *trans*-retinol, β and γ -tocopherol, and β and γ -tocotrienol isomers. So we mainly considered C₃₀ column and PFP column as alternative columns. Compared with the traditional column, the PFP column has a strong separation ability for easily polarizable substances such as aromatic

rings and heterocyclic compounds and has a better separation effect on isomers, and it was found that it could effectively achieve separation and detection of vitamin E isomers in a short period [26], but, in this study, we cannot effectively separate 9-*cis* retinol and 13-*cis* retinol by optimizing mobile phase conditions. What is more, it was found that the C₃₀ column can achieve the separation of vitamin E isomers, and, based on this study, it was found that when the proportion of the aqueous phase in the mobile phase reaches 17%, four retinol isomers can be separated. Finally, the full separation and detection of retinol and vitamin E 12 target substances can be achieved within 50 minutes by gradient elution, so the C₃₀ column was selected as the conditioned column for subsequent analysis.

3.1.2. Selection of Detector. The 4 kinds of retinols have a very high UV absorption characteristic spectrum, while vitamin E has strong FLR characteristics. Therefore, we used PDA and FLD detection to detect retinol and vitamin E, respectively, and the two detectors were used in series, and the standard solution separation chromatogram of retinol and vitamin E is shown in Figure 1.

3.2. Sample Pretreatment Conditions

3.2.1. Laboratory Environmental Conditions. Because of the unstable feature of retinol and vitamin E when exposed to light, heat, and oxygen, and under the light conditions, retinol was prone to degradation or isomerization [1]. Thus, sunlight should be avoided during the experiment, the pretreatment process should be completed in a dim environment, and the solution should be stored in glassware with a low photochemical rate as much as possible. During the actual sample extraction process, it is impossible to perform in a completely light-protected environment, so this study investigated the effects of different light conditions on the target components.

The standard solution of 12 components added with BHT antioxidants was separately aliquoted in a 1 mL transparent injection flask and three experimental environments (south-facing sun laboratory, north back sun laboratory, and windowless dark room) were chosen as different light sources, and each was put for 4 hours (the storage time covered the entire time for the pretreatment process), and the standard solution before storage was synchronized with the injection control; the loss rate is shown in Table 3, retinol was sensitive to ultraviolet light, and the loss rates of the four retinols were more than 75% when stored in the south-facing sun laboratory by the window. 11-*cis* retinol was the most unstable component, whether in the south-facing sun laboratory by the window or on the north side of the back sun laboratory against the window, and the loss rate was 100%. In addition, 8 tocopherols were relatively stable under the protection of the antioxidant BHT. Ultimately, our study found that, when using a red light (illuminance 20LUX) or a white LED lamp (illuminance 70LUX) in the darkroom with a white experimental table, the loss rate of 12 components is less than 4%.

TABLE 2: Standard storage solution correction parameters.

Name	Wavelength (nm)	$E_{1\text{cm}}^{1\%}$	Name	Wavelength (nm)	$E_{1\text{cm}}^{1\%}$
All- <i>trans</i> retinol	325	1830	γ -Tocopherol	298	91.4
9- <i>cis</i> retinol	323	1477	δ -Tocopherol	298	87.3
11- <i>cis</i> retinol	319	1220	α -Tocotrienol	292	86.0
13- <i>cis</i> retinol	328	1689	β -Tocotrienol	292	86.2
α -Tocopherol	292	75.8	γ -Tocotrienol	297	91.0
β -Tocopherol	296	89.4	δ -Tocotrienol	297	85.8

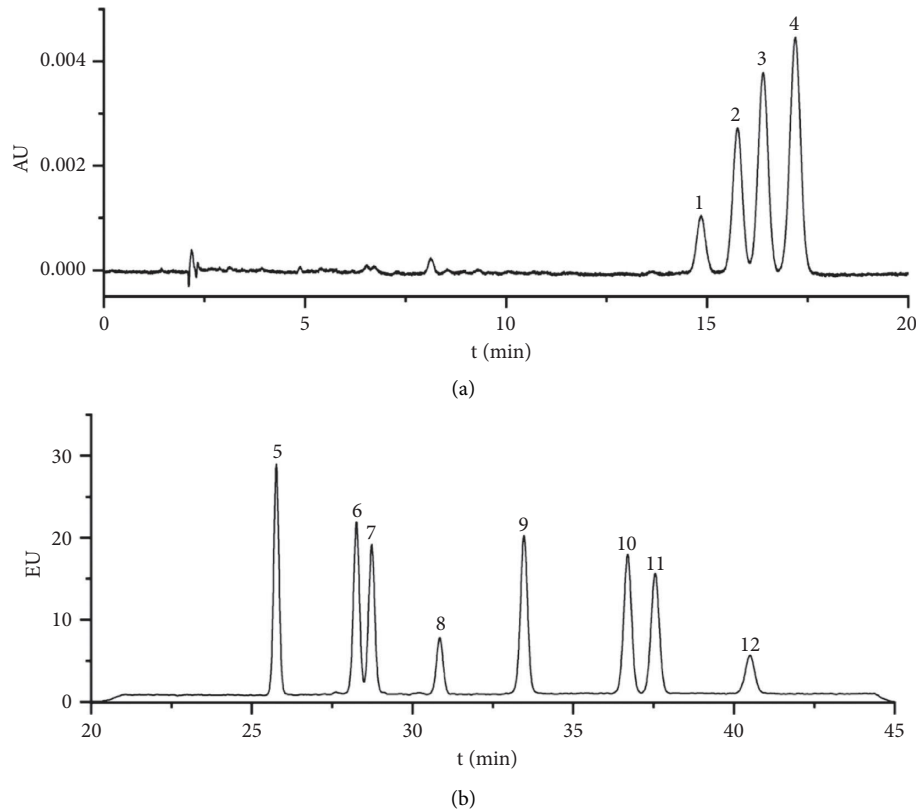


FIGURE 1: Standard solution chromatogram results. (a) UV = 325 nm; (b) FLR (Ex = 294 nm, Em = 328 nm) (1: 11-*cis* retinol; 2: 9-*cis* retinol; 3: 13-*cis* retinol; 4: all-*trans* retinol; 5: δ -tocotrienol; 6: γ -tocotrienol; 7: β -tocotrienol; 8: α -tocotrienol; 9: δ -tocopherol; 10: γ -tocopherol; 11: β -tocopherol; 12: α -tocopherol).

3.2.2. Saponification Conditions. Egg yolk powder is a powder obtained after a series of processes of fresh eggs as raw materials, which is a common health food and food additive on the market. Egg yolk powder is rich in various types of proteins, phospholipids, fatty acids, and so forth, with a strong emulsification function [27, 28]. Vitamins A and E are two main fat-soluble vitamins in food mainly combined with various types of lipid structures and coexist, so it is necessary to carry out a certain saponification treatment. As a common pretreatment method, the principle of saponification is to carry out an ester hydrolysis reaction under the catalytic action of alkali, to dissociate the target detection substance from the grease, which is conducive to the next step of enrichment extraction and detection. At present, the standard method for the determination of vitamins A, D, and E in food in China [29] recommends saponification conditions for 80°C constant temperature water bath oscillation for 30 min, and the saponification

conditions reported in the literature were overnight cold saponification at room temperature (25°C for 15 hours in the dark room) [30, 31]. This study mainly compared the two saponification conditions above and used low background egg yolk powder as a matrix sample, through the standard recovery experiment to compare the different results of the two methods by statistical analysis, and the comparison chart is shown in Figure 2. The results showed that there was no statistical difference in the recovery rate of 12 target components under two saponification conditions in this study ($P > 0.05$), and the recovery rate of each target component was above 83.02%, basically meeting the testing requirements.

3.2.3. Extraction Reagent. China's determination standards for vitamins A, D, and E in the recommended liquid extraction extractant are petroleum ether/ether mixture [29],

TABLE 3: Loss rate of target components in different experimental conditions (%).

Towards Placement	South			North			Dark room			
	By the window	By the corridor countertop	By the corridor countertop	By the window	By the corridor countertop	By the corridor countertop	Red light	Red light	LED light	LED light
Illuminance (LUX)	1496–3060	565–710	565–710	1490–1800	230–310	230–310	20	20	70	70
Table color	Black	Black	White	Black	Black	White	Black	White	Black	White
9- <i>cis</i> retinol	78.48	37.47	18.90	82.43	5.89	2.11	4.97	3.48	6.28	1.78
11- <i>cis</i> retinol	100.00	52.11	34.31	100.00	18.29	4.52	15.00	3.48	15.00	2.56
13- <i>cis</i> retinol	80.04	42.73	27.65	78.02	7.99	4.91	12.40	2.16	10.14	1.06
All- <i>trans</i> retinol	76.74	28.26	18.10	73.83	4.25	1.28	3.96	2.16	3.96	1.96
α -Tocopherol	2.29	2.27	3.02	3.74	3.93	4.86	3.21	2.68	2.22	2.29
β -Tocopherol	2.71	2.06	2.31	2.48	2.26	2.48	2.36	2.61	2.68	3.12
γ -Tocopherol	2.35	2.00	2.14	2.36	2.40	2.79	3.46	2.96	2.72	3.19
δ -Tocopherol	2.62	1.85	2.50	1.92	1.63	2.81	2.09	2.63	2.28	2.21
α -Tocotrienol	2.84	2.33	3.22	3.55	1.99	4.72	3.12	3.96	3.13	3.77
β -Tocotrienol	2.18	2.46	2.52	2.59	2.36	3.10	1.66	2.81	2.41	2.79
γ -Tocotrienol	2.44	1.82	2.60	3.04	2.28	3.18	1.21	3.24	3.01	3.27
δ -Tocotrienol	2.27	2.04	2.12	2.76	2.30	2.57	4.46	2.67	2.19	2.27

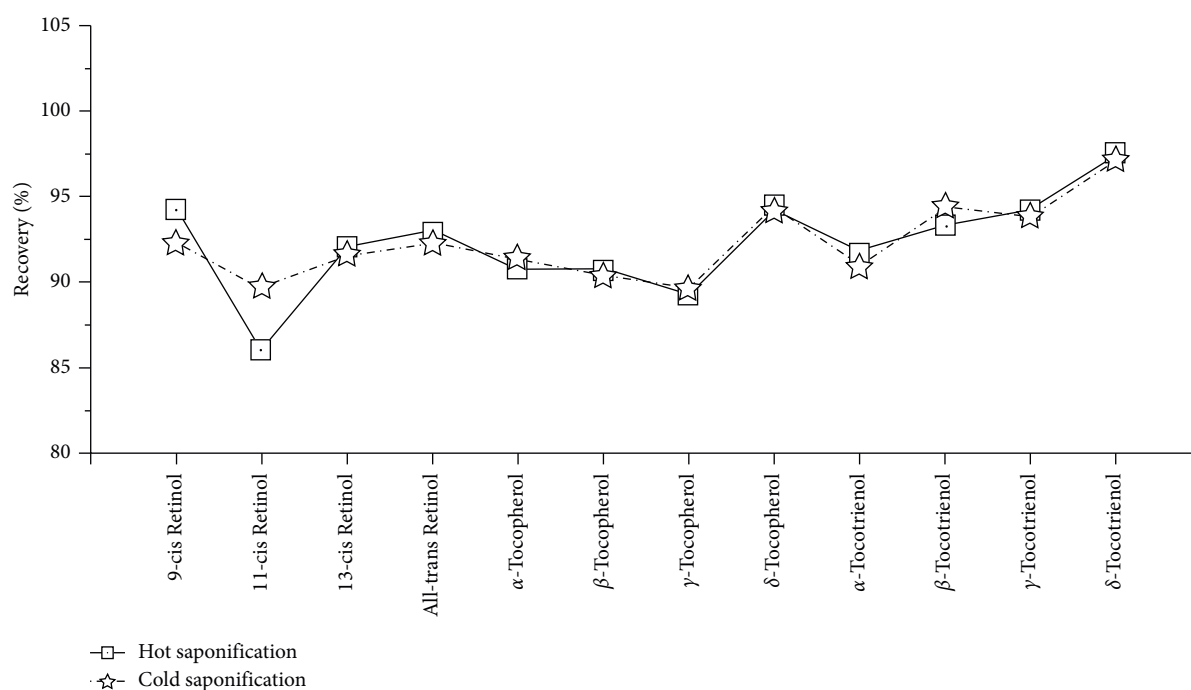


FIGURE 2: Recovery results for different saponification conditions.

but the extract has a special pungent odor and strong toxicity, which is not conducive to the experimenter's own protection. In recent years, some studies used n-hexane and other reagents instead of petroleum ether, ether, and other highly toxic reagents [13]. In this study, the extraction effects of six common extraction reagents (petroleum ether, ether, petroleum ether/ether, ethyl acetate, n-hexane, and ethyl acetate/n-hexane) were compared with the extraction effects of retinol and vitamin E, 6 samples were determined in

parallel with each reagent, and the target components were extracted twice in turn to achieve a better enrichment effect, and the final experimental results are shown in Figure 3. The results showed that when ethyl acetate/n-hexane was used as the extraction reagent, the recovery rate of the target components was comparable to that of petroleum ether/ether mixture, and the experimental error was even smaller, so ethyl acetate/n-hexane was selected as the extractant for this study.

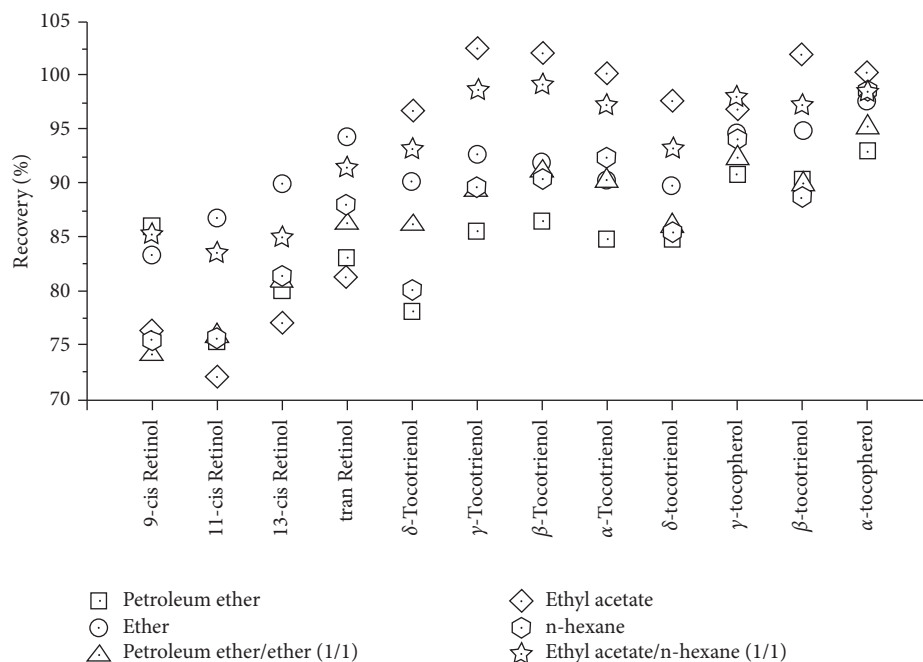


FIGURE 3: Results for different extraction reagents comparison.

3.3. Method Validation

3.3.1. Standard Curve Linear. The linearity calculation was based on the six increasing concentrations of each isomer. Ranged from 0.02 $\mu\text{g/mL}$ to 0.50 $\mu\text{g/mL}$ for retinols, and ranged from 0.10 $\mu\text{g/mL}$ to 2.50 $\mu\text{g/mL}$ for tocols. The standard curve was drawn with the concentration as the abscissa and the peak area as the ordinate, and the calibration curve and related coefficients are shown in Table 4.

3.3.2. Method Limit of Detection and Limit of Quantitation. Skimmed milk powder was selected as a blank background sample according to the method of sample preparation in 2.3.5, according to the signal-to-noise ratio (S/N) evaluation Limit of Detection and Limit of Quantitation, 3 times of the S/N is the method Limit of Detection value, and 10 times of the S/N is the method Limit of Quantitation value. The results showed that when the solid sample was weighed at 0.50 g and the volume was fixed to 5.00 mL; the Limits of Detection of 9-*cis* retinol, 11-*cis* retinol, 13-*cis* retinol, and all-*trans* retinol were 10 $\mu\text{g}/100\text{ g}$, and the Limits of Quantitation were 30 $\mu\text{g}/100\text{ g}$; and the Limits of Detection for the eight tocopherols were 0.05 mg/100 g and the Limits of Quantitation were 0.15 mg/100 g, respectively.

3.3.3. Method Precision and Accuracy. Blank background skimmed milk powder was selected as the standardized matrix; the standard recovery rate test was carried out at the three concentration levels of the lowest, intermediate, and highest points of the standard curve, respectively. Each concentration level was tested for 6 times, and the results were located in Table 5. The average recovery rate of low-level standardization was between 76.45% and 87.10%, RSD

was between 3.06% and 12.99%, the intermediate concentration recovery was between 80.72% and 92.50%, RSD was between 0.19% and 8.44%, and the high concentration standard recovery was between 78.52% and 93.52%, and RSD was between 0.44% and 2.75%; and the results indicated that the method established had great reproducibility and precision.

3.3.4. Detection of Certificated reference Materials. This study also used the certificated reference materials SRM 1869 and SRM 1849a provided by the National Institute of Standards and Technology (NIST) to verify the method; each reference standard underwent three parallel replicates to ensure the accuracy of the results, and the specific results are detailed in Table 6. From the experimental results, it can be seen that 11-*cis* retinol, β -tocotrienol, and δ -tocotrienol were not detected in the two certificated reference materials; the all-*trans* retinol of the two certificated reference materials was low compared to the nominal retinol values but was comparable to the declared values when the other isomers were counted; α -tocopherol's measurements were within the reference range of the indicated values; the detection values of β -tocopherol, γ -tocopherol, and δ -tocopherol in SRM 1869 were basically the same as those indicated. The detection values of the two certificated reference materials indicated that the test results of this method were true and reliable, and the method was suitable for the separation and detection of retinol and vitamin E isomers in real samples.

3.4. Actual Sample Results. This study also analyzed and detected the retinol and vitamin E isomer content in 15 kinds of formula milk powders and 6 kinds of egg yolk

TABLE 4: Linear range for retinol and tocopherol isomers.

Name	Range ($\mu\text{g/mL}$)	Calibration curve	R^2
9- <i>cis</i> retinol	0.02~0.50	$Y = 432.3 + 211783.7X$	0.9999
11- <i>cis</i> retinol	0.02~0.50	$Y = 488.7 + 82274.3X$	1.0000
13- <i>cis</i> retinol	0.02~0.50	$Y = 157.8 + 285759.4X$	0.9999
All- <i>trans</i> retinol	0.02~0.50	$Y = 119.1 + 389663.3X$	1.0000
α -Tocopherol	0.10~2.50	$Y = -69853.9 + 1116543.5X$	0.9993
β -Tocopherol	0.10~2.50	$Y = -42411.4 + 2535083.8X$	0.9998
γ -Tocopherol	0.10~2.50	$Y = -60077.5 + 2782667.2X$	0.9997
δ -Tocopherol	0.10~2.50	$Y = 663.2 + 3344578.7X$	1.0000
α -Tocotrienol	0.10~2.50	$Y = -91398.5 + 1004661.7X$	0.9992
β -Tocotrienol	0.10~2.50	$Y = -46799 + 2424243.3X$	0.9996
γ -Tocotrienol	0.10~2.50	$Y = -65585.5 + 2760020.3X$	0.9995
δ -Tocotrienol	0.10~2.50	$Y = -4499.3 + 2834712.8X$	0.9999

TABLE 5: Method precision and accuracy of experimental results.

Name	Addition level 1		Addition level 2		Addition level 3	
	Recovery (%)	RSD (%)	Recovery (%)	RSD (%)	Recovery (%)	RSD (%)
9- <i>cis</i> retinol	76.79	4.52	85.92	1.66	86.41	2.75
11- <i>cis</i> retinol	79.85	7.94	80.72	8.44	78.52	1.02
13- <i>cis</i> retinol	76.45	3.06	89.08	2.08	91.52	2.24
All- <i>trans</i> retinol	87.10	7.41	91.28	1.56	93.52	0.98
α -Tocopherol	76.56	2.62	88.46	3.31	90.07	0.44
β -Tocopherol	76.63	12.99	90.82	4.35	90.46	1.44
γ -Tocopherol	76.53	11.54	92.50	2.85	92.85	1.49
δ -Tocopherol	78.12	3.76	89.34	2.54	90.40	0.80
α -Tocotrienol	79.93	8.50	84.79	2.21	83.71	2.02
β -Tocotrienol	79.28	4.09	82.44	1.97	80.78	2.06
γ -Tocotrienol	80.73	4.22	84.53	1.92	83.68	1.99
δ -Tocotrienol	79.61	4.23	81.91	0.19	82.73	1.32

TABLE 6: Certificated reference materials test results.

Name	SRM 1869		SRM 1849a		
	Measured value (mg/kg)	Certified value (mg/kg)	Measured value (mg/kg)	Certified value (mg/kg)	
Retinol	9- <i>cis</i> retinol	0.45	19.27 \pm 0.32 (for retinol)	0.60	7.68 \pm 0.23 (for retinol)
	11- <i>cis</i> retinol	ND		ND	
	13- <i>cis</i> retinol	1.42		1.39	
	All- <i>trans</i> retinol	18.66		6.60	
Vitamin E	α -Tocopherol	214.7	217.2 \pm 6.2 (for total α -tocopherol)	204.70	219 \pm 16 (for total α -tocopherol)
	β -Tocopherol	3.79	4.22 \pm 0.69	6.30	—
	γ -Tocopherol	99.83	99.4 \pm 5.1	144.1	—
	δ -Tocopherol	33.21	32.5 \pm 2.9	82.3	—
	α -Tocotrienol	1.20	—	1.83	—
	β -Tocotrienol	ND	—	ND	—
	γ -Tocotrienol	0.41	—	1.20	—
δ -Tocotrienol	0.05	—	ND	—	

ND: not found; —: not referred.

powder commonly used in the market. Retinol examination results showed that three retinol isomers (9-*cis* retinol, 13-*cis* retinol, and all-*trans* retinol) could be detected in formula milk powder, and a small amount of 11-*cis* retinol can be detected; this may be due to the effect of steric resistance in space, making the presence of 11-*cis* retinol unstable in nature, making it impossible to obtain effective separation detection. In the egg yolk powder sample, only one of the

samples detected retinol isomers, and none of the remaining samples detected retinol; it may be that some processes in the production and processing destroy the retinol in it. Except for the four detectable *cis*- and *trans*-isomers of retinol, there was a high unknown peak between 11-*cis* retinol and 9-*cis* retinol during the detection of some actual samples, and if the content of the component was calculated by all-*trans* retinol, it accounted for 2.53% to 8.54% of the total all-*trans*

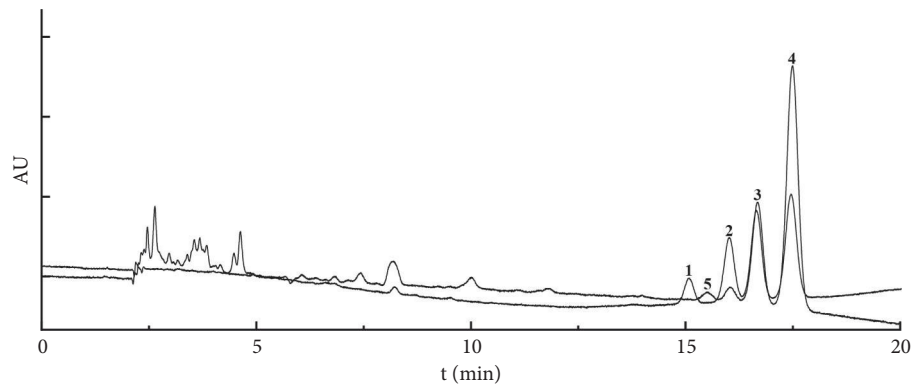


FIGURE 4: Sample and standard contrast chromatogram (1: 11-*cis* retinol; 2: 9-*cis* retinol; 3: 13-*cis* retinol; 4: all-*trans* retinol; 5: unknown component).

retinol, so the confirmation of the component needs to be further studied to confirm whether it is a retinol isomer or an impurity component. The detailed sample and the standard were compared to detect the chromatogram as shown in Figure 4, and the number 5 chromatographic peak in the figure was the unknown component chromatographic peak.

The test results of the vitamin E isomer showed that the presence of four tocopherols could be found in almost all samples, with the content being α -tocopherol > γ -tocopherol > δ -tocopherol > β -tocopherol; however, tocotrienols were detected less often, and the presence of various types of tocotrienols can be detected in some formula milk powders (such as four samples nos. 5, 6, 8, and 11). According to the biological activity equivalent of other forms of tocopherols known to the study, after conversion, it was found that the activity equivalent of other isomers detected in the sample accounted for 0.11% to 59.18%. Therefore, it is not perfect to evaluate the nutritional value of food only in line with α -tocopherol, and it is necessary to isolate and test other forms of tocopherol and include them in the calculation according to their active equivalent and improve the evaluation criteria further.

4. Conclusion

In this study, the influence of experimental light conditions on the degree of loss of the target components was considered for the first time, and, finally, the study found that, in the case of open red light (illuminance 20LUX) or white LED lamp (illuminance 70LUX) in the dark room, the loss rates of 12 target components were less than 4%. On this basis, the saponification conditions and liquid-liquid extraction solvents were studied, and it was found that there was no significant difference in the influence of hot saponification and cold saponification conditions on the target components of this study. The selection of ethyl acetate/*n*-hexane mixed solvent as the extraction solvent could meet the requirements of the extraction and detection of the target components while ensuring the safety of the experimenter. The optimized research method had the advantages of simple operation, high accuracy, and good repeatability, which can meet the simultaneous separation and detection of retinol

isomers and vitamin E homologues and can be effectively applied in dairy products.

Data Availability

The data used to support the findings of this study are included within the article.

Conflicts of Interest

The authors declare that they have no conflicts of interest.

References

- [1] *Vitamin Analysis for the Health and Food Sciences*, CRC Press, Boca Raton, FL, USA, 2nd edition, 2007.
- [2] L. M. Sivell, N. L. Bull, D. H. Buss, R. A. Wiggins, D. Scuffam, and P. A. Jackson, "Vitamin A activity in foods of animal origin," *Journal of the Science of Food and Agriculture*, vol. 35, no. 8, pp. 931–939, 1984.
- [3] H. Weiser and G. Somorjai, "Bioactivity of cis and trans isomers of vitamin A esters," *International Journal for Vitamin and Nutrition Research*, vol. 62, no. 3, pp. 201–208, 1992.
- [4] "Health industry standard of the people's republic of China Chinese dietary reference intakes—Part 4," *Lipid-Soluble Vitamin*, 2018.
- [5] Y. X. Yang, *Chinese Food Ingredient List*, Peking University Medical Press, Beijing, China, 6th edition, 2019.
- [6] T. Eitsuka, N. Tatewaki, H. Nishida, K. Nakagawa, and T. Miyazawa, "A combination of δ -Tocotrienol and ferulic acid synergistically inhibits telomerase activity in DLD-1 human colorectal adenocarcinoma cells," *Journal of Nutritional Science and Vitaminology*, vol. 62, no. 5, pp. 281–287, 2016.
- [7] C. Sato, S. Kaneko, A. Sato, N. Virgona, K. Namiki, and T. Yano, "Combination effect of δ -tocotrienol and γ -tocopherol on prostate cancer cell growth," *Journal of Nutritional Science and Vitaminology*, vol. 63, no. 5, pp. 349–354, 2017.
- [8] Y. Ding, J. Fan, Z. Fan, and K. Zhang, " γ -Tocotrienol reverses multidrug resistance of breast cancer cells through the regulation of the γ -Tocotrienol-NF- κ B-P-gp axis," *The Journal of Steroid Biochemistry and Molecular Biology*, vol. 209, Article ID 105835, 2021.

- [9] F. Fontana, R. M. Moretti, M. Raimondi et al., " δ -Tocotrienol induces apoptosis, involving endoplasmic reticulum stress and autophagy, and paraptosis in prostate cancer cells," *Cell Proliferation*, vol. 52, no. 3, Article ID e12576, 2019.
- [10] M. A. Pervez, D. A. Khan, A. U. R. Slehria, and A. Ijaz, "Delta-tocotrienol supplementation improves biochemical markers of hepatocellular injury and steatosis in patients with non-alcoholic fatty liver disease: a randomized, placebo-controlled trial," *Complementary Therapies in Medicine*, vol. 52, Article ID 102494, 2020.
- [11] W. Y. Wong, L. C. Ward, C. W. Fong, W. N. Yap, and L. Brown, "Anti-inflammatory γ - and δ -tocotrienols improve cardiovascular, liver and metabolic function in diet-induced obese rats," *European Journal of Nutrition*, vol. 56, no. 1, pp. 133–150, 2017.
- [12] H. Y. Peh, W. D. Tan, W. Liao, and W. F. Wong, "Vitamin E therapy beyond cancer: tocopherol versus tocotrienol," *Pharmacology & Therapeutics*, vol. 162, pp. 152–169, 2016.
- [13] B. Huang, Z. Cai, J. Zhang, and J. Xu, "An efficient solid-phase extraction-based liquid chromatography method to simultaneously determine diastereomers α -tocopherol, other tocopherols, and retinol isomers in infant formula," *Journal of Food Quality*, vol. 2021, Article ID 5591620, 8 pages, 2021.
- [14] B. Gleize, M. Steib, M. André, and E. Reboul, "Simple and fast HPLC method for simultaneous determination of retinol, tocopherols, coenzyme Q (10) and carotenoids in complex samples," *Food Chemistry*, vol. 134, no. 4, pp. 2560–2564, 2012.
- [15] M. Katsa, N. Papalouka, T. Mavrogianni et al., "Comparative study for the determination of fat-soluble vitamins in rice cereal baby foods using HPLC-DAD and UHPLC-APCI-MS/MS," *Foods*, vol. 10, no. 3, p. 648, 2021.
- [16] O. Heudi, M. J. Trisconi, and C. J. Blake, "Simultaneous quantification of vitamins A, D3 and E in fortified infant formulae by liquid chromatography-mass spectrometry," *Journal of Chromatography A*, vol. 1022, no. 1-2, pp. 115–123, 2004.
- [17] W. J. Shen, H. Wang, H. Y. Lu et al., "Determination of 8 vitamin E in vegetable oils by gas chromatography-mass spectrometry and their application in the identification of the authenticity of sesame oil," *Chinese Journal of Chromatography*, vol. 38, no. 05, pp. 595–599, 2020.
- [18] L. Olmo-GARCÍA, J. J. Polari, X. Li et al., "Deep insight into the minor fraction of virgin olive oil by using LC-MS and GC-MS multi-class methodologies," *Food Chemistry*, vol. 261, pp. 184–193, 2018.
- [19] S. H. Huang and L. T. Ng, "An improved high-performance liquid chromatographic method for simultaneous determination of tocopherols, tocotrienols and γ -oryzanol in rice," *Journal of Chromatography A*, vol. 1218, no. 29, pp. 4709–4713, 2011.
- [20] M. Podda, C. Weber, M. G. Traber, and L. Packer, "Simultaneous determination of tissue tocopherols, tocotrienols, ubiquinol, and ubiquinones," *Journal of Lipid Research*, vol. 37, no. 4, pp. 893–901, 1996.
- [21] E. D. Tsochatzis, K. Bladenopoulos, and M. Papageorgiou, "Determination of tocopherol and tocotrienol content of Greek barley varieties under conventional and organic cultivation techniques using validated reverse phase high-performance liquid chromatography method," *Journal of the Science of Food and Agriculture*, vol. 92, no. 8, pp. 1732–1739, 2012.
- [22] Y. B. Zheng, X. D. Pan, J. J. Xu, and B. F. Huang, "Simultaneous and quick determination of all eight vitamin E isomers in nuts by accelerated solvent extraction and hydrophilic interaction liquid chromatography," *Chinese Journal of Food Hygiene*, vol. 29, no. 6, pp. 698–702, 2017.
- [23] K. Knecht, K. Sandfuchs, S. E. Kulling, and D. Bunzel, "Tocopherol and tocotrienol analysis in raw and cooked vegetables: a validated method with emphasis on sample preparation," *Food Chemistry*, vol. 169, pp. 20–27, 2015.
- [24] P. Sookwong, K. Nakagawa, K. Murata, Y. Kojima, and T. Miyazawa, "Quantitation of tocotrienol and tocopherol in various rice brans," *Journal of Agricultural and Food Chemistry*, vol. 55, no. 2, pp. 461–466, 2007.
- [25] S. Strohschein, C. Rentel, T. Lacker, E. Bayer, and K. Albert, "Separation and identification of tocotrienol isomers by HPLC-MS and HPLC-NMR coupling," *Analytical Chemistry*, vol. 71, no. 9, pp. 1780–1785, 1999.
- [26] N. Grebenstein and J. Frank, "Rapid baseline-separation of all eight tocopherols and tocotrienols by reversed-phase liquid-chromatography with a solid-core pentafluorophenyl column and their sensitive quantification in plasma and liver," *Journal of Chromatography A*, vol. 1243, pp. 39–46, 2012.
- [27] S. Z. Chen, Y. C. Lei, S. Q. Huang, L. Gui, J. P. Gao, and X. Q. Cao, "Analysis of fatty acid composition and antioxidant effects in egg yolk oil," *Technology & Development of Chemical Industry*, vol. 51, pp. 30–33, 2022.
- [28] C. Y. Li, J. S. Ye, M. H. Wan, Q. Cheng, W. M. He, and J. Shi, "Optimization of reaction conditions for preparation of highly emulsifying egg yolk powder by TGase based on entropy weight method," *Genomics and Applied Biology*, vol. 39, no. 12, pp. 5526–5532, 2020.
- [29] *National Standard for Food Safety Determination of Vitamins A, D and E in Food*, National Health and Family Planning Commission of the People's Republic of China, China Food and Drug Administration (CFDA), 2016.
- [30] A. Gentili, F. Caretti, S. Bellante, S. Ventura, S. Canepari, and R. Curini, "Comprehensive profiling of carotenoids and fat-soluble vitamins in milk from different animal species by LC-DAD-MS/MS hyphenation," *Journal of Agricultural and Food Chemistry*, vol. 61, no. 8, pp. 1628–1639, 2013.
- [31] S. Q. Li, S. N. Chen, and Z. Li, "Cold saponification method for simultaneous determination of milk and milk products of vitamin by HPLC," *China Dairy Industry*, vol. 41, no. 10, pp. 40–42, 2013.

Research Article

Rapid Identification of Fupenzi (*Rubus chingii* Hu) and Its Adulteration by AuNP Visualization

Yuan Li ^{1,2}, Yixin Suo ³, Liuna Wei ³, Yue Zhang,² Youyou Wang ², Jiaxin Deng ³, Hengye Chen ³, Jian Yang ², Tiegui Nan ², Haiyan Fu ³, and Lanping Guo ^{1,2}

¹School of Traditional Chinese Medicine, Guangdong Pharmaceutical University, Guangzhou 510006, China

²State Key Laboratory Breeding Base of Dao-di Herbs, National Resource Center for Chinese Materia Medica, China Academy of Chinese Medical Sciences, Beijing 100700, China

³The Modernization Engineering Technology Research Center of Ethnic Minority Medicine of Hubei Province, School of Pharmaceutical Sciences, South-Central University for Nationalities, Wuhan 430074, China

Correspondence should be addressed to Lanping Guo; glp01@126.com

Received 11 November 2021; Revised 26 February 2022; Accepted 23 May 2022; Published 20 June 2022

Academic Editor: Nadica Maltar Strmečki

Copyright © 2022 Yuan Li et al. This is an open access article distributed under the Creative Commons Attribution License, which permits unrestricted use, distribution, and reproduction in any medium, provided the original work is properly cited.

Fupenzi (*Rubus chingii* Hu) is a dried and immature fruit in East China, which has effects of nourishing kidneys, solidifying essence, and otherwise. Because Fupenzi was often adulterated and replaced with inferior things, this paper had researched Fupenzi and its adulterant raspberry. A new type of visible sensor was constructed by using Au nanoparticles (AuNPs), which was modified by the surface-active agent and combined with the ultraviolet-visible (UV-vis) spectrum technology. It was found that the change in particle size after the interaction of AuNPs and adulterants will lead to color change. In this paper, the RGB (red, green, and blue) values of the solution were extracted to correlate the color with the concentration of adulterants, and the relationship between the absorption peak intensity and the concentration of adulterants was established. The results showed that the intensity of an absorption peak is related to adulteration concentration, and the color of the solution changed from red to gray as the particle size changed. The visual sensor constructed based on the above principle is a fast and precise method to detect adulteration with different concentrations, which has a potential application value in real-time and rapid detection of Fupenzi's quality.

1. Introduction

Food and drug safety has always been the focus of people's concern. At present, in the Chinese traditional medicine market, the phenomenon of adulteration of traditional Chinese medicine is not uncommon, especially some valuable medicinal materials such as saffron, *Panax ginseng*, and *Panax quinquefolium* L.. Therefore, the identification of adulteration of Chinese medicinal materials is an important problem that perplexes consumers and relevant regulatory departments; at present, it is very necessary to develop a technical method for rapid detection of adulteration of Chinese medicinal materials.

Fupenzi (*Rubus chingii* Hu), a wild raspberry in China, is usually picked when it is not ripe. Fupenzi has different

applications in the food and pharmaceutical industry because of its nutritional value and pharmacological activity. Fupenzi is rich in vitamins, amino acids, and mineral elements, which can be used to make fruit juice drinks and health products [1, 2]. So far, more than 235 chemical constituents have been isolated and identified from *R. chingii* [2]. These compounds include 15 triterpenoids, 15 diterpenoids, 18 flavonoids, 7 alkaloids, 95 volatile compounds, 5 coumarins, 9 steroids, 56 organic acids, and 15 other compounds [2], which have the pharmacological effects of reducing blood sugar and blood lipids [3], antitumor [4], antioxidation [5, 6], anti-aging [6], and anti-inflammation properties [7], so it has been used in traditional Chinese medicine for a long time. Reducing costs and increasing profits are the main reasons for the frequent adulteration in

the Chinese herbal medicine market, and Fupenzi is no exception. The adulteration way of Fupenzi in the market is mainly to use other plant materials with similar appearance but different or no effect as adulterants, in which raspberry (*Rubus corchorifolius* L. f.) is commonly used as Fupenzi adulteration. The adulteration of Fupenzi can not only harm the right of consumers and break the market orders but also cannot achieve the same therapeutic effect as Fupenzi. Thus, it is necessary to identify a detection method for Fupenzi adulteration.

There are a variety of identification methods and techniques for food and drugs. These techniques include analytical, physical, chemical, and most recent DNA-based molecular techniques [8]. In the aspects of qualitative and quantitative analysis and quality control of compounds, chromatographic techniques such as high performance liquid chromatography (HPLC), gas chromatography (GC), and chromatography-mass spectrometry technology are often used. Generally, those chromatography and mass spectrometry technologies are often used in metabonomics. For example, by detecting as many of these small molecules as possible, untargeted metabolomics approaches enable a holistic analysis in comparing complex samples [9], and it is an accurate method to identify the adulteration. In addition to chromatography and mass spectrometry technology, the spectroscopic technique is a common method to detect adulterants as well. Universal spectral techniques include near-infrared (NIR) and mid-infrared (MIR) spectroscopies, ultraviolet-visible (UV-vis) spectrum, and fluorescence spectrum. These spectral techniques are often used to detect adulteration of edible oil [10], honey [11, 12], and rare medicinal materials [13, 14]. In addition, with the development of molecular biology techniques, many molecular biology techniques have been applied to identify the adulteration of food and drugs. For example, the adulteration identification of food and drugs such as plant oil [15] and *Fritillariae cirrhosae* bulbus [16] was realized by using DNA barcoding technology. Except for those methods, a stable isotope technique can also be used to identify adulterants [17, 18]. To improve the sensitivity of identification, chemometrics methods are often used in combination with the aforementioned methods. Such as using near-infrared (NIR) spectroscopy and mid-infrared (MIR) spectroscopy combined with principal component analysis (PCA), partial least squares discriminant analysis (PLS-DA), and partial least squares regression (PLS-R) to identify saffron and its adulteration [14]. Vieira et al. [19] used Fourier transform near-infrared (FT-NIR) and PLS-DA to establish a separate model to distinguish adulterated extravirgin olive oil samples.

Although these methods can be used to identify food quality sensitively, there are still some shortcomings. Chromatography, spectroscopy, and molecular biology techniques rely on large-scale instruments and time-consuming sample preparations, and operators should possess a high level of skill for those instruments. On the basis of these methods, chemometrics combined with nanomaterial methods came into being. In recent years, new methods based on nanomaterials combined with spectroscopy have

been applied to fruit juice adulteration, drug adulteration, and food corruption [20–22]. These new methods can distinguish adulterants effectively and have application prospects in the future. In recent years, by integrating metal nanoparticles into the detection process, an ultraviolet-visible (UV-Vis) spectrum has considerably improved the application of ultraviolet detection of various chemical substances [23–26]. It has been applied in the detection of target analyses with high selectivity and high sensitivity, and the performance has been improved to a level comparable to that of precision instruments [27]. The surface plasmon resonance (SPR) effect significantly exists in nanonoble metal materials, and it occurs when the vibration frequency of the metal free conduction electron is equal to that of the incident light. SPR absorption of Au nanoparticles (AuNPs) is extremely sensitive to their size, shape, surrounding media, and interparticle distances [28]. With the change in the shape and size of AuNPs and the physical properties of the environment medium, the position of the plasmon resonance absorption peak is different, and the accumulation of AuNPs results in red shift of SPR, which changes the solution from red to blue or gray [28, 29]. For example, Rohit et al. [30], based on the color change in AuNPs from red to blue, developed a colorimetric sensor for the determination of quinalphos in water and food samples. At present, a AuNP colorimetric sensor is widely used in the detection of antibiotics, pesticide residues, heavy metals, and so on [29, 31, 32].

Since gold nanoparticles have SPR characteristics and color changes can be seen intuitively by naked eyes, we choose AuNPs as a colorimetric sensor in this article. At present, there is no report on the application of AuNP colorimetric sensors in the adulteration identification of Fupenzi. In our research study, Fupenzi and its adulterants were quantitatively characterized according to the color change characteristics of AuNPs, and the detection results were compared and verified by UV-Vis spectroscopy. The results showed that the detection method was consistent with the results of UV-Vis spectroscopy, which proved that the method of Fupenzi adulteration rapid detection by AuNPs combined with the RGB value was feasible. The method could achieve simple, rapid, efficient, and sensitive detection of the Fupenzi adulteration effect. And it can be applied not only to the rapid identification of adulteration of other Chinese medicinal materials but also to a variety of fields, including food, biometric identification and drug quality control.

2. Experiment

2.1. Materials, Reagents, and Equipment. A total of 18 batches of Fupenzi were purchased from Zhejiang, Shanghai, Anhui, Guizhou, Guangdong, Guangxi, Chongqing, Fujian, Sichuan, and Yunan. Adulterated raspberries (*Rubus corchorifolius* L. f.) were purchased from a market in Wuhan, Hubei. Anhydrous methanol, anhydrous ethanol, and chloroauric acid were purchased from Yongda Chemical Reagent Co. Ltd (Tianjin, China). A microporous filtration membrane was purchased from Jiaying Haining Kono

Filtration Equipment Co. Ltd (Zhejiang, China). Sodium borohydride was purchased from Hongrui Chemical Co. Ltd (Shanghai, China). All the reagents used in the experiment are analytically pure, and the water used in the experiment is ultrapure water. A buckle-type small grinder was purchased from Guangzhou Xulang Machinery Equipment Co. Ltd (Guangdong, China). A total of 50 and 100 mesh screens were purchased from Xinxiang Jinhe Machinery Co. Ltd (Henan, China). The KQ-500DE CNC ultrasonic cleaner was purchased from Kunshan Ultrasonic Instrument Co. Ltd (Jiangsu, China). The TD4 small desktop centrifuge was purchased from Hetian Scientific Instrument Co. Ltd (Shanghai, China). Analytical ultrapure water equipment was purchased from Shanghai Moller Scientific Instrument Co. Ltd (Shanghai, China). The BSA224S analytical balance was purchased from Sedolis Instrument System Co. Ltd (Beijing, China). The UV-5800 (PC) ultraviolet-visible spectrophotometer was purchased from Yuanxi Instrument Co. Ltd (Shanghai, China). The high-resolution transmission electron microscopy TF20 Joel 2100 F microscope was purchased from Japan Electronics Corporation Company.

2.2. Preparation of AuNPs. The synthesis of AuNPs was performed in the previous report and modified in [33]. 2 mL chloroauric acid (1%) was taken into a round bottom flask, 6.5 mL water was added and stirred at room temperature for 15 min, 1.5 mL 0.1 mol·L⁻¹ cetyltrimethyl ammonium bromide (CTAB) was added, and 3 mL sodium borohydride (0.4 mol·L⁻¹) was slowly added under the stirring state after 10 min and continued stirring for 3 h at room temperature. Finally, the color of the solution changed from light yellow to dark red.

2.3. Preparation of Pure and Adulterated Fupenzi. Fupenzi and adulterants were crushed in a grinder, and the powder was passed through a 50 mesh sieve for reserve. A 0.1 g Fupenzi powder which was shifted was taken and put into a flask, and we added 20 mL boiling water into Fupenzi, soaked for 20 min, kept the temperature at 50°C and ultrasonic for 30 min, centrifuged for 10 min at 4000 r min⁻¹, took the supernatant, and filtered through a 0.22 μm microporous membrane to obtain Fupenzi and adulterant stock solutions. Similarly, the Fupenzi powder was mixed with different proportions of the adulterated powder, and the same extraction method was used to obtain the Fupenzi mixture of 1%, 2%, 5%, 10%, and 20% adulterated powders.

2.4. Condition Optimization. The influence of the pH, reaction time, and reaction temperature on the ultraviolet absorbance was investigated. There are three parallel tests for each condition optimization. When AuNPs were mixed with the adulterants, the pH value of the solution was changed to observe the ultraviolet absorbance peak intensity of the solution at different pH values. The gradient of the reaction time was set at 0, 5, 10, 20, 30, 45, and 60 min, respectively; and the temperature of the reaction was set at 5, 15, 25, 35, 45, 55, 65, 75, 85, and 95°C, respectively.

2.5. FT-IR Spectral Analysis. In order to characterize the functional groups, the prepared AuNPs, the AuNPs-Fupenzi mixture, and the AuNPs-adulterant mixture were ground and pressed with the KBr powder and placed at wavenumbers of 4000 to 400 cm⁻¹ for FT-IR analysis.

2.6. Detection of Fupenzi Adulteration. In order to quickly detect the raspberry adulteration, 1 mL of Fupenzi and the stock solution of the adulteration were added into the colorimetric dish to detect and record the absorbance. Then, the absorbance of the Fupenzi mixture was detected. After that, 900 μL mixture and 100 μL AuNPs were added into the cuvette, the combined mixture was kept for 1 min, and its absorbance was detected. 900 μL ultrapure water was mixed with 100 μL AuNPs, which was left standing for 1 min as in the blank control group. Finally, transmission electron microscopy (TEM) was used to observe the diameter of the different concentrations of the AuNP mixture. Then, the RGB value was applied to obtain the color information of the different concentrations of the AuNP mixture solution. The flowchart of experimental steps is shown in Figure 1.

Through UV-Vis spectrum, the limit of detection (LOD) was used to measure the low detection limit of the detection method. The LOD is expressed as the following function:

$$\text{LOD} = \frac{3.3\delta}{S}, \quad (1)$$

where δ is the RSD of blank samples and S is the slope of the calibration curve.

2.7. Data Processing. The UV-vis spectrum data, FT-IR data, and other statistical analyses were plotted by Origin 2018 (Massachusetts, USA). Data obtained by TEM were imported into nanomeasure particle size measurement software (Laboratory of Surface Chemistry and Catalysis, Department of Chemistry, Fudan University). The RGB values were extracted by Microsoft Office PowerPoint 2019 (Microsoft, USA).

3. Results and Discussion

3.1. Condition Optimization. According to the maximum absorption peak of the ultraviolet absorption spectrum, the pH value, reaction time, and temperature of the solution were optimized. It can be seen that when the pH value of the solution was 8–10, the absorbance was stable (Figure 2(a)). Though the reaction time was negatively correlated with the absorption intensity, the absorbance changed slowly and leveled off with the increase in time after 20 min (Figure 2(b)). However, when the reaction temperature rose gradually, the maximum absorption peak intensity did not change significantly before 65°C. However, when the reaction temperature was greater than 65°C, the absorbance showed an overall upward trend (Figure 2(c)).

3.2. UV-Vis Spectra of Fupenzi and AuNP Mixtures. The UV-vis absorption spectra of the Fupenzi stock solution,

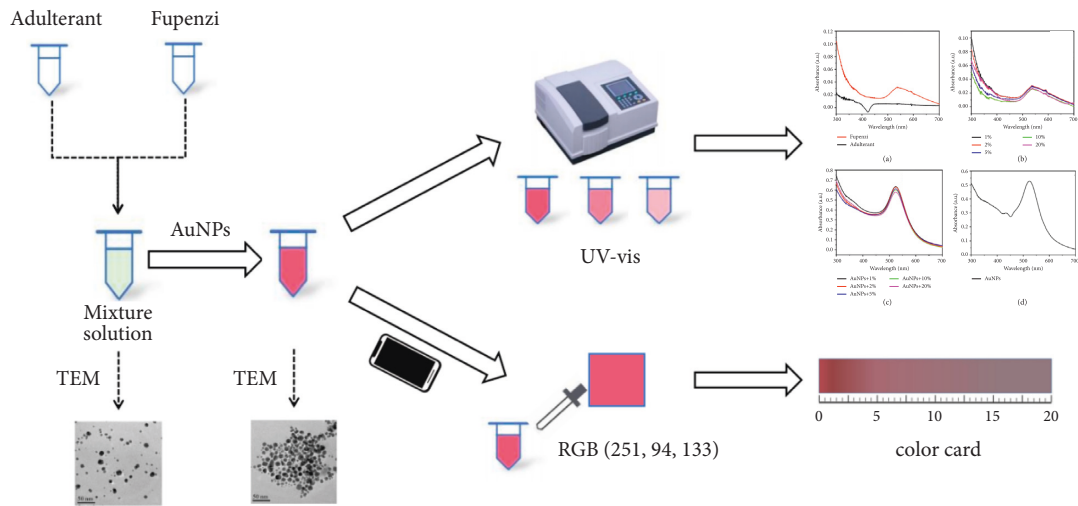


FIGURE 1: The flowchart of adulteration detection of Fupenzi.

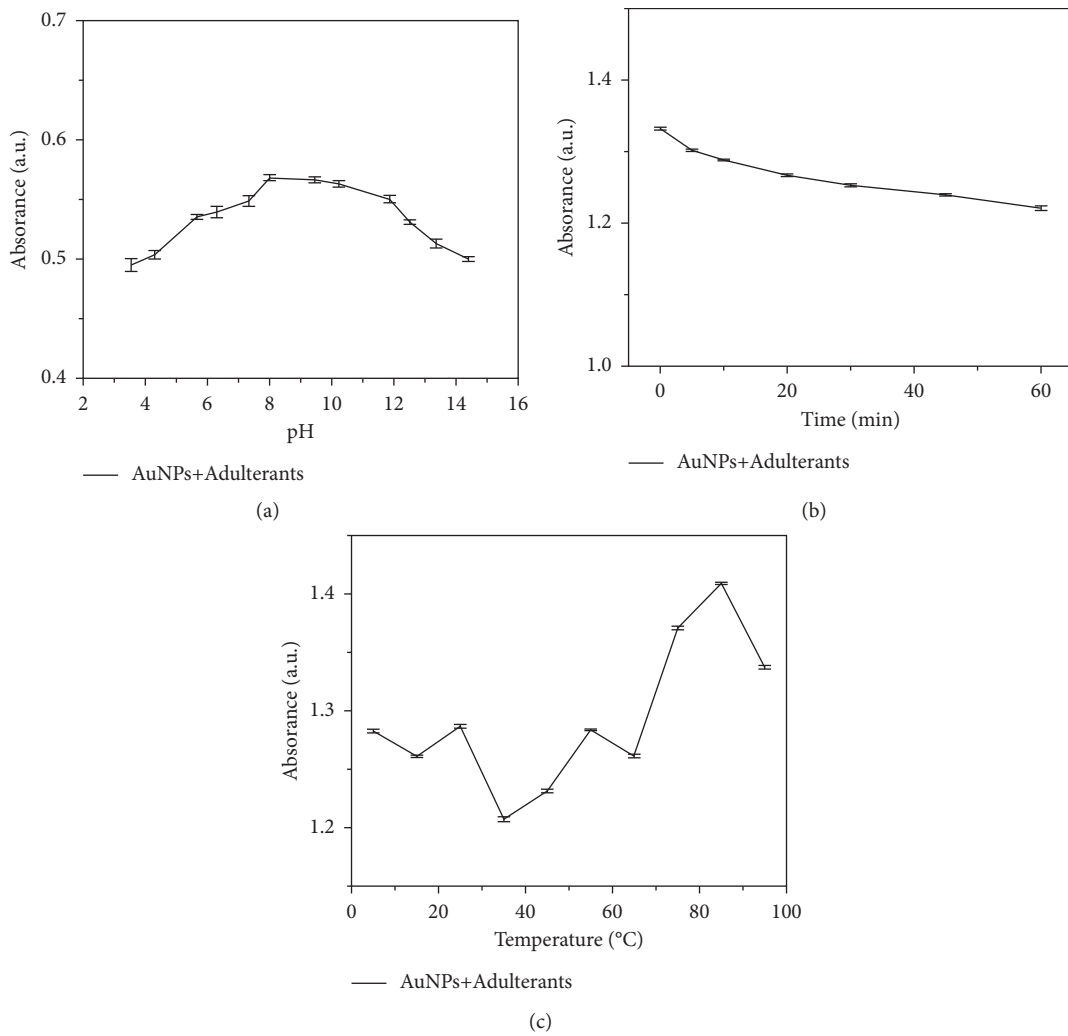


FIGURE 2: Condition optimization. (a) The pH value and absorbance of solution during reaction. (b) The reaction time and absorbance of solution during reaction. (c) The reaction temperature and absorbance of solution during reaction.

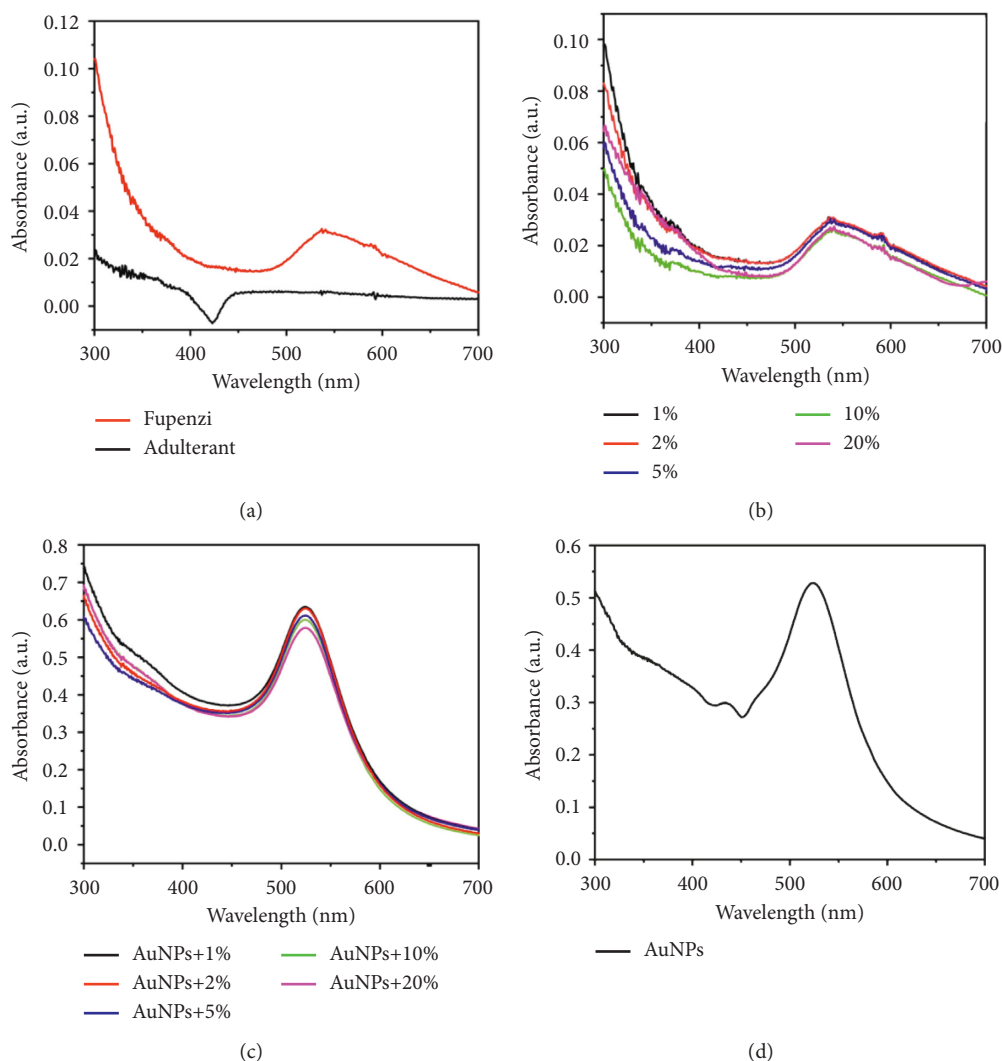


FIGURE 3: UV-vis spectrum of Fupenzi, AuNPs, and adulterants. (a) UV-vis spectrum of raspberry and adulterants; (b) UV-vis spectrum of mixtures with different concentrations; (c) UV-vis spectrum of AuNPs combined with mixtures of different concentrations; (d) AuNP UV-vis spectrum in ultrapure water.

adulterated stock solution, AuNPs, and mixtures of various concentrations are shown in Figure 3. It can be seen that the Fupenzi stock solution has a characteristic absorption peak at 540 nm, while the adulteration stock solution has almost no absorption peak (Figure 3(a)). When the Fupenzi stock solution was added with a small amount of adulterants, the absorption peak did not change and the shape of the peak did not change significantly with the increase in the proportion of adulterants (Figure 3(b)). However, the absorbance of the mixture decreased after the addition of AuNPs, and compared with that before the addition of AuNPs, it could be seen that the absorbance gradually decreased with the increase in the proportion of adulterants (Figure 3(c)). The absorbance of AuNPs and the concentration of the mixture showed a good linear relationship in the range of 1%–20%. The formula for the standard curve is $y = -0.0034x + 0.6366$, $R^2 = 0.9962$. By setting a blank control group (Figure 3(d)), it can be found that the intensity of the absorption peak of AuNPs changed significantly after the combination of the Fupenzi stock solution,

which can be accurately distinguished by different concentrations from 1% to 20%. In addition, according to formula (1), the LOD of this method can be calculated. The LOD of the method that we proposed is 0.2%.

In order to correlate the concentration with the color, the visualization experiment in the reagent bottle was carried out. In the course of the experiment, it was found that the color of the mixed solution of AuNPs and Fupenzi without adulterants was red. With the increasing proportion of adulterants, the color of solution gradually changed from red to gray, and the proportion of the adulterants was 1%, 2%, 5%, 10%, and 20%, respectively, (Figure 4(a)). This shows that the relationship between absorbance and adulterant concentrations can be transformed into the relationship between color and adulterant concentrations.

3.3. FT-IR Spectral Analysis. The functional groups in Fupenzi and its adulterants were characterized by infrared

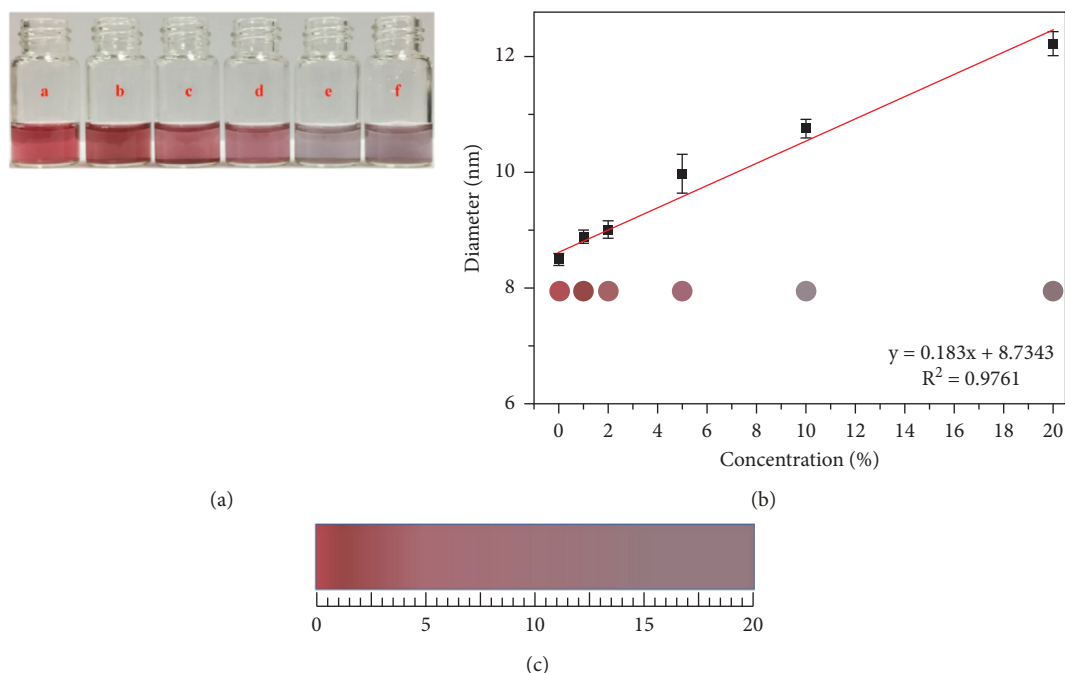


FIGURE 4: The relationship between concentration of different adulterants and particle size of AuNPs and solution color. (a) A–F represent the color of the AuNP mixture solution at the concentration of 0%, 1%, 2%, 5%, 10%, and 20% adulterants, respectively. (b) The linear fitting diagram of the concentration of different adulterants against the particle size of AuNP mixtures. (c) According to the relationship between the concentration of different adulterants and the color of the solution-produced color card. ($R^2 = 0.9761$).

spectroscopy, the interaction of AuNPs with them was studied, and the results are shown in Figure 5. The strong and wide band near 3380 cm^{-1} is O-H stretching vibration, and the band at 2920 cm^{-1} is C-H stretching vibration. The absorption peak at 1730 cm^{-1} is attributed to the stretching vibration of C=O [34]. The bands of 1640 and 1470 cm^{-1} are attributable to the C=O asymmetric and symmetric stretching vibration [35]. The strong absorption band of 1190 cm^{-1} is due to the O-H out-of-plane bending vibration. The absorption bands of 960 and 920 cm^{-1} were represented rhamnogalacturonan I and D-glucopyranosyl, respectively, [34, 36]. These groups indicated that there were abundant phenols and carboxylic acid compounds in Fupenzi and its adulterants, such as ellagic acid and its glycoside derivatives [1]. When these phenolic acid compounds combined with the negatively charged CTAB-AuNPs, AuNPs were aggregated (Figure 5).

3.4. TEM Images of AuNPs. In order to verify the mechanism of color change, we used TEM to observe particle size change. All the particles in the TEM image were measured diameter through the Nano Measure particle size measurement software. As can be seen that the mixed solution of AuNPs and Fupenzi without adulterants was well dispersed with the mean particle size of 7.5 nm (Figure 6(a)). However, the AuNPs were significantly aggregated with the mean particle size of 12.3 nm when the concentration of adulterate is 20% (Figure 6(f)). With the increase of the concentration of adulterants, the aggregation degree of AuNPs increased and the particle size became larger, resulting in the color of

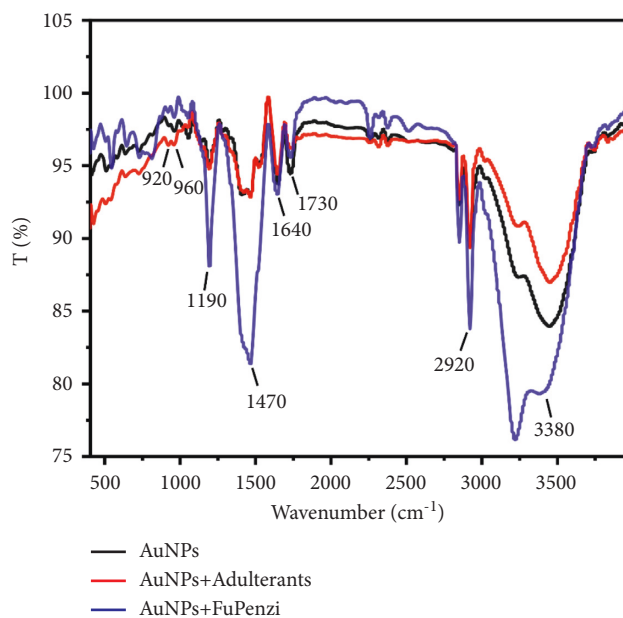


FIGURE 5: FT-IR spectrum of Fupenzi, adulterants, and AuNP mixtures.

gold nanoparticles from red to grey. The standard curve was drawn according to the relationship between the particle size of AuNPs and the concentration of adulterants (Figure 4(b)), which indicated that there was a certain linear relationship between the particle size of AuNPs and the concentration of adulterants ($y = 0.2026x + 8.3405$, $R^2 = 0.9761$). The possible

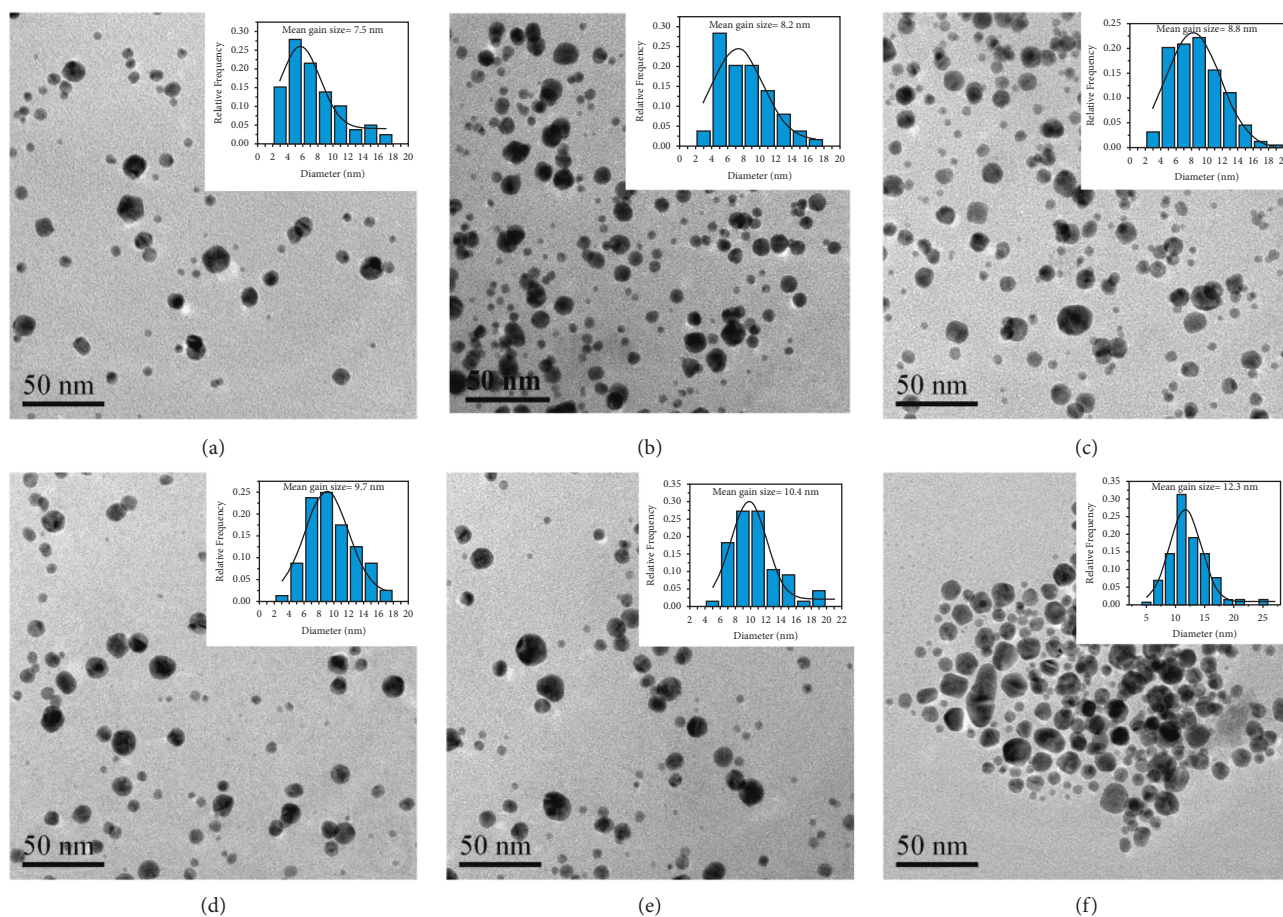


FIGURE 6: TEM images and frequency histograms of AuNP mixtures with different concentrations (a–f) Adulterant concentrations of 0%, 1%, 2%, 5%, 10%, and 20%, respectively).

reason for this phenomenon is the positive charge of CTAB modified AuNPs, and there were negatively charged acids and compounds with carboxyl and hydroxyl groups in raspberry. These negatively charged compounds combined with CTAB with ammonium state to aggregate AuNPs and increase the particle size. At the same time, the color of solution became red to gray with the increase in the AuNP particle diameter.

3.5. Identification of Fupenzi Adulteration. The color of AuNPs changed with the particle size, and it can be speculated that the adulteration of raspberry can be judged by the color of AuNPs. Based on the relationship between the solution color and adulterant concentration, we made the colorimetric card of the Fupenzi mixture solution of AuNPs with different concentrations of adulterants (Figure 4(c)). We introduced the concept of the RGB color mode to characterize the color of solution. RGB (red, green, and blue) is applied in many areas, such as electronics, medicine, and food [37–39]. In order to achieve the purpose of rapid detection, we needed to eliminate instruments. The pipette function was added on the basis of colorimetry to achieve more portable quantitative analysis, in which the qualitative color changes were converted into the quantitative RGB

values. Therefore, the RGB values could be used to bridge the color variation with the mixture concentration.

The average RGB values (any 10 points) of the known concentration of adulteration with AuNP Fupenzi mixtures were measured to make a colorimetric card by using the pipette function using Microsoft Office PowerPoint 2019 software. Secondly, after obtaining the average RGB values (any 10 points) of the unknown sample photos in the same way, similar RGB values were searched and located in the color comparison card. Finally, quantitative information could be obtained by converting RGB values into mixture concentrations.

In order to verify the accuracy of the colorimetric method, two AuNP samples (5% concentration and 10% concentration of the mixture) were selected for testing. The two samples were treated under the same conditions, and the average RGB values were (156, 109, and 118) and (157, 145, and 149). Similar RGB values were found in the colorimetric card (155, 109, and 119) and (158, 146, and 151). The concentrations of the mixture were $(5.02 \pm 0.32)\%$ and $(9.74 \pm 0.52)\%$ through calculation, respectively, and the recovery rate was good. Then, mixtures containing 5% and 10% adulterants were analyzed by UV-vis. $100 \mu\text{L}$ AuNPs and $900 \mu\text{L}$ 5% mixture solution were added into the colorimetric dish to detect the absorbance. It can be found that

TABLE 1: The concentration of adulterants in mixtures containing AuNPs was determined by colorimetry, and the results were verified by UV-vis.

Sample	Method	Adulteration concentration (%)	Actual adulteration concentration \pm standard deviation (%)	RSD (%)	Recovery (%)
1	Colorimetry	5.0	5.02 ± 0.32	6.3	99.6
2		10.0	9.74 ± 0.52	5.2	102.7
3	UV-vis	5.0	5.06 ± 0.07	1.4	98.8
4		10.0	9.94 ± 0.18	1.8	100.6

the mixture concentrations of the two samples quantitatively obtained by the UV-vis spectrophotometer are $(5.06 \pm 0.07)\%$ and $(9.94 \pm 0.18)\%$, respectively. The results are shown in Table 1. By comparison, it can be found that the quantitative results of colorimetry and UV-vis spectroscopy are similar, but the colorimetric method does not rely on large instruments and can achieve real-time on-site identification, and the operation is more convenient and rapid.

4. Conclusion

In this paper, a new type of a visual sensor was constructed by using surfactant-modified AuNPs as sensing materials, combined with UV-vis spectroscopy, which was successfully applied to the identification of Fupenzi adulteration. The changes in the solution color and absorbance caused by AuNPs can reflect the degree of Fupenzi adulteration. After adding AuNPs, the absorbance was linearly correlated with the concentration of adulterants, and the range of detection is 0%–20%. The correlation coefficient between the particle size of AuNPs and the concentration of adulterants was 0.9761, which indicated that the adulterants interacted with AuNPs. The relationship between the mixture concentration and AuNP color was constructed according to RGB values. Compared with UV-vis spectroscopy, the accuracy of the quantitative results is almost the same, and the accuracy and effectiveness of this method have been confirmed. Nano-labeling technology shows a broad application prospect in the on-site rapid detection of adulteration of traditional Chinese medicine. However, because of the complexity of the components of traditional Chinese medicine, there are still some challenges in the detection of traditional Chinese medicine. For example, the content of some characteristic chemical components in traditional Chinese medicine will change with the extension in storage time and resulting in false positive results, which will have certain interference in the identification of traditional Chinese medicine. To solve the problem of interference component diversity, the next step of this paper is to establish a reliable detection standard by studying the differences in Fupenzi components from different producing areas, which lays a foundation for adulteration analysis of traditional Chinese medicine products on the spot and ensuring the quality and safety of traditional Chinese medicine.

Data Availability

The data used to support the findings of this study are included in the article.

Disclosure

Yuan Li and Yixin Suo should be considered joint first author.

Conflicts of Interest

The authors declare they have no conflicts of interest regarding the publication of this article.

Authors' Contributions

Yuan Li was involved in conceptualization and was responsible for writing, reviewing and editing the manuscript. Yixin Suo was involved in data curation and investigation. Liuna Wei was involved in data curation and investigation and wrote the manuscript. Yue Zhang, Youyou Wang, and Jiabin Deng were responsible for investigation. Hengye Chen was responsible for Methodology. Jian Yang was responsible for resources and supervision. Tiegui Nan was responsible for supervision. Haiyan Fu was involved in conceptualization, funding acquisition and supervision. Lanping Guo was responsible for resources, supervision, conceptualization, and funding acquisition.

Acknowledgments

This work was supported by the National Key R&D Program of China (Grant nos. 2020YFC1712700 and 2017YFC1700701), Scientific and Technological Innovation Project of the China Academy of Chinese Medical Sciences (Grant nos. CI2021A04005 and CI2021A01809), the Fundamental Research Funds for the Central Public Welfare Research Institutes (Grant no. ZZXT201906), and the Key Project at Central Government Level: the Ability Establishment of Sustainable Use for Valuable Chinese Medicine Resources (Grant no. 2060302).

References

- [1] J.-Y. Sheng, S.-Q. Wang, K.-H. Liu et al., "Rubus chingii Hu: an overview of botany, traditional uses, phytochemistry, and pharmacology," *Chinese Journal of Natural Medicines*, vol. 18, no. 6, pp. 401–416, 2020.
- [2] G. Yu, Z. Luo, W. Wang, Y. Li, Y. Zhou, and Y. Shi, "Rubus chingii Hu: a review of the phytochemistry and pharmacology," *Frontiers in Pharmacology*, vol. 10, p. 799, 2019.
- [3] Y. Chen, Z. Chen, Q. Guo et al., "Identification of ellagittannins in the unripe fruit of *Rubus chingii* Hu and evaluation of its potential antidiabetic activity," *Journal of Agricultural and Food Chemistry*, vol. 67, no. 25, pp. 7025–7039, 2019.

- [4] K. Li, M. Zeng, Q. Li, and B. Zhou, "Identification of polyphenolic composition in the fruits of *Rubus chingii* Hu and its antioxidant and antiproliferative activity on human bladder cancer T24 cells," *Journal of Food Measurement and Characterization*, vol. 13, no. 1, pp. 51–60, 2018.
- [5] Y. He, S. Jin, Z. Ma et al., "The antioxidant compounds isolated from the fruits of Chinese wild raspberry *Rubus chingii* Hu," *Natural Product Research*, vol. 34, no. 6, pp. 872–875, 2020.
- [6] Y. Chen, L. Xu, Y. Wang et al., "Study on the active polyphenol constituents in differently colored *Rubus Chingii* Hu and the structure-activity relationship of the main ellagitannins and ellagic acid," *Lebensmittel-Wissenschaft & Technologie*, vol. 121, Article ID 108967, 2020.
- [7] T.-T. Zhang, M. Wang, L. Yang, J.-G. Jiang, J.-W. Zhao, and W. Zhu, "Flavonoid glycosides from *Rubus chingii* Hu fruits display anti-inflammatory activity through suppressing MAPKs activation in macrophages," *Journal of Functional Foods*, vol. 18, pp. 235–243, 2015.
- [8] S. Bansal, A. Singh, M. Mangal, A. K. Mangal, and S. Kumar, "Food adulteration: sources, health risks, and detection methods," *Critical Reviews in Food Science and Nutrition*, vol. 57, no. 6, pp. 1174–1189, 2017.
- [9] E. D. Wallace, D. A. Todd, J. M. Harnly, N. B. Cech, and J. J. Kellogg, "Identification of adulteration in botanical samples with untargeted metabolomics," *Analytical and Bioanalytical Chemistry*, vol. 412, no. 18, pp. 4273–4286, 2020.
- [10] S. Popa, M. S. Milea, S. Boran et al., "Rapid adulteration detection of cold pressed oils with their refined versions by UV-Vis spectroscopy," *Scientific Reports*, vol. 10, no. 1, Article ID 16100, 2020.
- [11] F. Huang, H. Song, L. Guo et al., "Detection of adulteration in Chinese honey using NIR and ATR-FTIR spectral data fusion," *Spectrochimica Acta Part A: Molecular and Biomolecular Spectroscopy*, vol. 235, Article ID 118297, 2020.
- [12] M. F. González, E. E. Bellido, L. G. Cueto, M. Palma, C. G. Barroso, and G. F. Barbero, "Rapid quantification of honey adulteration by visible-near infrared spectroscopy combined with chemometrics," *Talanta*, vol. 188, pp. 288–292, 2018.
- [13] J. Yang, C. Yin, X. Miao, X. Meng, Z. Liu, and L. Hu, "Rapid discrimination of adulteration in *Radix Astragali* combining diffuse reflectance mid-infrared Fourier transform spectroscopy with chemometrics," *Spectrochimica Acta Part A: Molecular and Biomolecular Spectroscopy*, vol. 248, Article ID 119251, 2021.
- [14] A. Amirvaresi, N. Nikounezhad, M. Amirahmadi, B. Daraei, and H. Parastar, "Comparison of near-infrared (NIR) and mid-infrared (MIR) spectroscopy based on chemometrics for saffron authentication and adulteration detection," *Food Chemistry*, vol. 344, Article ID 128647, 2021.
- [15] A. O. Uncu and A. T. Uncu, "A barcode-DNA analysis method for the identification of plant oil adulteration in milk and dairy products," *Food Chemistry*, vol. 326, Article ID 126986, 2020.
- [16] Q. Chen, X. Wu, and D. Zhang, "Comparison of the abilities of universal, super, and specific DNA barcodes to discriminate among the original species of *fritillariae cirrhosae* bulbus and its adulterants," *PLoS One*, vol. 15, no. 2, Article ID e0229181, 2020.
- [17] K. El Hawari, M. Al Iskandarani, F. Jaber et al., "Evaluation of honey authenticity in Lebanon by analysis of carbon stable isotope ratio using elemental analyzer and liquid chromatography coupled to isotope ratio mass spectrometry," *Journal of Mass Spectrometry*, vol. 56, no. 6, Article ID e4730, 2021.
- [18] M. Perini, L. Strojnik, M. Paolini, and F. Camin, "Gas chromatography combustion isotope ratio mass spectrometry for improving the detection of authenticity of grape must," *Journal of Agricultural and Food Chemistry*, vol. 68, no. 11, pp. 3322–3329, 2020.
- [19] L. S. Vieira, C. Assis, M. E. L. R. de Queiroz, A. A. Neves, and A. F. de Oliveira, "Building robust models for identification of adulteration in olive oil using FT-NIR, PLS-DA and variable selection," *Food Chemistry*, vol. 345, Article ID 128866, 2021.
- [20] L. Xu, L. Wei, Q. Shi, C. Cai, H.-Y. Fu, and Y.-B. She, "Non-targeted detection of multiple frauds in orange juice using double water-soluble fluorescence quantum dots and chemometrics," *Food Analytical Methods*, vol. 12, no. 11, pp. 2614–2622, 2019.
- [21] L. Xu, Q. Shi, D. Lu et al., "Simultaneous detection of multiple frauds in kiwifruit juice by fusion of traditional and double-quantum-dots enhanced fluorescent spectroscopic techniques and chemometrics," *Microchemical Journal*, vol. 157, Article ID 105105, 2020.
- [22] Z. Mohammadi and S. M. Jafari, "Detection of food spoilage and adulteration by novel nanomaterial-based sensors," *Advances in Colloid and Interface Science*, vol. 286, Article ID 102297, 2020.
- [23] C. Karami, A. Alizadeh, M. A. Taher, Z. Hamidi, and B. Bahrami, "UV-visible spectroscopy detection of iron (III) ion on modified gold nanoparticles with a hydroxamic acid," *Journal of Applied Spectroscopy*, vol. 83, no. 4, pp. 687–693, 2016.
- [24] S. Pandey and K. K. Nanda, "Au nanocomposite based chemiresistive ammonia sensor for health monitoring," *ACS Sensors*, vol. 1, no. 1, pp. 55–62, 2015.
- [25] S. Pandey, G. K. Goswami, and K. K. Nanda, "Green synthesis of biopolymer-silver nanoparticle nanocomposite: an optical sensor for ammonia detection," *International Journal of Biological Macromolecules*, vol. 51, no. 4, pp. 583–589, 2012.
- [26] M. Hassanisaadi, G. H. S. Bonjar, A. Rahdar, S. Pandey, A. Hosseinipour, and R. Abdolshahi, "Environmentally safe biosynthesis of gold nanoparticles using plant water extracts," *Nanomaterials*, vol. 11, no. 8, p. 2033, 2021.
- [27] L. B. Roa, J. Hill, S. Notman et al., "Analogues with fluorescent leaving groups for screening and selection of enzymes that efficiently hydrolyze organophosphorus nerve agents," *Journal of Medicinal Chemistry*, vol. 49, no. 1, pp. 246–255, 2006.
- [28] E. Deymehkar, M. A. Taher, C. Karami, and A. Arman, "Synthesis of SPR nanosensor using gold nanoparticles and its application to copper (II) determination," *Silicon*, vol. 10, no. 4, pp. 1329–1336, 2017.
- [29] C. Karami, S. Y. Mehr, E. Deymehkar, and M. A. Taher, "Naked eye detection of Cr^{3+} and Co^{2+} ions by gold nanoparticle modified with azomethine," *Plasmonics*, vol. 13, no. 2, pp. 537–544, 2017.
- [30] J. V. Rohit, H. Basu, R. K. Singhal, and S. K. Kailasa, "Development of p-nitroaniline dithiocarbamate capped gold nanoparticles-based microvolume UV-vis spectrometric method for facile and selective detection of quinalphos insecticide in environmental samples," *Sensors and Actuators B: Chemical*, vol. 237, pp. 826–835, 2016.
- [31] J. Sun, J. Ge, W. Liu, Z. Fan, H. Zhang, and P. Wang, "Highly sensitive and selective colorimetric visualization of streptomycin in raw milk using Au nanoparticles supramolecular assembly," *Chemical Communications*, vol. 47, no. 35, p. 9888, 2011.
- [32] R. Zhang, N. Li, J. Sun, and F. Gao, "Colorimetric and phosphorimetric dual-signaling strategy mediated by inner

- filter effect for highly sensitive assay of organophosphorus pesticides,” *Journal of Agricultural and Food Chemistry*, vol. 63, no. 40, pp. 8947–8954, 2015.
- [33] Y. Xia, X. Wu, J. Zhao et al., “Three dimensional plasmonic assemblies of AuNPs with an overall size of sub-200 nm for chemo-photothermal synergistic therapy of breast cancer,” *Nanoscale*, vol. 8, no. 44, Article ID 18692, 2016.
- [34] Y. Chen, Y. Wang, L. Xu et al., “Ultrasound-assisted modified pectin from unripe fruit pomace of raspberry (*Rubus chingii* Hu): structural characterization and antioxidant activities,” *Lebensmittel-Wissenschaft & Technologie*, vol. 134, Article ID 110007, 2020.
- [35] H. Ke, T. Bao, and W. Chen, “Polysaccharide from *Rubus chingii* Hu affords protection against palmitic acid-induced lipotoxicity in human hepatocytes,” *International Journal of Biological Macromolecules*, vol. 133, pp. 1063–1071, 2019.
- [36] Y. Chen, L. Xu, Y. Wang, Z. Chen, M. Zhang, and H. Chen, “Characterization and functional properties of a pectin/tara gum based edible film with ellagitannins from the unripe fruits of *Rubus chingii* Hu,” *Food Chemistry*, vol. 325, Article ID 126964, 2020.
- [37] T.-T. Wang, C. k. Lio, H. Huang et al., “A feasible image-based colorimetric assay using a smartphone RGB camera for point-of-care monitoring of diabetes,” *Talanta*, vol. 206, Article ID 120211, 2020.
- [38] J. Yang and Y. Xu, “Prediction of fruit quality based on the RGB values of time-temperature indicator,” *Journal of Food Science*, vol. 86, no. 3, pp. 932–941, 2021.
- [39] S. Hong, D.-W. Zheng, Q.-L. Zhang et al., “An RGB-emitting molecular cocktail for the detection of bacterial fingerprints,” *Chemical Science*, vol. 11, no. 17, pp. 4403–4409, 2020.

Research Article

Determining the Geographical Origin of Fuji Apple from China by Multivariate Analysis Based on Soluble Sugars, Organic Acids, and Stable Isotopes

Hui Zhang ¹, Jiyun Nie ², Zhaoguo Tong,³ Jing Li,¹ An Li,⁴ Youming Shen,¹ Jia Zhang,¹ and Lixue Kuang¹

¹Institute of Pomology, Chinese Academy of Agricultural Sciences (CAAS), Laboratory of Quality and Safety Risk Assessment for Fruit, Quality Inspection and Test Center for Fruit and Nursery Stocks, Ministry of Agriculture and Rural Affairs, Xingcheng 125100, China

²College of Horticulture, Qingdao Agricultural University, Laboratory of Quality & Safety Risk Assessment for Fruit (Qingdao), Ministry of Agriculture and Rural Affairs, National Technology Centre for Whole Process Quality Control of FSEN Horticultural Products (Qingdao), Qingdao Key Lab of Modern Agriculture Quality and Safety Engineering, Qingdao 266109, China

³College of Agricultural Science, Xichang University, Xichang 615013, China

⁴Beijing Research Center for Agricultural Standards and Testing, Beijing 100097, China

Correspondence should be addressed to Jiyun Nie; jiyunnie@163.com

Received 14 January 2022; Accepted 23 March 2022; Published 28 April 2022

Academic Editor: Yong-Jie Yu

Copyright © 2022 Hui Zhang et al. This is an open access article distributed under the Creative Commons Attribution License, which permits unrestricted use, distribution, and reproduction in any medium, provided the original work is properly cited.

The aim of this study was to explore the regional characteristics of soluble sugars, organic acids, and stable isotopes ($\delta^2\text{H}$, $\delta^{18}\text{O}$, and $\delta^{13}\text{C}$) in Fuji apple and the viability of tracing the geographical origin. Totally, 181 Fuji apple samples from 2017 and 2018 from three main apple production regions in China, Bohai Bay (BHB), Loess Plateau (LP), and Northwest region (NW) were collected. The parameters of soluble sugars, organic acids, and stable isotopes in samples were analyzed with HPLC, IC, and IRMS, respectively. The results of regional difference analysis, multiway variance analysis, and correlation analysis indicated that sorbitol (Sor), glucose (Glu), fructose (Fru), sucrose (Sucr), $\delta^2\text{H}$, and $\delta^{13}\text{C}$ can be used to distinguish the samples from the three regions. Stepwise linear discriminant analysis (SLDA) showed that the correct discriminant rate of samples from the advantageous production areas of apples in China (BHB and LP) was 82.2%, and the most effective indexes were Glu, Fru, Sucr, and $\delta^2\text{H}$. Moreover, satisfactory classification can be achieved in samples from BHB and NW, with a correct classification rate of 90.0%, and Sor, Glu, and Fru were included in the discrimination model. Furthermore, the validity of the discriminant model was verified by the prediction set. The study also found that organic acids were not suitable to distinguish the apple samples from the three regions. In addition, soluble sugars and stable isotopes could not effectively distinguish LP and NW samples, which was also the reason that the samples from the three main apple production regions could not be distinguished well.

1. Introduction

In recent years, due to the occurrence of food safety issues such as heavy metal pollution, pesticide residues, adulteration, and fake and inferior agricultural products [1], consumers want to know more relevant information to confirm the safety of the food they purchase [2]. In this situation, consumers are more inclined to buy agricultural products

with a clear geographical origin, especially certified foods, such as agricultural products with geographical indications, which comply with relevant standards [3, 4]. However, some unauthorized operators may use false labels to impersonate agricultural products with clear geographical indications in order to obtain higher profits, as the agricultural products with guaranteed origin will charge a high premium, which will damage the interests of operators and consumers [5].

Therefore, the development of suitable analytical techniques for tracing the origin of agricultural products is highly desirable for consumers, production operators, and government regulators [6].

Due to the different principles and characteristics, especially the limitations of technology in the application, it is difficult to accurately trace the origin of agricultural products with only one traceability technology [7–9]. For example, stable isotope ratios analysis technology is an increasingly accepted tool for tracing the geographical origin of agricultural products, but the isotopic composition is mainly affected by geographic and climatic conditions, such as latitude, distance from the sea, altitude, temperature, and precipitation [10]. Therefore, the isotopic compositions of agricultural products from areas with similar climates and topography may not be effectively distinguished [5]. Using organic fingerprints to trace the origin of agricultural products, the discriminant rates were varied greatly due to the selected indexes. Therefore, screening out the organic ingredients which are unique or closely related to environmental conditions is the key to use organic compounds fingerprint analysis technology to trace the origin of agricultural products [11]. Therefore, it is the current development trend to use multiple technologies and multiple indexes to trace the origin of agricultural products. For instance, by combining the stable isotopes with volatile compounds, organic compounds, and multiple elements, the geographical origin of potatoes, kiwifruit, apple juices, and red wine can be well classified, and the total correct discrimination rate was varied from 83.9% to 100% [8, 12–14].

The cultivation of apples in China is mainly distributed in the advantageous production areas of apple, Bohai Bay (BHB), and Loess Plateau (LP), including the seven major apple-producing provinces of Shaanxi, Shandong, Henan, Shanxi, Hebei, Liaoning, and Gansu. In 2018, the apple cultivated area and the yield in BHB and LP accounted for 84.22% and 89.12% of the total cultivated area and yield in China [15]. Xinjiang and Ningxia are characteristic apple-producing areas in China and belong to the Northwest region (NW). In recent years, the cultivation area and yield of apples in the NW have continued to increase; moreover, with the changes in the layout of apple production, Xinjiang has gradually become an important apple-producing area in China. Furthermore, the Fuji apple is the main cultivated variety, and its cultivation proportion accounts for 72.7% of the total cultivated area [16]. As we all know, the quality and price of agricultural products will be different due to their geographic origin [17]; in addition, studies have found that the physiological quality of apples was related to the latitude, longitude, and altitude of the growing area [18]. For example, fructose has the highest proportion in the soluble sugars in Fuji apple from Shaanxi Province which belongs to the LP [19], with a higher price than in other provinces; moreover, apples in some specific areas of Shaanxi have been recognized as “protected designation of origin” (PDO) products [20]. Therefore, tracing the origin of the Fuji apple in the three main apple production regions in China is of great significance to achieving the traceability of apple and protecting the regional advantages of agricultural products.

What’s more, there has not been literature that specifically studied the use of organic compounds and stable isotope fingerprint characteristics to trace the origin of the Fuji apple.

Since the isotope ratios of carbon, hydrogen, and oxygen were altitude-, latitude-, and climate-dependent, these three stable isotope ratios can provide information about the geographic origin and metabolism of plants, so the isotopic ratios of carbon, hydrogen, and oxygen are suitable for tracking the geographical origin of agricultural products related to regional climate conditions [17, 21–23]. In addition, soluble sugars and organic acids were important nutrients in apples, as well as the main flavor compounds in apples. Moreover, studies have found that soluble sugars and organic acid compounds in Fuji apple were different between regions [19]. Therefore, the soluble sugars, organic acids, and stable isotopes ($\delta^2\text{H}$, $\delta^{18}\text{O}$, and $\delta^{13}\text{C}$) will be used to study the effectiveness of multi-index in tracking the origin of Fuji apples from the three main apple producing areas (BHB, LP, and NW) in China. It is expected to provide references for tracing the origin of apples.

2. Materials and Methods

2.1. Sample Collection. A total of 181 Fuji apple samples were collected from the 2017 and 2018 harvests from three main apple production regions in China, BHB (Hebei, Shandong, and Liaoning provinces), LP (Shaanxi, Gansu, Shanxi, and Henan provinces), and NW (Ningxia and Xinjiang autonomous regions). For each sample, approximately 5 kg of fruit was collected at the harvest maturity stage from September to November. Samples were transported to the laboratory 3 days after collection. The information on samples was shown in Table 1.

2.2. Sample Preparation. About 2.0 kg of fruit was ground into a powder in liquid nitrogen by a SPEX Sample Prep system (New Jersey, USA) and stored at -20°C for the determination of soluble sugars and organic acids. For the rest of the samples, wipe the surface of the peel and core; then the sample was homogenized by a homogenizer (JT C, Jintian, China), which was used for the determination of stable isotope ratios. The extraction of soluble sugars and organic acids was carried out according to the previously reported method [24, 25] and the extracted solution was stored at -20°C and analyzed by the instrument later. The homogenized sample was placed in the sample chamber of a vacuum freeze dryer (VFD-1000, Bilon, China); then, the sample was freeze-dried for 72 hours under the instrument conditions of -40°C and under 15pa. The dried sample was passed through a sieve (100 mesh, Huafeng, China) immediately. Finally, a powdered sample was obtained to detect the isotope ratio $^{13}\text{C}/^{12}\text{C}$ in samples.

2.3. Instrument Conditions

2.3.1. High-Performance Liquid Chromatography (HPLC) Measurement Conditions [25,26]. After filtered through a

TABLE 1: The region information of apple samples.

Location	Province/region	Longitude (E)	Latitude (N)	Altitude (m)	Years	Mean annual temperature (°C)	Annual precipitation (mm)	Number of samples
BHB	Hebei	113°27'–119°50'	36°05'–42°40'	3–386	2017	11.3	499.6	14
					2018	11.8	549.0	15
BHB	Liaoning	118°53'–125°46'	38°43'–43°26'	10–39	2017	10.3	368.0	2
					2018	10.6	477.5	3
BHB	Shandong	114°19'–122°43'	34°22'–38°23'	33–305	2017	13.5	622.4	2
					2018	14.2	750.1	9
LP	Shaanxi	105°29'–111°15'	31°42'–39°35'	580–969	2017	19.0	591.0	23
					2018	16.9	525.6	23
LP	Gansu	92°13'–108°46'	32°31'–42°57'	1085–1421	2017	9.8	546.1	1
					2018	13.5	725.8	5
LP	Shanxi	110°14'–114°33'	34°34'–40°43'	365–778	2017	13.8	503.6	9
					2018	17.7	386.0	7
LP	Henan	110°21'–116°39'	31°23'–36°22'	504–626	2017	15.0	641.1	3
					2018	14.8	525.7	4
NW	Ningxia	104°17'–107°39'	35°14'–39°23'	1111–1226	2017	10.8	224.5	24
					2018	10.6	280.1	8
NW	Xinjiang	73°40'–96°23'	34°22'–49°10'	663–1104	2017	12.2	70.2	17
					2018	11.6	101.4	12

* BHB, the Bohai Bay; LP, the Loess Plateau; NW, Northwest Region.

0.22 μm pore filter (Fine, Japan), the extracted solution was used to detect the organic acid compounds directly, using HPLC (LC-10A, Shimadzu, Japan), with SPD-10A UV-VIS detector, and a C18 column (Ultimate LP-C18, 4.6 mm \times 300 mm, 5 μm , Ultimate, China). A total of five organic acid compounds, including oxalic acid (Oxa), tartaric acid (Tar), quinic acid (Qui), malic acid (Mal), and shikimic acid (Shi), were identified by comparison with the standards. The calibration curves were prepared by plotting different concentrations ranging from 0.05 to 50 mg/L (for Mal, the concentrations ranging from 25 to 400 mg/L) of standards versus the area measurements in UPLC ($R^2 \geq 0.9992$). Results were expressed as mg/g. The reproducibility of the chromatographic separation of the organic acid compounds was carried out according to the previously reported method (Wu et al., Wang). The results of the reproducibility of chromatographic separation for organic acids were expressed as relative standard deviation (RSD%) as follows: 0.63 for Oxa, 1.41 for Tar, 0.43 for Qui, 0.62 for Mal, and 0.81 for Shi. The content of total acid in the samples was the sum of the contents of the five organic acids.

2.3.2. Ion Chromatograph (IC) Measurement Conditions [24, 25]. The soluble sugars were detected by an Ion Chromatograph (ICS-5000, Dionex, USA) with a conductivity detector, an anion exchange analytical column (Dionex CarboPac™ PA10, 4 mm \times 250 mm, Thermo Fisher Scientific, USA), and a guard column (IonPac AG23, 4 mm \times 50 mm, Dionex, USA). The extracted solution after being diluted 50 times with deionized water can be used to measure sorbitol (Sor), glucose (Glu), fructose (Fru), and sucrose (Sucr) in the samples. The soluble sugars were identified by comparison with the standards. The calibration curves were prepared by plotting different concentrations ranging from 0.5 to 100 mg/L of standards versus the area measurements in IC ($R^2 \geq 0.9965$). The result was expressed

as mg/g. The results of the reproducibility of chromatographic separation for soluble sugars, expressed as RSD%, were as follows: 1.75 for Sucr, 1.52 for Glu, 1.69 for Fru, and 0.37 for Sor. The content of total sugar in the samples was the sum of the contents of the four soluble sugars.

2.3.3. Isotopic Ratio Mass Spectrometer (IRMS) Measurement Conditions

- (1) **Stable Hydrogen and Oxygen Isotope Determination Conditions** [27,28]. About 2 g of the homogenized sample was weighed and placed in a glass sample bottle. The fully automatic vacuum condensed water extraction system (LI-2100, LICA, China) was used to extract the water in the samples; then, the extracted water was put into the automatic sampling tray of the element analyzer (Flash HT2000, Thermo Fisher Scientific, USA). The elements of H and O in the samples were converted into H_2 and CO by splitting at 1,400°C. After passing through the chromatographic column, H_2 and CO successively entered the stable isotope mass spectrometer (MAT 253, Thermo Fisher Scientific, USA) to detect the isotope ratios $^2\text{H}/^1\text{H}$ and $^{18}\text{O}/^{16}\text{O}$. The flow rates of helium carrier gas and helium purge gas were both 100 mL/min.
- (2) **Stable Carbon Isotope Determination Conditions** [27,28]. About 0.8 mg of the powder sample was weighed, which was wrapped in a tin cup, and placed in the element analyzer. The element of C in the sample was converted into CO_2 in a combustion furnace at 960°C. After passing through the chromatographic column, CO_2 entered the stable isotope mass spectrometer for the determination of the isotope ratio $^{13}\text{C}/^{12}\text{C}$. The flow rates of helium carrier gas and helium purge gas were both 100 mL/min.

(3) *The Calculated Stable Isotope Ratios.* The isotope values were calibrated against standard materials, which were Vienna Standard Mean Ocean Water (V-SMOW), USGS45 ($\delta^2\text{HVSMOW} = -10.3\text{‰}$, $\delta^{18}\text{OVSMOW} = -2.238\text{‰}$), USGS46 ($\delta^2\text{HVSMOW} = -235.8\text{‰}$, $\delta^{18}\text{OVSMOW} = -29.8\text{‰}$), and USGS40 ($\delta^{13}\text{CVPDB-LSVEC} = -26.39\text{‰}$, $\delta^{14}\text{NAIR} = -4.52\text{‰}$). According to the equation, R was the isotope ratio of heavy isotope to light isotope abundance in the samples ($^{18}\text{O}/^{16}\text{O}$, $^2\text{H}/^1\text{H}$, and $^{13}\text{O}/^{12}\text{O}$). R_{sample} and R_{standard} were the isotope ratio of the samples and the international standards. Results were referenced to Vienna Pee Dee Belemnite (V-PDB) for $\delta^{13}\text{C}$ and Vienna Standard Mean Ocean Water (V-SMOW) for $\delta^2\text{H}$ and $\delta^{18}\text{O}$. The analytical precision was 2‰, 0.4‰, and 0.2‰ for H, O, and C, respectively. The stable isotope ratios were calculated as follows:

$$\delta(\text{‰}) = \left[\frac{(R_{\text{sample}} - R_{\text{standard}})}{R_{\text{standard}}} \right] \times 1000 \quad (1)$$

2.4. Statistical Analysis. When data conformed to both normality and homogeneity assumptions, a regional different analysis was performed by one-way analysis of variance (ANOVA) (P value < 0.05), and the Pearson correlation analysis was used to investigate the relationship between indexes and regional conditions. When data conformed to the normality assumption but failed on the homogeneity of variances, analysis of variance was performed using Welch's test. For not normally distributed data, Kruskal-Wallis (K-W) was used for the analysis of regional differences, and Spearman correlation analysis was used to investigate the relationship between indexes and regional conditions. Multiway ANOVA was applied to quantify the contributions of geographical origin, harvest year, and their interactions to the total variance in stable isotope ratio, soluble sugars, and organic acids levels. In addition, the sample set was randomly split up into two groups, with three-quarters of the total samples as a training set and the remaining one-quarter of samples as a prediction set. According to F-value, the training set was used to create the discriminant model by Linear Discriminant Analysis (LDA), and the predictive ability of the discriminant model was estimated by the prediction set. Stepwise linear discriminant analysis (SLDA) was used to select necessary and optimal indexes to incorporate into the discriminant model, and the coefficients of the indexes in the discriminant model were standardized coefficients. The statistical analysis of the data was performed with SPSS 26.0 software (SPSS, IBM Corp., USA).

3. Results

3.1. Analysis of Soluble Sugars in Apples. The proportion of each sugar component in samples from high to low was Fru, Sucr, Glu, and Sor. For BHB, LP, and NW samples, the proportion of Fru to total sugars was 45.93%, 49.65%, and

49.33%, respectively (Figure 1(a)), which was the main soluble sugar component, in addition, the proportion of Sucr (26.44%, 23.03%, and 28.36%, respectively) was higher than Glu (23.12%, 22.51%, and 16.19%, respectively), and the lowest content was Sor (4.51%, 4.81%, and 6.12%, respectively). Moreover, the radar chart showed that the soluble sugar content in samples from different regions had different patterns (Figure 2(a)).

Regional differences of soluble sugars were shown in Table 2, and the contents of soluble sugars were expressed as means \pm standard deviation (SD). In LP samples, the average content of Fru was 59.5 ± 12.8 mg/g FW, which was higher than in BHB and NW samples, which are 54.3 ± 9.41 mg/g FW and 55.2 ± 13.3 mg/g FW, respectively. The average content of Sucr in LP samples was 27.4 ± 9.21 mg/g FW, which was lower than BHB and NW samples (31.6 ± 9.34 mg/g FW and 32.2 ± 10.0 mg/g FW, respectively). The contents of Fru and Sucr in the LP samples were significantly different from the BHB and NW samples ($P < 0.05$), and the content of Sucr was significantly different in LP and NW samples ($P < 0.01$), while the differences in Fru and Sucr contents in BHB and NW samples were not significantly ($P > 0.05$). The content of Glu in NW samples was significantly different from that in BHB and LP samples ($P < 0.01$). In addition, the content of Sor was significantly different between the BHB and NW samples ($P < 0.05$).

3.2. Analysis of Organic Acids in Apples. Different from soluble sugars, the content characteristics of organic acids had similar patterns among regions, and the content of organic acids in descending order was Mal, Qui, Oxa, Tar, and Shi (Figure 2(b)). In the samples from BHB, LP, and NW, Mal accounted for 85.18%, 85.66%, and 88.73% of the total acids, respectively (Figure 1(b)), indicating that Mal occupies an absolute advantage in the total acid content.

Regional differences of organic acids are shown in Table 2, and the contents of organic acids were expressed as means \pm standard deviation (SD). Mal was the main organic acid component in Fuji apple; the average content of Mal in BHB, LP, and NW samples was 4.11 ± 1.31 mg/g FW, 3.70 ± 0.828 mg/g FW, and 3.85 ± 1.20 mg/g FW, respectively; however, the differences in the three regions were not significant ($P > 0.05$). The average content of Qui in the BHB samples was significantly different from NW samples ($P < 0.01$). The content of Tar in NW samples was significantly different from that in BHB and LP samples ($P < 0.05$). The average content of Oxa and Shi in samples from the three main production regions was not significantly different ($P > 0.05$).

3.3. Analysis of Stable Isotopes in Apples. The characteristics of the $\delta^{18}\text{O}$ and $\delta^{13}\text{C}$ values in the samples from the three main apple-producing areas showed similar patterns, while the $\delta^2\text{H}$ value in the BHB samples was higher than that in NW and LP samples (Figure 2(c)). The mean $\delta^2\text{H}$ value of the BHB samples was -39.6‰ , which was higher than that of the LP and NW samples (-44.6‰ and -44.4‰ , respectively), and the results of ANOVA showed that the $\delta^2\text{H}$ value

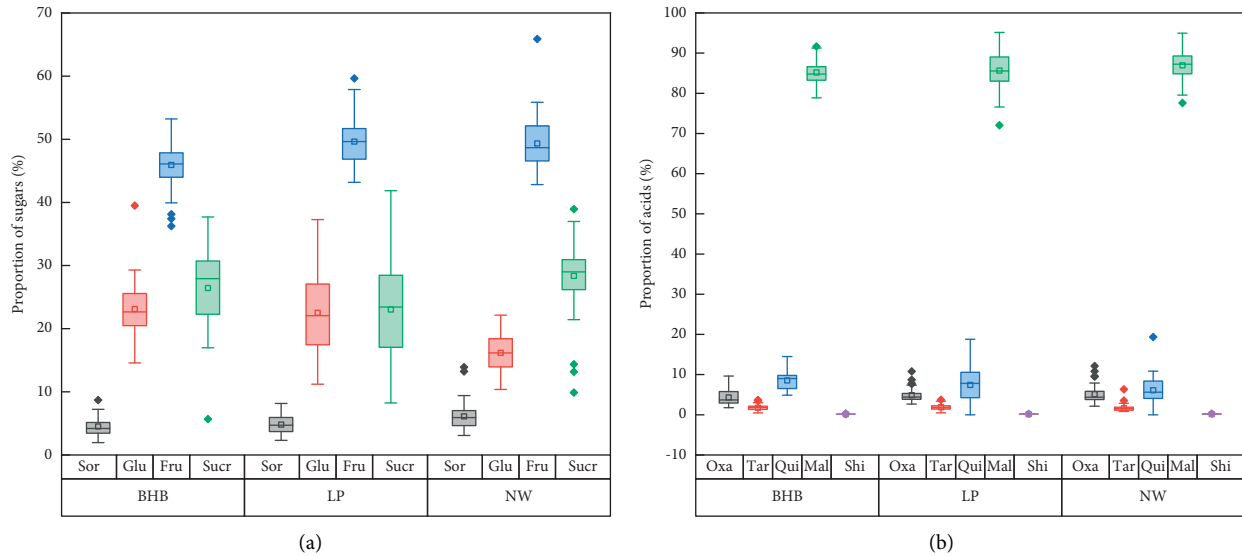


FIGURE 1: The proportions of soluble sugars (a) and organic acids (b) in samples.

of BHB samples was different from LP and NW samples, and the difference was significant ($P < 0.01$). In addition, there was no significant difference in the mean $\delta^2\text{H}$ values between LP and the NW samples ($P > 0.05$). The distribution of $\delta^{18}\text{O}$ values in the samples was similar to the $\delta^2\text{H}$ value; the mean $\delta^{18}\text{O}$ value of BHB samples was higher than that of LP and NW samples, which were -4.67% , -5.26% , and -5.22% , respectively. The results of ANOVA showed that the mean $\delta^{18}\text{O}$ value in the BHB samples was significantly different from the LP sample ($P < 0.05$). In addition, the mean $\delta^{18}\text{O}$ value of NW samples was not significantly different from BHB and LP samples ($P > 0.05$). The distribution of the $\delta^{13}\text{C}$ value of samples roughly showed that the $\delta^{13}\text{C}$ value of the NW samples was higher than that of LP samples, while the $\delta^{13}\text{C}$ value of the BHB samples was the lowest, and the mean $\delta^{13}\text{C}$ values of NW, LP, and BHB samples were -25.5% , -25.7% , and -26.3% , respectively. The results of ANOVA analysis showed that the mean $\delta^{13}\text{C}$ value of BHB samples was different from the LP and NW samples, and the difference was significant ($P < 0.01$). In addition, the mean $\delta^{13}\text{C}$ value of LP and NW samples was not significantly different ($P > 0.05$) (Table 2).

3.4. Multiway ANOVA. A combined analysis of variance of two years and three geographical origins was performed using the general linear model (GLM). Harvest year and geographical origin were considered as the fixed factors. The effects were partitioned into different sources: year, region, and region \times year (Table 3). Oxa was not statistically significant in this analytical model ($P > 0.05$). Sor, Glu, Fru, Sucr, Tar, Qui, Mal, Shi, $\delta^2\text{H}$ value, and $\delta^{18}\text{O}$ value were significantly influenced by year ($P < 0.01$). Sor, Glu, Fru, Sucr, $\delta^2\text{H}$ value, and $\delta^{13}\text{C}$ value were significantly affected by region ($P < 0.01$). Qui, Mal, and $\delta^{18}\text{O}$ values were significantly affected by region ($P < 0.05$). Region \times year had a significant effect on Sucr ($P < 0.05$) and $\delta^{13}\text{C}$ ($P < 0.01$). The results showed that geographical origin was the most

important source of the concentration variations of $\delta^{13}\text{C}$ value, and the contribution percentage was 44.76%. The harvest year was the most source of variation for soluble sugars, organic acids, $\delta^2\text{H}$, and $\delta^{18}\text{O}$.

3.5. Correlation between Indexes and Regional Conditions. To identify the relationship between indexes and regional conditions (longitude, latitude, altitude, mean annual temperature, and annual precipitation), correlation analysis was employed to assess whether or not positive/negative correlation patterns existed. The results showed that longitude was significantly negatively correlated with Sor ($r = -0.150$, $P < 0.05$) and $\delta^{13}\text{C}$ value ($r = -0.244$, $P < 0.01$) had a significant positive correlation with Glu ($r = 0.320$, $P < 0.01$) and $\delta^2\text{H}$ value ($r = 0.228$, $P < 0.01$) (Table 4). Latitude was negatively correlated with Glu ($r = -0.328$, $P < 0.01$) and Fru ($r = -0.205$, $P < 0.01$) and significantly positively correlated with Sucr ($r = 0.189$, $P < 0.05$). Altitude was significantly positively correlated with Sor ($r = 0.290$, $P < 0.01$) and $\delta^{13}\text{C}$ value ($r = 0.336$, $P < 0.01$) and was correlated with Glu ($r = -0.326$, $P < 0.01$) and Tar ($r = -0.170$, $P < 0.05$) showing a significant negative correlation. The temperature was significantly positively correlated with Glu ($r = 0.199$, $P < 0.01$) and was significantly negatively correlated with Sucr ($r = -0.222$, $P < 0.01$) and Mal ($r = -0.162$, $P < 0.05$). There was a significant negative correlation between precipitation and Sor ($r = -0.196$, $P < 0.01$) and $\delta^{13}\text{C}$ value ($r = -0.178$, $P < 0.05$), and there was a significant positive correlation with Glu ($r = 0.398$, $P < 0.01$), Tar ($r = 0.160$, $P < 0.05$), and $\delta^2\text{H}$ value ($r = 0.181$, $P < 0.05$). In addition, in the sample collection area, Oxa, Qui, Shi, and $\delta^{18}\text{O}$ values had no correlation with the regional conditions studied. Therefore, geographical location has a significant impact on most soluble sugars, organic acids, and stable isotopes studied ($P < 0.05$), which provides a basis for distinguishing the samples from different geographical regions by using soluble sugars, organic acids, and stable isotopes.

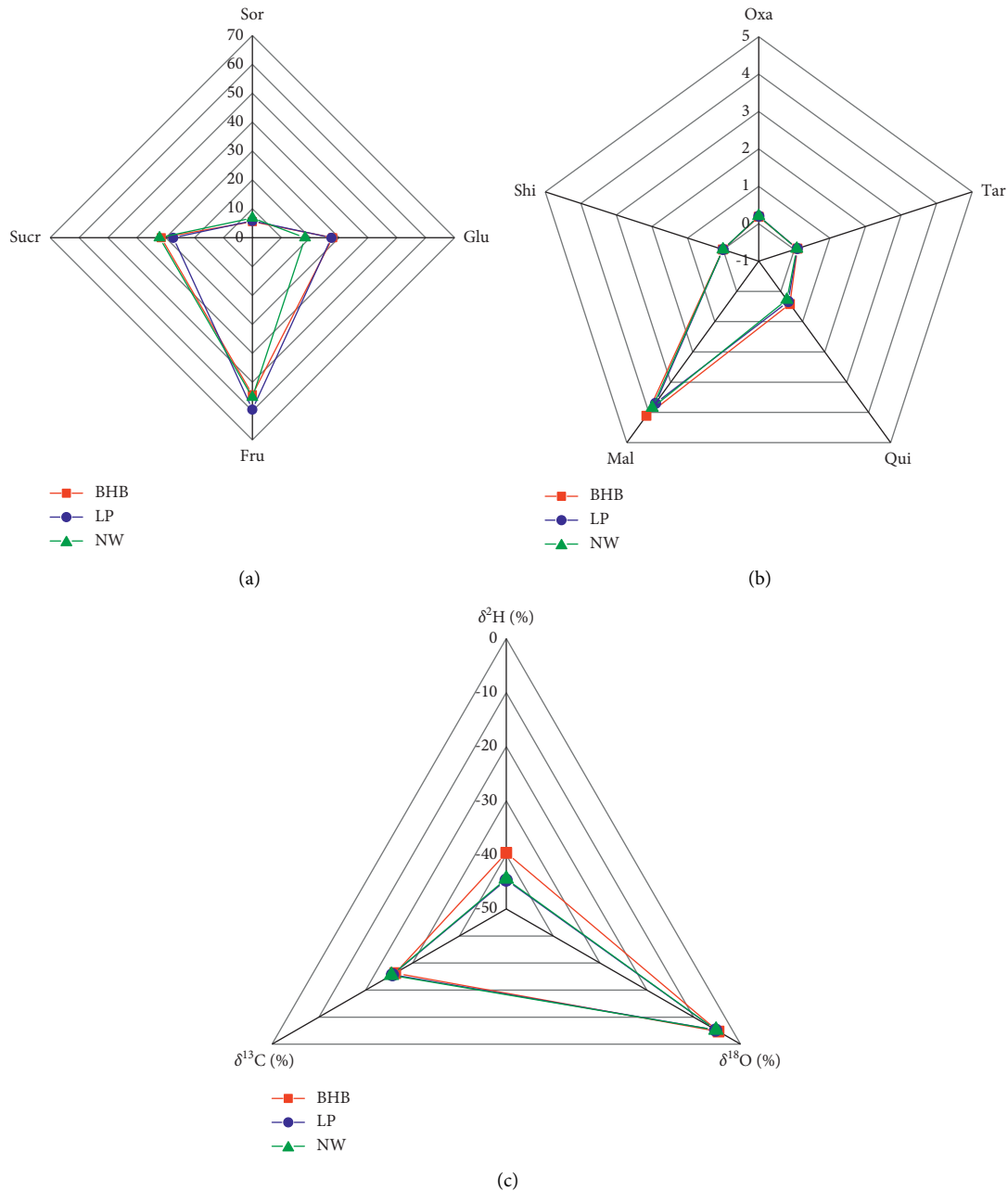


FIGURE 2: The content characteristics of soluble sugars (a), organic acids (b), and stable isotopes (c) in samples from different regions.

3.6. Linear Discriminant Analysis (LDA). In order to explore the effectiveness of soluble sugars, organic acids, and stable isotopes in tracing the origin of the Fuji apple in China, the indexes had significant differences between regions ($P < 0.05$) and were significantly affected by regional factors ($P < 0.05$); besides, the selected indexes were significantly correlated with the regional conditions. Finally, Sor, Glu, Fru, Sucr, $\delta^2\text{H}$, and $\delta^{13}\text{C}$ were selected for stepwise discriminant analysis (SLDA) of BHB, LP, and NW samples. About three-quarters of the samples (136 samples) were used as training set and the remaining 45 samples, BHB (11 samples), LP (19 samples), and NW (15 samples), were used as prediction set to verify the stability of the discriminant models.

SLDA was used to classify Fuji apple samples from BHB, LP, and NW. The classification of the training set by the canonical discriminant functions was shown in Figure 3; it can be seen that BHB, NW, and LP samples were overlapped, mainly because the LP samples were misjudged as BHB and NW samples, and the correct classification rate and cross-validation rate were only 69.1% and 67.6% (Table 5); in addition, Sor, Glu, Fru, Sucr, and $\delta^2\text{H}$, which had a significant impact on sample discrimination ($P < 0.001$), were included in the discriminant model, and the correct discrimination rate of the discriminant model for the prediction set was only 75.6% (for BHB, NW, and LP samples was 81.8%, 80.0%, and 68.4%, respectively) (Table 6). In addition,

TABLE 2: Analysis of the regional differences of soluble sugars, organic acids, and stable isotopes in samples.

Composition	Location	Means \pm SD	Range	Variation coefficient (%)
Sor	BHB	5.57 \pm 2.76 b	2.04–14.4	49.5
	LP	5.86 \pm 2.22ab	1.77–10.9	37.8
	NW	6.81 \pm 2.75a	2.39–14.4	40.4
Glu	BHB	27.8 \pm 8.03a	12.8–48.9	28.9
	LP	27.3 \pm 10.2a	11.4–52.0	37.4
	NW	18.2 \pm 5.82 b	8.90–34.8	31.9
Fru	BHB	54.3 \pm 9.41 b	38.2–87.0	17.3
	LP	59.5 \pm 12.8a	34.0–106.1	21.6
	NW	55.2 \pm 13.3 b	36.6–126	24.0
Sucr	BHB	31.6 \pm 9.34a	5.21–53.2	29.6
	LP	27.4 \pm 9.21 b	9.59–49.1	33.6
	NW	32.2 \pm 10.0a	6.74–74.5	31.1
Oxa	BHB	0.187 \pm 0.0417a	0.110–0.301	22.3
	LP	0.204 \pm 0.0686a	0.0811–0.641	33.6
	NW	0.207 \pm 0.0839a	0.108–0.482	40.6
Tar	BHB	0.0852 \pm 0.0368a	0.0191–0.175	43.2
	LP	0.0812 \pm 0.0318a	0.0191–0.143	39.1
	NW	0.0684 \pm 0.0331 b	0.0295–0.180	48.4
Qui	BHB	0.416 \pm 0.171a	0.146–0.901	41.1
	LP	0.339 \pm 0.216ab	0.000–0.943	63.7
	NW	0.276 \pm 0.230 b	0.00–1.58	83.4
Mal	BHB	4.11 \pm 1.31a	2.00–7.72	31.8
	LP	3.70 \pm 0.828a	1.79–6.10	22.4
	NW	3.85 \pm 1.20a	2.12–8.60	31.3
Shi	BHB	0.00670 \pm 0.00137a	0.00460–0.0110	20.4
	LP	0.00631 \pm 0.00146a	0.00310–0.0103	23.2
	NW	0.00632 \pm 0.00169a	0.00360–0.0105	26.8
$\delta^2\text{H}$	BHB	–39.6 \pm 6.88a	–57.6––21.8	17.4
	LP	–44.6 \pm 5.77b	–59.5––32.7	12.9
	NW	–44.4 \pm 7.66b	–73.9––25.6	17.2
$\delta^{18}\text{O}$	BHB	–4.67 \pm 1.44a	–8.48––1.85	30.9
	LP	–5.26 \pm 1.57b	–8.58––1.59	29.8
	NW	–5.22 \pm 1.51ab	–8.26––1.86	28.9
$\delta^{13}\text{C}$	BHB	–26.3 \pm 0.973b	–28.1––24.5	3.70
	LP	–25.7 \pm 0.834a	–28.0––23.3	3.25
	NW	–25.5 \pm 0.963a	–27.3––22.3	3.78

* The different letters in the same column mean significant difference ($P < 0.05$); the coefficient of variation of stable isotopes was the absolute value of the original value.

it was found that the classification effect of the samples from two producing areas was better (Figure 3). So, SLDA was performed on samples from the two production regions to explore the effectiveness of the combination of soluble sugars and stable isotopes in distinguishing the regions of samples.

Glu, Fru, Sucr, and $\delta^2\text{H}$ were selected by SLDA to classify Fuji apple samples from the advantageous production areas of apple in China (BHB and LP). The correct classification rate and cross-validation rate of the training set of BHB and LP samples were both 82.2% (Table 5), and the correct discrimination rate of the prediction set was 80.0% (Table 6). When SLDA was used to classify Fuji apple samples from BHB and NW, a satisfactory classification was obtained, and the correct classification rate of the training set and cross-validation rate were 90.0% and 86.3%, respectively (Table 5); moreover, the discriminant model, including Sor, Glu, and Fru, had a correct discrimination rate of 84.6% for prediction set (Table 6). However, it was found that the samples from the LP and NW were not easy to be distinguished, and

the correct classification rate of the training set was only 71.6% (Table 5), which was the reason that the classification of samples from the three production regions was not satisfactory.

4. Discussion

In this study, Fru was the main soluble sugar in samples, accounting for 45.93%–49.65% of the total sugar content, and Mal was the main organic acid, accounting for 85.18%–88.73% of the total acid, which was consistent with previous studies [24,29]. For apple fruits, the formation and accumulation of the flavor substances (soluble sugars and organic acids) were closely related to ecological and climatic conditions such as temperature, light intensity, and altitude. In this study, LP (Shaanxi, Gansu, Shanxi, and Henan) is next to BHB (Shandong, Hebei, and Liaoning) and NW (Ningxia and Xinjiang). The altitude and annual average temperature of provinces on the LP are similar to those of BHB and NW, such as Gansu, Ningxia, and Xinjiang. This may cause the

TABLE 3: The contribution of each factor to the content variability of soluble sugars, organic acids, and stable isotopes.

Dependent variable	Calibrate model			Year			Region			Region × year			Error Contribution rates (%)
	F-Value	Significance (p value)	Contribution rates (%)										
Sor	5.469	≤0.001	70.22	≤0.001	24.93	0.002	1.10	0.746	3.75				
Glu	47.318	≤0.001	82.29	≤0.001	15.70	≤0.001	1.37	0.125	0.65				
Fru	23.314	≤0.001	92.69	≤0.001	5.37	0.005	0.94	0.389	0.99				
Sucr	4.527	≤0.001	43.37	0.005	35.09	0.002	16.25	0.049	5.29				
Oxa	1.137	0.343	34.91	0.186	0.07	0.996	45.25	0.105	19.77				
Tar	46.865	≤0.001	98.09	≤0.001	0.50	0.337	0.95	0.132	0.46				
Qui	57.677	≤0.001	96.90	≤0.001	1.60	0.021	1.09	0.071	0.40				
Mal	22.227	≤0.001	93.43	≤0.001	3.33	0.026	2.35	0.074	0.89				
Shi	21.697	≤0.001	95.85	≤0.001	1.96	0.130	1.24	0.273	0.95				
δ ² H	7.315	≤0.001	53.56	≤0.001	35.32	≤0.001	6.64	0.229	4.47				
δ ¹⁸ O	39.428	≤0.001	96.64	≤0.001	2.17	0.025	0.62	0.345	0.58				
δ ¹³ C	8.473	≤0.001	15.12	0.077	44.76	≤0.001	35.35	≤0.001	4.77				

TABLE 4: Correlations of soluble sugars, organic acids, and stable isotopes with regional conditions.

	Sor	Glu	Fru	Sucr	Oxa	Tar	Qui	Mal	Shi	$\delta^2\text{H}$	$\delta^{18}\text{O}$	$\delta^{13}\text{C}$
Longitude	-0.150*	0.320**	0.023	-0.002	-0.045	-0.012	0.121	0.090	-0.045	0.228**	0.081	-0.244**
Latitude	0.017	-0.328**	-0.205**	0.189*	-0.100	-0.039	-0.005	0.006	0.132	-0.112	-0.032	-0.035
Altitude	0.290**	-0.326**	0.140	0.073	0.114	-0.170*	-0.090	0.020	-0.073	-0.123	-0.011	0.336**
Mean annual temperature	-0.065	0.199**	0.051	-0.222**	0.022	0.070	-0.070	-0.162*	-0.127	0.045	-0.049	0.056
Annual precipitation	-0.196**	0.398**	0.069	-0.129	-0.063	0.160*	0.112	0.080	0.058	0.181*	0.076	-0.178*

**Significant correlation ($P < 0.01$). *Significant correlation ($P < 0.05$).

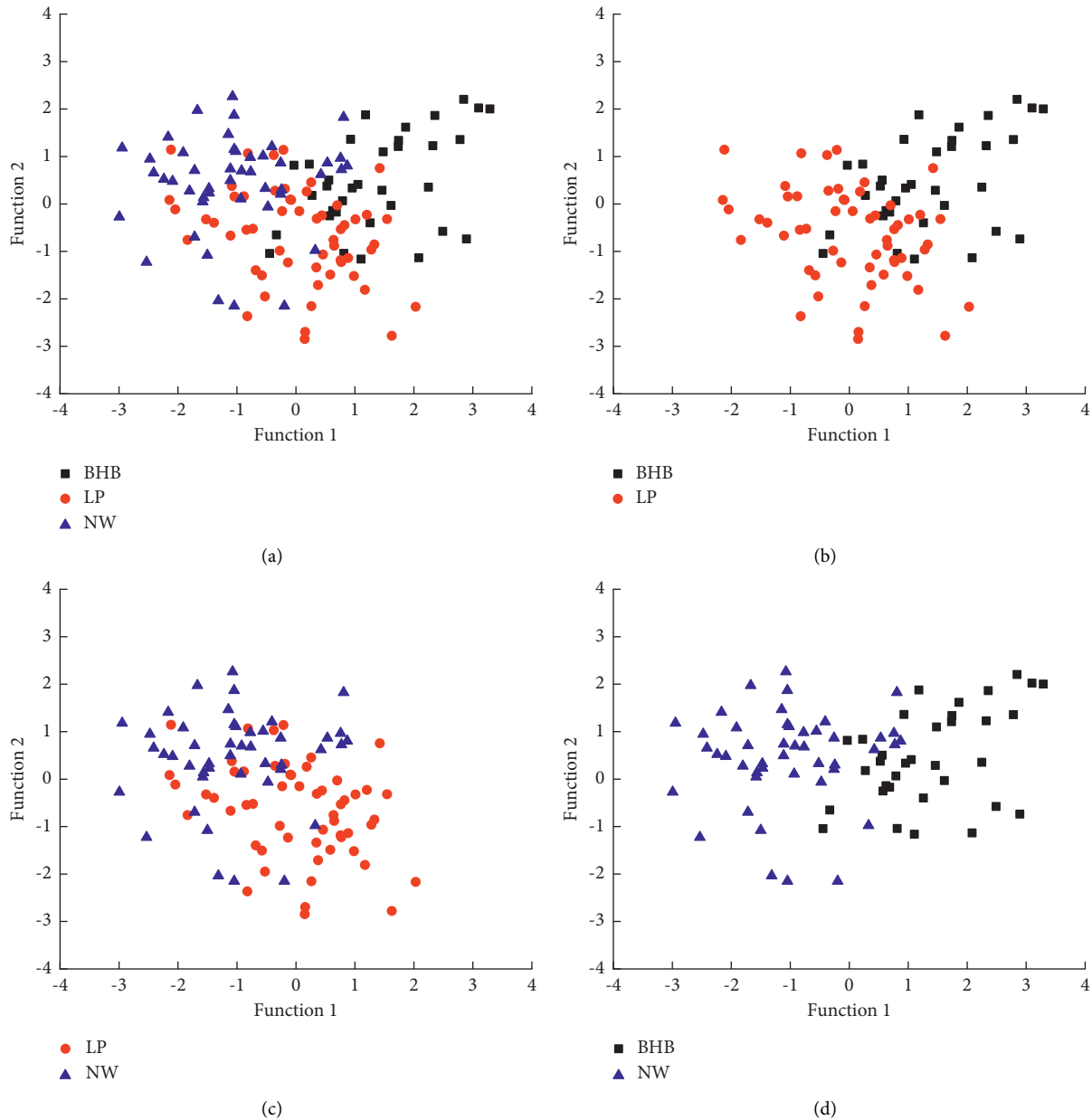


FIGURE 3: Scatter plot of the scores of apple samples from the three major apple-producing areas on the canonical discriminant functions.

content of soluble sugar in the LP sample to be similar to the NW and BHB samples, making it difficult to be classified from BHB and NW samples. In fact, acid metabolism and regulation in apples are very complex, and the acid content is

jointly regulated by the relevant genes and enzymes [30]. In addition, it is also affected by many factors such as environment and cultivation conditions. For example, a certain degree of deficit irrigation will affect the content of total acid

TABLE 5: The correct classification rate (%) of the training set obtained by SLDA.

Sample groups	BHB	LP	NW	Total	
				Original	Cross-validated
BHB-LP-NW	73.5	60.7	76.1	69.1	67.6
BHB-LP	73.5	87.5		82.2	82.2
LP-NW		71.4	71.7	71.6	71.6
BHB-NW	91.2		89.1	90.0	86.3

TABLE 6: The correct discrimination rate of discrimination model for prediction set.

Sample groups	Discriminant models	Prediction set (%)	
		Total	
BHB-LP-NW	BHB = $-0.653 \text{ Sor} + 1.973 \text{ Glu} - 1.829 \text{ Fru} + 1.468 \text{ Sucr} + 0.859 \delta^2\text{H} - 2.166$	81.8	75.6
	LP = $-0.134 \text{ Sor} + 0.285 \text{ Glu} + 0.448 \text{ Fru} - 0.568 \text{ Sucr} - 0.477 \delta^2\text{H} - 1.313$	68.4	
	NW = $0.646 \text{ Sor} - 1.805 \text{ Glu} + 0.806 \text{ Fru} - 0.393 \text{ Sucr} - 0.054 \delta^2\text{H} - 1.744$	80.0	
BHB-LP	BHB = $0.847 \text{ Glu} - 1.375 \text{ Fru} + 0.998 \text{ Sucr} + 0.927 \delta^2\text{H} - 1.320$	81.8	80.0
	LP = $-0.514 \text{ Glu} + 0.835 \text{ Fru} - 0.606 \text{ Sucr} - 0.563 \delta^2\text{H} - 0.924$	78.9	
LP-NW	LP = $-0.417 \text{ Sor} + 0.698 \text{ Glu} - 0.886$	68.4	73.5
	NW = $0.508 \text{ Sor} - 0.849 \text{ Glu} - 0.979$	80.0	
BHB-NW	BHB = $-0.594 \text{ Sor} + 2.436 \text{ Glu} - 1.106 \text{ Fru} - 1.609$	81.8	84.6
	NW = $0.439 \text{ Sor} - 1.800 \text{ Glu} + 0.817 \text{ Fru} - 1.193$	86.7	

in fruit [31,32]. Moreover, fruit acidity rather than sweetness was likely to have undergone selection during apple domestication [26]. In this study, it was found that the organic acids were not suitable for distinguishing the Fuji apple samples from these three producing regions. Therefore, it was speculated that organic acids are less affected by temperature, light, and altitude than soluble sugars, which was consistent with the results of correlation analysis of soluble sugars, organic acids, and regional conditions (Table 4).

The fractionation of hydrogen isotopes was affected by distance from the sea, temperature, rainfall, and atmospheric humidity. In this study, BHB (including Hebei Province) is located on the east coast of China and will be affected by coastal climate, so the $\delta^2\text{H}$ value will be different from the samples in inland areas (LP and NW), which can be used to distinguish samples from coastal and inland areas, even from different coasts [10,28]. In addition, the altitude of BHB was lower than LP and NW; these factors will lead to the enrichment of heavy isotopes of hydrogen in BHB samples [33]. Therefore, the decreasing order of $\delta^2\text{H}$ value in samples from the three production regions was BHB (-39.6‰), NW (-44.4‰), and LP (-44.6‰), and the $\delta^2\text{H}$ value in BHB samples was significantly different from LP and NW samples ($P < 0.01$). Oxygen isotopes in plants were affected by latitude, distance from the sea, altitude, and degree of evaporation (mainly affected by humidity and temperature) [34–36]. In addition, in samples in coastal areas, the $\delta^{18}\text{O}$ value was high [37], so it was speculated that the content characteristics of the $\delta^{18}\text{O}$ value in the three production regions were consistent with $\delta^2\text{H}$. The study found that the decreasing order of $\delta^{18}\text{O}$ value was BHB (-4.67‰), NW (-5.22‰), and LP (-5.26‰), and there was a significant difference between BHB and LP samples ($P < 0.05$), but NW samples had no significant difference with BHB and LP samples ($P > 0.05$), possibly because the increase of solar

radiation and the decrease of precipitation in NW lead to the enrichment of oxygen heavy isotopes in samples [36]; furthermore, as the hydrogen isotopes in plants only come from water, the coastal climate had a greater impact on $\delta^2\text{H}$ than $\delta^{18}\text{O}$ [10]. Therefore, the variation in $\delta^{18}\text{O}$ values within NW samples was observed. The $\delta^{13}\text{C}$ value in plants is related to atmospheric photosynthetic carbon sequestration during growth and some environmental factors [38], such as water availability, relative humidity, light intensity, and temperature in the plant environment (atmospheric and soil water) [36,39,40]. In this study, the altitude of NW was higher than LP, and the altitude of BHB was the lowest, and the average $\delta^{13}\text{C}$ value roughly conforms to the characteristics that it increases with the increase of altitude. The average $\delta^{13}\text{C}$ value of samples from high to low was NW (-25.5‰), LP (-25.7‰), and BHB (-26.3‰). This phenomenon was considered to be related to the physiological changes of plants adapting to their growth conditions and the changes of carbon dioxide content with the rise of sea level [41–43].

The fingerprint characteristics of soluble sugars, organic acids, and stable isotopes formed under the influence of geographic and climatic conditions tend to distinguish samples without LP samples, and the correct discrimination rates of the training set were above 82.2%; furthermore, the correct discrimination rates of prediction set were above 80%. The storage time and the sample preparation for detecting sugars and acids in 2017 samples were different from 2018 samples, which may increase the differences in indexes between years (except $\delta^{13}\text{C}$ value); however, the correct discrimination rates of the prediction set were similar to the training set, indicating that although the year may be the main source of variance, there is a variation of soluble sugar, organic acid, and $\delta^2\text{H}$ value, and the discriminant model still has a certain stability. In addition, organic acids were not suitable for distinguishing the

samples from the three main apple production regions, while soluble sugars and stable isotopes were not satisfactorily distinguishing LP and NW samples; therefore, in the following research, it is necessary to add indexes, suitable for distinguishing LP and NW samples, to improve the correct discrimination rate of samples from the three production regions.

5. Conclusions

In this study, as the soluble sugar, organic acid, and stable isotope studied were closely related to the regional conditions, which lead to the poor discrimination rate of LP and NW samples, the correct discrimination rate of the samples from the three main apple production regions was only 69.1%. Nevertheless, it can still be used for many specific applications, such as Glu, Fru, Sucr, and $\delta^2\text{H}$ which can be used to distinguish the samples from the advantageous production areas of apple in China (BHB and LP), and the correct discrimination rates of the training set and prediction set were 82.2% and 80.0%, respectively. In addition, BHB and NW samples can be satisfactorily distinguished by Sor, Glu, and Fru, and the correct discrimination rates of the training set and prediction set were 90.0% and 84.6%, respectively.

Data Availability

Data are included within this article.

Conflicts of Interest

The authors declare that they have no conflicts of interest.

Acknowledgments

This research was supported by the Earmarked Fund for China Agriculture Research System (No. CARS-27), the Agricultural Science and Technology Innovation Program of Chinese Academy of Agricultural Sciences (No. CAAS-ASTIP), and the National Program for Quality and Safety Risk Assessment of Agricultural Products of China (No. GJFP2018003).

References

- [1] Y. m. Wei, B. l. Guo, S. Wei, S. Sun, and H. y. Zhao, "The principle of food geographical origin traceability and authenticity technique," *Scientia Agricultura Sinica*, vol. 45, no. 24, pp. 5073–5081, 2012, in Chinese.
- [2] S. Hunt and L. J. Frewer, "Trust in sources of information about genetically modified food risks in the UK," *British Food Journal*, vol. 103, no. 1, pp. 46–62, 2001.
- [3] C. f. Zeng, L. f. Zhang, J. d. Xu, J. Shu, and D. h. Liu, "Research progress in traceability technology about geographical origin of agricultural products," *Science and Technology of Food Industry*, vol. 34, no. 06, pp. 367–371, 2013, in Chinese.
- [4] X. Zhao, M. Kneafsey, and D. Finlay, "Food safety and Chinese geographical indications," *British Food Journal*, vol. 118, no. 1, pp. 217–230, 2016.
- [5] S. A. Wadood, G. Boli, Z. Xiaowen, I. Hussain, and W. Yimin, "Recent development in the application of analytical techniques for the traceability and authenticity of food of plant origin," *Microchemical Journal*, vol. 152, Article ID 104295, 2020.
- [6] D. M. A. M. Luykx and S. M. Van Ruth, "An overview of analytical methods for determining the geographical origin of food products," *Food Chemistry*, vol. 107, no. 2, pp. 897–911, 2008.
- [7] F. Longobardi, A. Ventrella, G. Casiello et al., "Instrumental and multivariate statistical analyses for the characterisation of the geographical origin of Apulian virgin olive oils," *Food Chemistry*, vol. 133, no. 2, pp. 579–584, 2012.
- [8] Y. y. Ma, B. l. Guo, Y. m. Wei, and S. Wei, "Identification of Kiwi fruit geographical origin using stable isotopes and organic compounds," *Journal of Chinese Institute of Food Science and Technology*, vol. 15, no. 08, pp. 238–244, 2015, in Chinese.
- [9] A. Mahne Opatić, M. Nečemer, S. Lojen, and J. Masten, "Determination of geographical origin of commercial tomato through analysis of stable isotopes, elemental composition and chemical markers," *Food Control*, vol. 89, pp. 133–141, 2018.
- [10] L. Bontempo, F. Camin, R. Larcher, G. Nicolini, M. Perini, and A. Rossmann, "Coast and year effect on H, O and C stable isotope ratios of Tyrrhenian and Adriatic Italian olive oils," *Rapid Communications in Mass Spectrometry*, vol. 23, no. 7, pp. 1043–1048, 2009.
- [11] H. Shi, S. Liu, and X. g. Zhao, "Application of stable hydrogen and oxygen Isotope in water circulation," *Journal of Soil and Water Conservation*, vol. 17, no. 02, pp. 163–166, 2003, in Chinese.
- [12] D. McCarroll and N. J. Loader, "Stable isotopes in tree rings," *Quaternary Science Reviews*, vol. 23, no. 7–8, pp. 771–801, 2004.
- [13] F. Longobardi, G. Casiello, D. Sacco, L. Tedone, and A. Sacco, "Characterisation of the geographical origin of Italian potatoes, based on stable isotope and volatile compound analyses," *Food Chemistry*, vol. 124, no. 4, pp. 1708–1713, 2011.
- [14] H. Wu, T. Yue, and Y. Yuan, "Authenticity tracing of apples according to variety and geographical origin based on electronic nose and electronic tongue," *Food Analytical Methods*, vol. 11, no. 2, pp. 522–532, 2018.
- [15] J. t. Zhou, D. y. Zhao, Y. h. Chen, G. d. Kang, and C. g. Cheng, "Analysis of apple producing area changes in China," *Journal of Fruit Science*, vol. 38, pp. 1–15, 2021, in Chinese.
- [16] L. X. Kuang, J. Y. Nie, Y. P. Li, Y. Cheng, and Y. M. Shen, "Quality evaluation of Fuji apples cultivated in different regions of China scientia," *Agricultura Sinica*, vol. 53, no. 11, pp. 2253–2263, 2020, in Chinese.
- [17] M. T. Osorio, A. P. Moloney, O. Schmidt, and F. J. Monahan, "Multielement isotope analysis of bovine muscle for determination of international geographical origin of meat," *Journal of Agricultural and Food Chemistry*, vol. 59, no. 7, pp. 3285–3294, 2011.
- [18] Z. Li, Y. R. Guo, L. J. Sun, Q. I. Liu, J. J. Liu, and C. C. Fu, "Quality differences of Nagafu 2 apple from different habitats and its correlation with geographical coordinates," *Journal of Shaanxi Normal University (Natural Science Edition)*, vol. 40, no. 04, pp. 98–103, 2012, in Chinese.
- [19] X. Wang, *Research on Quality Evaluation and Processing Suitability of Fuji Apple from Different Chinese Origins*, Chinese Academy of Agricultural Sciences, Beijing, China, 2013, in Chinese.

- [20] J. Guo, T. Yue, Y. Yuan, and Y. Wang, "Chemometric classification of apple juices according to variety and geographical origin based on polyphenolic profiles," *Journal of Agricultural and Food Chemistry*, vol. 61, no. 28, pp. 6949–6963, 2013.
- [21] S. Kelly, K. Heaton, and J. Hoogewerff, "Tracing the geographical origin of food: the application of multi-element and multi-isotope analysis," *Trends in Food Science & Technology*, vol. 16, no. 12, pp. 555–567, 2005.
- [22] B. I. Guo, Y. m. Wei, and J. r. Pan, "Progress in the application of isotopic fingerprint analysis to food origin traceability," *Transactions of the CSAE*, vol. 23, no. 3, pp. 284–289, 2007.
- [23] P. Zhou, Z. Li, L. Ouyang et al., "A multi-element stable isotope approach coupled with chemometrics for the determination of Tieguanyin tea geographical origin and harvest season," *Analytical Methods*, vol. 11, no. 3, pp. 346–352, 2019.
- [24] L. j. Zheng, J. Y. Nie, Z. Yan et al., "Studies on the characteristics of the composition and content of soluble sugars in apple fruit," *Acta Horticulturae Sinica*, vol. 42, no. 05, pp. 950–960, 2015, in Chinese.
- [25] J. Zhang, J.-y. Nie, J. Li et al., "Evaluation of sugar and organic acid composition and their levels in highbush blueberries from two regions of China," *Journal of Integrative Agriculture*, vol. 19, no. 9, pp. 2352–2361, 2020.
- [26] B. Ma, J. Chen, H. Zheng et al., "Comparative assessment of sugar and malic acid composition in cultivated and wild apples," *Food Chemistry*, vol. 172, pp. 86–91, 2015.
- [27] A. Li, Q. S. Chen, L. G. Pan et al., "Discriminations of the geographical origin of peach based on stable isotope and rare earth element fingerprint characteristics," *Food Science*, vol. 41, no. 06, pp. 322–328, 2020, in Chinese.
- [28] A. Li, J. Zhao, J. Xi et al., "Geographical authentication of peach in China based on stable isotope combined with multielement analysis of peach juice," *Food Control*, vol. 127, Article ID 108126, 2021.
- [29] J. Wu, H. Gao, L. Zhao et al., "Chemical compositional characterization of some apple cultivars," *Food Chemistry*, vol. 103, no. 1, pp. 88–93, 2007.
- [30] J. Shi, F. F. Li, H. Ma, Z. Y. Li, and J. Z. Xu, "Effects of different dwarfing interstocks on key enzyme activities and the expression of genes related to malic acid metabolism in Red Fuji apples," *Genetics and Molecular Research*, vol. 14, no. 4, pp. 17673–17683, 2015.
- [31] A. Thakur and Z. Singh, "Responses of "Spring Bright" and "Summer Bright" nectarines to deficit irrigation: fruit growth and concentration of sugars and organic acids," *Scientia Horticulturae*, vol. 135, pp. 112–119, 2012.
- [32] X.-J. Xu, Q.-Y. Li, X.-H. Song, S. Qi-Rong, and D. Cai-Xia, "Dynamic regulation of nitrogen and organic acid metabolism of cherry tomato fruit as affected by different nitrogen forms," *Pedosphere*, vol. 22, no. 1, pp. 67–78, 2012.
- [33] M. Brencic and P. Vreca, "Identification of sources and production processes of bottled waters by stable hydrogen and oxygen isotope ratios," *Rapid Communications in Mass Spectrometry*, vol. 20, no. 21, pp. 3205–3212, 2006.
- [34] L. Bontempo, F. Camin, L. Manzocco et al., "Traceability along the production chain of Italian tomato products on the basis of stable isotopes and mineral composition," *Rapid Communications in Mass Spectrometry*, vol. 25, no. 7, pp. 899–909, 2011.
- [35] H. Jeon, S.-C. Lee, Y.-J. Cho, J.-H. Oh, K. Kwon, and B. H. Kim, "A triple-isotope approach for discriminating the geographic origin of Asian sesame oils," *Food Chemistry*, vol. 167, pp. 363–369, 2015.
- [36] K. Bizjak Bat, K. Eler, D. Mazej et al., "Isotopic and elemental characterisation of Slovenian apple juice according to geographical origin: preliminary results," *Food Chemistry*, vol. 203, pp. 86–94, 2016.
- [37] H. Wu, L. Tian, B. Chen et al., "Verification of imported red wine origin into China using multi isotope and elemental analyses," *Food Chemistry*, vol. 301, Article ID 125137, 2019.
- [38] M. F. Cengiz, O. Turan, D. Ozdemir, Y. Albayrak, F. Perincek, and H. Kocabas, "Geographical origin of imported and domestic teas (*Camellia sinensis*) from Turkey as determined by stable isotope signatures," *International Journal of Food Properties*, vol. 20, no. 12, pp. 3234–3243, 2017.
- [39] F. Camin, R. Larcher, M. Perini et al., "Characterisation of authentic Italian extra-virgin olive oils by stable isotope ratios of C, O and H and mineral composition," *Food Chemistry*, vol. 118, no. 4, pp. 901–909, 2010.
- [40] D. Potočnik, M. Nečemer, I. Perišić et al., "Geographical verification of Slovenian milk using stable isotope ratio, multi-element and multivariate modelling approaches," *Food Chemistry*, vol. 326, Article ID 126958, 2020.
- [41] K. A. Hobson, L. I. Wassenaar, B. Mila, I. Lovette, C. Dingle, and T. B. Smith, "Stable isotopes as indicators of altitudinal distributions and movements in an Ecuadorean hummingbird community," *Oecologia*, vol. 136, no. 2, pp. 302–308, 2003.
- [42] L. Bontempo, F. Camin, M. Paolini, C. Micheloni, and K. H. Laursen, "Multi-isotopic signatures of organic and conventional Italian pasta along the production chain," *Journal of Mass Spectrometry*, vol. 51, no. 9, pp. 675–683, 2016.
- [43] S. A. Wadood, G. Boli, and W. Yimin, "Geographical traceability of wheat and its products using multielement light stable isotopes coupled with chemometrics," *Journal of Mass Spectrometry*, vol. 54, no. 2, pp. 178–188, 2019.

Research Article

A Study on the Volatile Compounds in *Elaeagnus angustifolia* L. Flowers during Flowering Season by Gas Chromatography-Mass Spectrometry Coupled with Advanced Chemometrics

Zhijing Liu,¹ Degang Ding,¹ Huapeng Cui ,² Chuanchuan Wang,¹ Juntao Liu,¹ Li Chen,² Meijuan Fan,² and Guangwei Geng ¹

¹Faculty of Science, Henan University of Animal Husbandry and Economics, Zhengzhou, China

²Zhengzhou Tobacco Research Institute of CNTC, Zhengzhou, China

Correspondence should be addressed to Huapeng Cui; cuihuapeng516@126.com and Guangwei Geng; gengguangwei@hotmail.com

Received 17 August 2021; Accepted 11 September 2021; Published 27 September 2021

Academic Editor: Yong-Jie Yu

Copyright © 2021 Zhijing Liu et al. This is an open access article distributed under the Creative Commons Attribution License, which permits unrestricted use, distribution, and reproduction in any medium, provided the original work is properly cited.

The flowers of *Elaeagnus angustifolia* L. have been used as a homologous variety in China, whose quality seriously relies on the compositions during the flowering period. Unfortunately, studies on the variations of volatile compounds during the flowering season are rarely reported. Herein, a gas chromatography-mass spectrometry-based untargeted metabolomic methodology was proposed for the comprehensive analysis of volatile compounds in *E. angustifolia* flowers to classify various flowering stages. Samples from four flowering stages were collected, including the initial bloom stage, pre-full bloom stage (70–80% of flowers), full bloom stage, and ending of the bloom stage. Simultaneous distillation extraction was used for the extraction of volatile compounds in the flowers, which was then analyzed by a newly developed chemometric data analysis tool, autoGCMSDataAnal. An advantage of the developed methodology is that compounds can be accurately screened and identified. Finally, 59 compounds that showed significant difference among four flowering stages were screened and 31 compounds were identified. Sample clustering results from principal component analysis and hierarchical clustering analysis suggested that flowers from the pre-full bloom stage and full bloom stage may be more suitable when used as raw materials for industrial products.

1. Introduction

As a homologous variety, the flowers of *Elaeagnus angustifolia* L. (oleaster, Russian olive, or wild olive) have been used in the west zones of China [1–4]. Traditionally, the flowers were used as a medicine [5] for chronic bronchitis and tetanus [6], asthma [7–9], arthritis, and cough [10, 11]. Additionally, it can also be used as a material of food additive for flavor treatment of some wines [12, 13]. *E. angustifolia* flowers are widely used as tea beverage in northwest zone of China [14]. It was reported that *E. angustifolia* flowers have anti-saccharification effect and can be used as a food additive to inhibit the undesirable saccharification reaction in food processing [15]. The essential oils of *E. angustifolia* flowers and leaves have been extracted and identified as preservatives in the food industry and natural pesticides in agriculture [7].

In China, *E. angustifolia* has been widely planted in the northwest zones, including Ningxia, Qinghai, Gansu, and Xinjiang provinces [16]. Usually, the flowering season lasts about 20–30 days and mostly ranges from May to June in Ningxia province of China. During this period, the flowers were collected for extracting essential oil [17]. However, the volatile compounds in the flowers changed rapidly during the flowering season, which can thus seriously influence the quality of product.

A number of works had been published for characterizing the compounds in the flowers of *E. angustifolia*. For instance, Torbati et al. [7] utilized gas chromatography-mass spectrometry (GC-MS) for studying the compounds in the essential oil, and about 53 compounds can be quantified, including ethyl cinnamate, hexahydrofarnesyl acetone, palmitic acid, etc., which accounted for about 96.59%

content in the essential oil. Chen et al. [18] and Han et al. [9] separated a number of new compounds in the flowers of *E. angustifolia* and characterized them by nuclear magnetic resonance (NMR), which involved macrocyclic flavonoid glycoside, triterpenoid saponin, and lignan glycosides [18]. Most of published works focused on the employment of GC-MS for characterizing the compounds in the flowers or related products [19]. Very little work had been reported for studying the volatile compounds during the flowering season.

In this work, a GC-MS-based untargeted metabolomic strategy [20] was proposed for performing compound identification and characterization of the content variations during the flowering season. The recently proposed automatic GC-MS data analysis software, autoGCMSDataAnal [21], was introduced for analyzing flower samples of *E. angustifolia* for the first time. Samples from Ningxia province were collected as examples for demonstrating the developed strategy. Coeluted compounds in the GC-MS can be reasonably separated with the aid of chemometric mathematical separation algorithm and accurately qualified.

2. Experiment

2.1. Sample Collection. The flower samples were collected during the flowering season between 16 May and 2 June in Yinchuan, Ningxia province of China, with a sampling interval of 4 or 5 days. Four flowering stages were manually divided, i.e., the initial bloom stage (with about 25% flowers, the perianth is not open), the pre-full bloom stage (70–80% flowers, the perianth opens), the full bloom stage (100% flowers, the perianth is completely open), and the ending of the bloom stage (100% flowers with some abscission, the perianth began to wilt) [22]. A total of 34 samples from different trees in the same area were collected, including 8 samples from the initial bloom stage, 10 samples from the pre-full bloom stage, 8 samples from the full bloom stage, and 8 samples from the ending of the bloom stage. After collection, all the samples were treated in the lab for analysis.

2.2. Sample Pretreatment. A simultaneous distillation extraction (SDE) procedure was utilized for volatile compound extraction. For each sample, about 20 g of flowers was weighed into a 1 L round-bottom flask, and then 350 mL of pure water (Watsons, China) and 40 g of NaCl were added. CH_2Cl_2 (ThermoFisher, USA) was selected as the extraction solvent and about 40 mL was added into a 250 mL round-bottom flask. The SDE was performed for about 2 h. Then, about 10 mL of extraction solvent was transformed into a 25 mL flat-bottom flask and 2 g of anhydrous sodium sulfate was added. Finally, 1 μL of solvent was injected for GC-MS analysis.

2.3. Preparation for Quality Control Sample. A quality control (QC) sample was prepared by equally mixing the extraction solutions of 34 samples. During the sample injection procedure, the QC sample was injected after every 6 samples.

2.4. Instrumental Analysis. Agilent GC-MS was used for data collection. A DB-WAXETR (30 m \times 0.25 mm, 0.25 μm) column was used. He (99.999%) was used as carrier gas. The temperature of front injection was set as 250°C, with a split ratio of 5 : 1. The oven temperature was started with 50°C and maintained for 3 min, followed by an increment of 3°C/min to 250°C. A 15 min post-run was used under the temperature of 250°C. The solvent delay time was set as 4 min.

The parameters of mass spectrometry were optimized. The full scan mode was used with the scan range of 50–500 Da and the scan speed of 5 spectra/s. The EI temperature was 230°C, and the collision energy was 70 eV.

2.5. Data Analysis. All collected GC-MS data were transformed into the “mzdata.xml” file format and imported into autoGCMSDataAnal platform for performing total ion current chromatogram (TIC) peak detection, peak deconvolution, time-shift correction, component registration, and statistical analysis like analysis of variance (ANOVA), principal component analysis (PCA), and hierarchical clustering analysis (HCA). The resolved spectra of screened compounds from autoGCMSDataAnal were finally used for compound identification in National Institute of Standards and Technology (NIST).

3. Results and Discussion

3.1. TIC Peak Detection and Deconvolution. The success of GC-MS data analysis seriously relied on the compound information extraction. The performance of autoGCMSDataAnal on TIC peak detection was firstly investigated in this work. A typical example is shown in Figure 1, where about 107 TIC peaks were detected. A major peak eluted at 43.49 min can be clearly found in the TIC signal, which occupied about 64.42% of content in the sample. The margined plot in Figure 1 shows the peak detection results of some minor peaks in more detail. Evidently, the minor components can be successfully extracted by autoGCMSDataAnal.

In complex sample analysis, it is very common to find coeluted compounds, whose TIC peaks were overlapped with each other [23]. In this case, compound identification based on the mass spectrum collected under the peak apex may provide inaccurate results. It will be reasonable to perform a peak deconvolution at first. Usually, analysts may resort to the AMIDS for TIC peak deconvolution. However, the AMDIS can provide a number of false-positive compound resolution results. Herein, the TIC peak deconvolution was performed based on the multivariate curve resolution-alternating least squares algorithm (MCR-ALS) [24], which was implemented in autoGCMSDataAnal. An advantage of MCR-ALS is that it is insensitive to initialized parameters by using the iterative strategy. autoGCMSDataAnal can automatically provide the initialized parameters, like the number of components, chromatographic profiles of components under a TIC peak, and so on, for MCR-ALS, which will be iteratively optimized to retrieve the underlying chromatographic and mass spectral profiles of compounds.

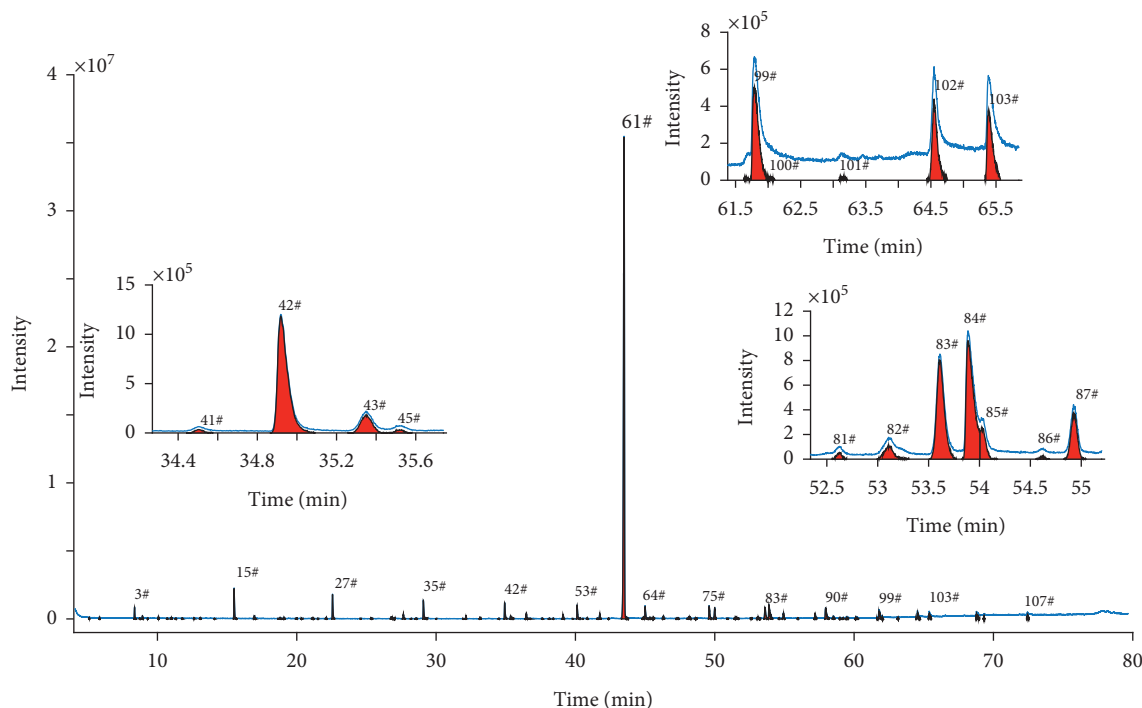


FIGURE 1: A typical example for TIC peak detection results of *Elaeagnus angustifolia* L. flowers. Margined plot shows TIC peaks in detail.

An example of the TIC peak deconvolution in autoGCMSDataAnal is shown in Figure 2. Figure 2(a) provides a TIC peak that was extracted by autoGCMSDataAnal. The extracted ion chromatograms (EICs) under various m/z values are shown in Figure 2(b). Figure 2(c) shows the smoothed EICs after baseline correction. autoGCMSDataAnal classified these EICs into two clusters for generating initialized chromatograms for MCR-ALS. Finally, two compounds were retrieved from the TIC peak, with the resolved chromatographic profiles shown in Figure 2(d).

The benefit of compound identification after TIC peak deconvolution is shown in Figures 2(e) and 2(f). The mass spectrum of the resolved compound eluted under the apex of the -32# was matched with the compound heptacosane by NIST with a match factor (MF) of 761. The other retrieved compound (33#) was identified as benzeneacetaldehyde by NIST with a MF of 915. It seems that both compounds can be matched with acceptable match factors. However, a further investigation indicated that the resolved compound benzeneacetaldehyde can be accurately identified. Results in Figure 2 indicated that compounds under detected TIC peaks can be successfully retrieved by autoGCMSDataAnal. Thus, in the following part of this work, autoGCMSDataAnal was used for TIC peak deconvolution and compound registration to screen compounds showing significant difference among various flowering stages.

3.2. Compound Screening and Statistical Analysis. With the aid of autoGCMSDataAnal, a registered compound list (266×34) was obtained, where 266 and 34 were the number of compounds and samples, respectively. A further analysis

indicated that 59 compounds can be found in at least 80% of samples. The compound screening was performing by ANOVA with p value < 0.05 , and compounds that could not be detected by 80% of samples were removed. Finally, 59 compounds were screened.

The PCA and HCA were used to analyze grouping characteristics of samples on the basis of the screened compounds. Figure 3(a) provides sample distributions on the first two principal components, which explained approximately 78.6% of information in the dataset. It can be seen that samples from the first (initial bloom) and the fourth (ending of the bloom) stages of the flowering season can be clearly separated with the others, i.e., the pre-full bloom stage and the full bloom stage. Samples from the second (pre-full bloom) and the third (full bloom) flowering stages were located quite close to each other in the PCA plot (Figure 3(a)), with their ellipses calculated under 95% level partly overlapped.

Similar results can be found from HCA (Figure 3(b)), as samples from the second and the third flowering stages were firstly clustered, followed by the fourth and the first flowering stages. A very possible reason is that volatile compounds varied dramatically during the first and the fourth flowering seasons. In fact, sample clustering results were consistent with practical realizations, as the flavor characteristics of the second and the third were similar. With respect to the fourth flowering stage, the flavor content released by flowers decreased gradually.

3.3. Compound Identification. Mass spectra of the screened 59 compounds were written in an MSP file by autoGCMSDataAnal, which were then imported into the

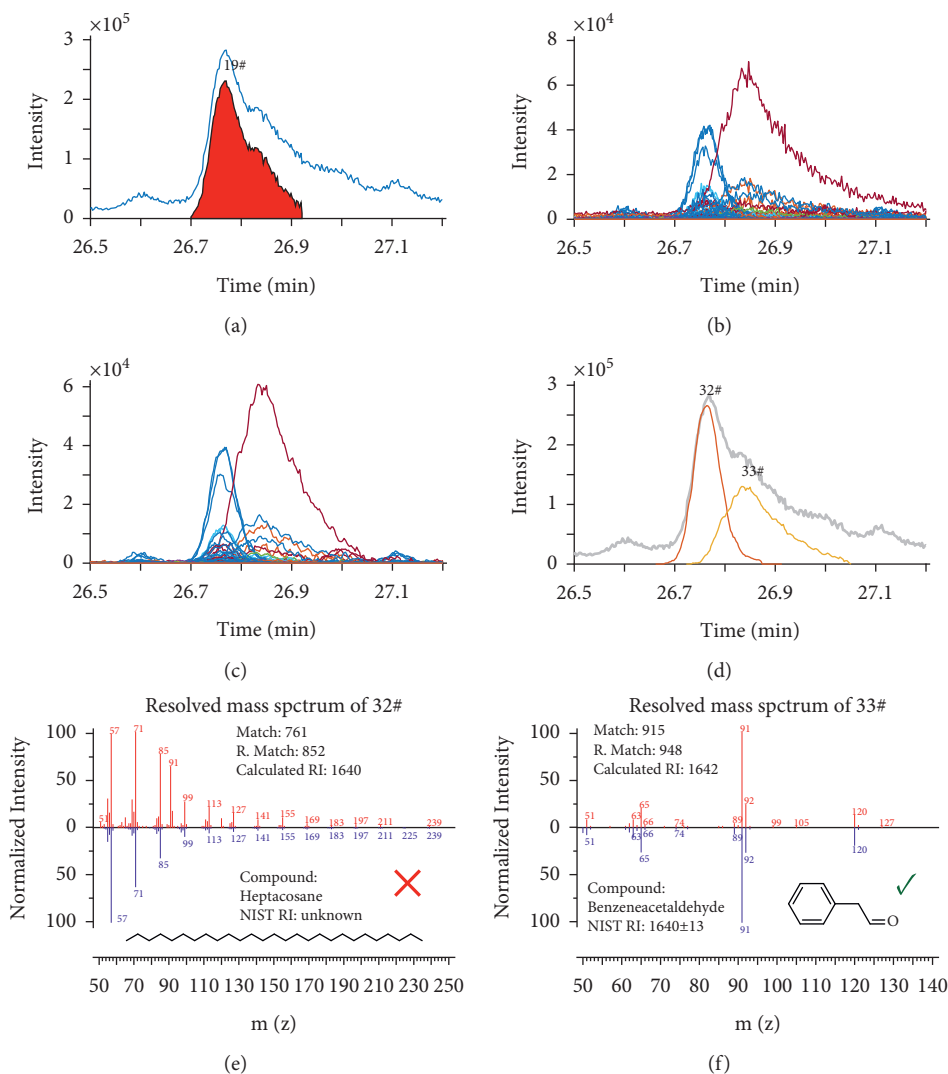


FIGURE 2: Illustration of TIC peak deconvolution by autoGCMSDataAnal. (a) Detected TIC peaks. (b) Original acquired EICs under the TIC peak. (c) EICs with baseline correction by autoGCMSDataAnal. (d) Retrieved compounds for the TIC peak. (e) Identified compound for 32# compound. (f) Identified compound for 33# compound.

NIST for compound identification. Linear retention index (RI) was used to limit the number of candidates. In this work, the tolerance of RI was set at 30. An example of the compound identification is shown in Figure 4. Figure 4(a) provides resolved chromatogram and mass spectrum of a screened compound, whose content was gradually decreased from the first to the fourth flowering stages. The resolved chromatographic and mass spectral profiles of this compound by autoGCMSDataAnal are depicted in Figure 4(b). The importation of the resolved mass spectrum into NIST resulted in a number of candidate compounds. Figure 4(c) provides several acceptable candidates on the basis of MF. In this case, one may find it hard to identify the matched compound, especially for the first two compounds in Figure 4(c). With the aid of RI, the candidate can be limited to only one candidate, which is the first one in the candidate compound table (Figure 4(c)). Finally, the resolved compound was confirmed by standard compound.

A combination of autoGCMSDataAnal with NIST suggested that among the screened 59 compounds, 31 compounds can be matched by NIST with MFs above 700 and RI error below 30, which involved 11 esters (hexanoic acid ethyl ester, benzoic acid ethyl ester, benzenoic acid ethyl ester, benzenopropanoic acid ethyl ester, ethyl cinnamate, 2-propenoic acid-3-phenyl methyl ester, 2-propenoic acid-3-phenyl ethyl ester, 2-propenoic acid-3-phenyl-2-methylpropyl ester, hexadecanoic acid ethyl ester, octadecanoic acid ethyl ester, and 9-octadecenoic acid ethyl ester), 7 aldehydes (hexanal, heptanal, 2-hexenal, nonanal, furfural, benzaldehyde, and benzeneacetaldehyde), 4 alcohols (benzyl alcohol, phenylethyl alcohol, 3-phenyl-2-propen-1-ol, and phytol), 3 organic acids (2-methylbutanoic acid, heptanoic acid, and *n*-hexadecanoic acid), 2 phenols (2-methoxy-4-vinylphenol, and *trans*-isoeugenol), and 4 unclassified compounds. Detailed information of matched compounds including retention time, RI, MF, and so on is shown in Table 1.

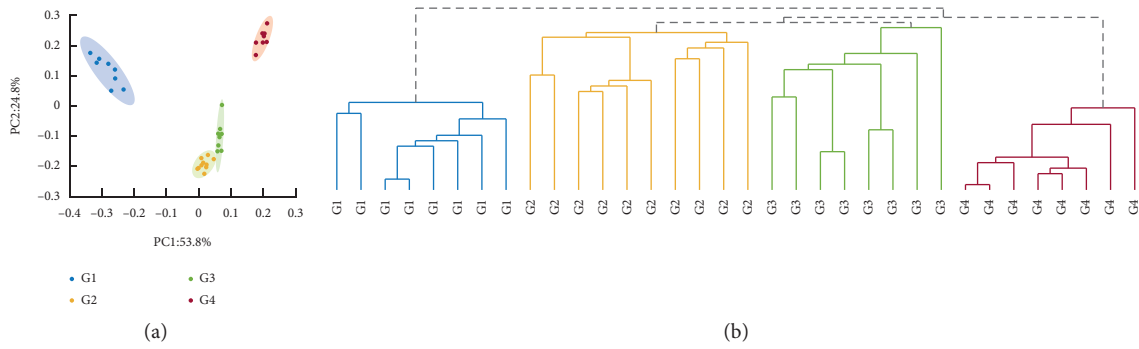


FIGURE 3: PCA (a) and HCA (b) clustering results. “G1,” “G2,” “G3,” and “G4” represent the initial bloom stage, the pre-full bloom stage, the full bloom stage, and the ending of the bloom stage, respectively.

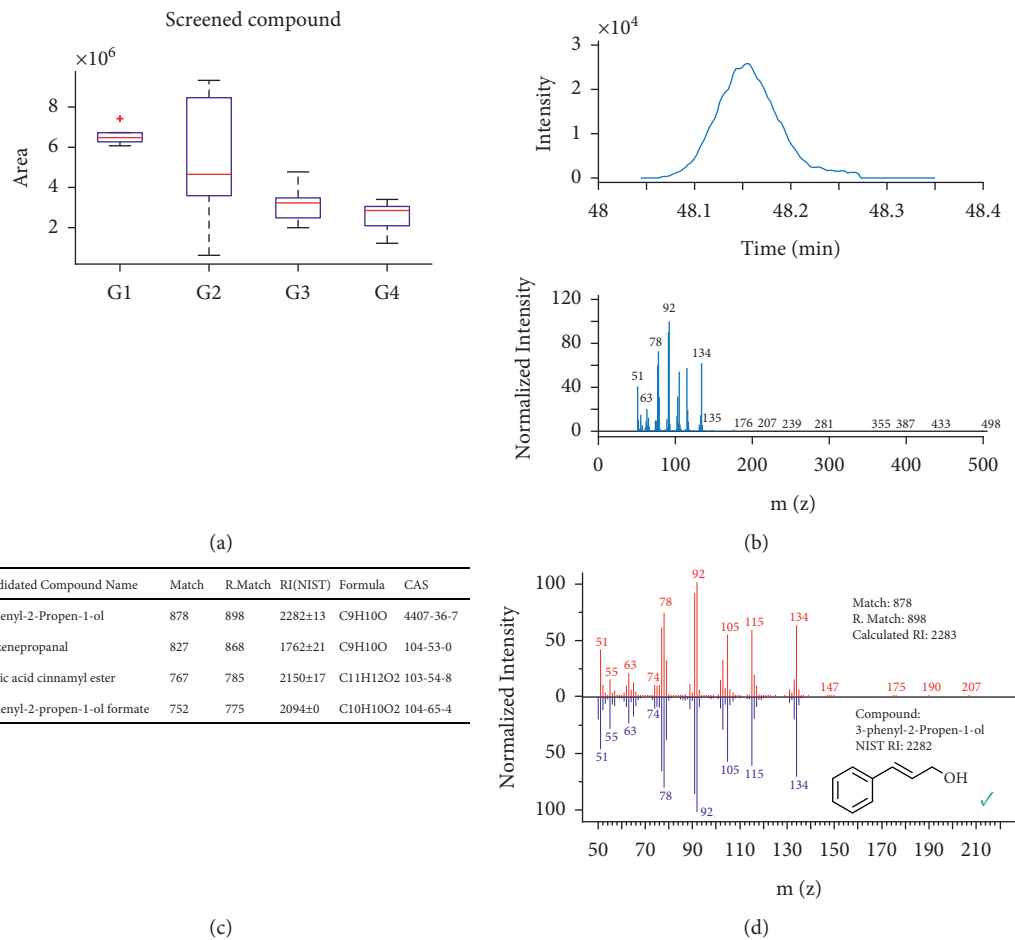


FIGURE 4: Illustration of compound identification procedure in the present work. (a) A screened compound. (b) The resolved chromatogram and mass spectrum of the compound. (c) Candidates in the NIST. (d) With the aid of RI, a candidate was finally accepted and confirmed. “G1,” “G2,” “G3,” and “G4” represent the initial bloom stage, the pre-full bloom stage, the full bloom stage, and the ending of the bloom stage, respectively.

The content variations of identified compounds during flowering season are shown in a heatmap in Figure 5. As can be seen, ten ester compounds showed higher expression level at the first stage (initial bloom), such as 9-octadecenoic acid ethyl ester, isobutyl cinnamate, benzoic acid ethyl ester, benzeneacetic acid ethyl ester, ethyl cinnamate, hexanoic acid ethyl ester, 2-propenoic acid-3-phenyl methyl ester, octadecanoic acid ethyl ester, 2-propenoic acid-3-phenyl

ethyl ester, and hexadecanoic acid ethyl ester. By contrast, fifteen compounds show more content at the fourth flowering stage, including benzyl alcohol, nonanal, heptanal, heptanoic acid, 2-methoxy-4-vinylphenol, phenylethyl alcohol, 2-hexenal, hexanal, 6,10,14-trimethyl-2-pentadecanone, furfural, benzenepropanoic acid ethyl ester, n-hexadecanoic acid, 2-methylbutanoic acid, benzeneacetaldehyde, and benzaldehyde. Notably, all of the identified

TABLE 1: Information of identified compounds.

ID	RT (min)	Calculated RI	NIST RI	Compound	Formula	CAS	MW	MF
1	5.821	1068	1083	Hexanal	C ₆ H ₁₂ O	66-25-1	100	741
2	8.928	1183	1184	Heptanal	C ₇ H ₁₄ O	111-71-7	114	922
3	10.070	1218	1216	2-Hexenal	C ₆ H ₁₀ O	6728-26-3	98	899
4	10.687	1233	1233	Hexanoic acid ethyl ester	C ₈ H ₁₆ O ₂	123-66-0	144	836
5	11.333	1250	1235	3,7-Dimethyl-1,3,6-octatriene	C ₁₀ H ₁₆	3338-55-4	136	853
6	16.966	1392	1391	Nonanal	C ₉ H ₁₈ O	124-19-6	142	912
7	19.968	1468	1461	Furfural	C ₅ H ₄ O ₂	98-01-1	96	854
8	22.116	1521	1520	Benzaldehyde	C ₇ H ₆ O	100-52-7	106	879
9	26.833	1642	1640	Benzeneacetaldehyde	C ₈ H ₈ O	122-78-1	120	899
10	27.661	1664	1658	Benzoic acid ethyl ester	C ₉ H ₁₀ O ₂	93-89-0	150	938
11	28.200	1679	1662	2-Methylbutanoic acid	C ₅ H ₁₀ O ₂	116-53-0	102	755
12	32.138	1785	1783	Benzeneacetic acid ethyl ester	C ₁₀ H ₁₂ O ₂	101-97-3	164	935
13	35.341	1878	1870	Benzyl alcohol	C ₇ H ₈ O	100-51-6	108	924
14	35.523	1883	1893	Benzenepropanoic acid ethyl ester	C ₁₁ H ₁₄ O ₂	2021-28-5	178	843
15	36.470	1911	1906	Phenylethyl alcohol	C ₈ H ₁₀ O	60-12-8	122	953
16	38.100	1959	1950	Heptanoic acid	C ₇ H ₁₄ O ₂	111-14-8	130	907
17	39.113	1989	2012	Ethyl cinnamate	C ₁₁ H ₁₂ O ₂	4610-69-9	176	880
18	41.748	2072	2056	2-Propenoic acid-3-phenyl methyl ester	C ₁₀ H ₁₀ O ₂	103-26-4	162	897
19	43.422	2125	2131	6,10,14-Trimethyl-2-pentadecanone	C ₁₈ H ₃₆ O	502-69-2	268	884
20	43.487	2127	2130	2-Propenoic acid-3-phenyl ethyl ester	C ₁₁ H ₁₂ O ₂	4192-77-2	176	943
21	45.594	2195	2188	2-Methoxy-4-vinylphenol	C ₉ H ₁₀ O ₂	7786-61-0	150	814
22	46.320	2220	2243	Isobutyl cinnamate	C ₁₃ H ₁₆ O ₂	122-67-8	204	811
23	47.301	2254	2251	Hexadecanoic acid ethyl ester	C ₁₈ H ₃₆ O ₂	628-97-7	284	716
24	48.154	2283	2282	3-Phenyl-2-propen-1-ol	C ₉ H ₁₀ O	4407-36-7	134	834
25	49.996	2347	2354	trans-Isoeugenol	C ₁₀ H ₁₂ O ₂	5932-68-3	164	941
26	51.534	2400	2399	Isolemicin	C ₁₂ H ₁₆ O ₃	487-12-7	208	855
27	52.608	2441	2445	Indole	C ₈ H ₇ N	120-72-9	117	774
28	53.116	2459	2451	Octadecanoic acid ethyl ester	C ₂₀ H ₄₀ O ₂	111-61-5	312	817
29	53.613	2478	2476	9-Octadecenoic acid ethyl ester	C ₂₀ H ₃₈ O ₂	6114-18-7	310	916
30	57.203	2613	2622	Phytol	C ₂₀ H ₄₀ O	150-86-7	293	921
31	64.546	2915	2931	<i>n</i> -Hexadecanoic acid	C ₁₆ H ₃₂ O ₂	57-10-3	256	903

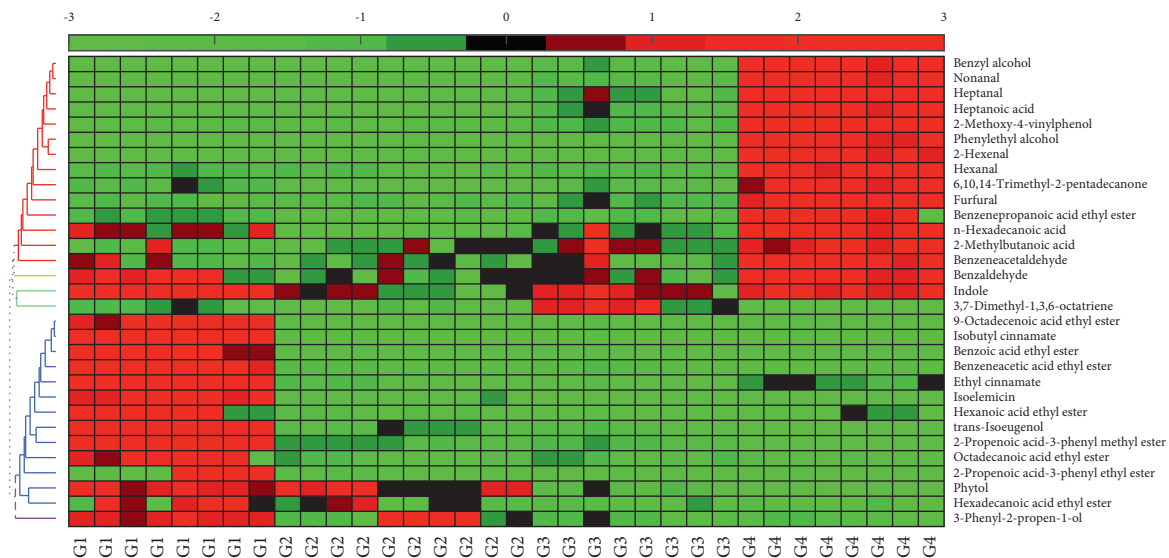


FIGURE 5: Heatmap of identified compounds. “G1,” “G2,” “G3,” and “G4” represent the initial bloom stage, the pre-full bloom stage, the full bloom stage, and the ending of the bloom stage, respectively.

aldehydes were significantly increased at the fourth stage. A similar report was found by Hou et al. [25], which suggested that aldehydes will be gradually increased during the maturation stage.

Results indicated that most of compounds were changed slowly during the second and the third flowering stages. Compounds in the first and the fourth stages were quite different with the other stages. The compound distribution

characteristics can be found in the sample clustering results, as samples from the second and third stages were classified at first (Figure 3). The relatively constant factor in composition of *E. angustifolia* flowers is the evaluation criterion for industrial products. According to the results shown in this work, the quality of *E. angustifolia* flowers can be maintained during the second and the third flowering stages, which may be more suitable when used as a raw material for industrial products.

4. Conclusion

This work proposed a strategy for investigating the volatile compounds in the *E. angustifolia* flowers during the flowering season. Samples from four flowering stages including the initial bloom stage, the pre-full bloom stage, the full bloom stage, and the ending of the bloom stage were collected for studying. 31 compounds were finally screened and identified. Both PCA and HCA indicated that samples from the second and third stages were closer than the remaining two stages. In conclusion, flowers from the second and third stages were more suitable when used as raw materials for industrial products.

Data Availability

The data used to support the findings of this study are included within the article.

Conflicts of Interest

The authors declare that they have no potential conflicts of interest.

Acknowledgments

This study was supported by Henan University of Animal Husbandry and Economy (grant nos. 2018HNUAHEDF014, XKYCXJJ2020002, and 2019HNUAHEDF007).

References

- [1] Y. Wang, S.-Z. Zhou, C.-M. Zhao et al., "Antioxidant and antitumor effect of different fractions of ethyl acetate part from *Elaeagnus angustifolia* L.," *Advance Journal of Food Science and Technology*, vol. 6, no. 5, pp. 707–710, 2014.
- [2] Z. Huang, M. Liu, B. Chen, T. Uriankhai, C. Xu, and M. Zhang, "Distribution and interspecific correlation of root biomass density in an arid *Elaeagnus angustifolia*-*Achnatherum splendens* community," *Acta Ecologica Sinica*, vol. 30, no. 1, pp. 45–49, 2010.
- [3] R. Hamidpour, S. Hamidpour, M. Hamidpour et al., "Russian olive (*Elaeagnus angustifolia* L.): from a variety of traditional medicinal applications to its novel roles as active antioxidant, anti-inflammatory, anti-mutagenic and analgesic agent," *Journal of Traditional and Complementary Medicine*, vol. 7, no. 1, pp. 24–29, 2017.
- [4] S. Çakmakçı, E. F. Topdaş, P. Kalın et al., "Antioxidant capacity and functionality of oleaster (*Elaeagnus angustifolia* L.) flour and crust in a new kind of fruity ice cream," *International Journal of Food Science & Technology*, vol. 50, no. 2, pp. 472–481, 2015.
- [5] Z. Hassanzadeh and H. Hassanpour, "Evaluation of physicochemical characteristics and antioxidant properties of *Elaeagnus angustifolia* L.," *Scientia Horticulturae*, vol. 238, pp. 83–90, 2018.
- [6] F. Saboonchian, R. Jamei, and S. Hosseini Sarghein, "Phenolic and flavonoid content of *Elaeagnus angustifolia* L. (leaf and flower)," *Avicenna Journal of Phytomedicine*, vol. 4, no. 4, pp. 231–238, 2014.
- [7] M. Torbati, S. Asnaashari, and F. Heshmati Afshar, "Essential oil from flowers and leaves of *Elaeagnus Angustifolia* (*Elaeagnaceae*): composition, radical scavenging and general toxicity activities," *Advanced Pharmaceutical Bulletin*, vol. 6, no. 2, pp. 163–169, 2016.
- [8] S. Faramarz, G. Dehghan, and A. Jahanban-Esfahlan, "Antioxidants in different parts of oleaster as a function of genotype," *Bioimpacts*, vol. 5, no. 2, pp. 79–85, 2015.
- [9] J. Han, X. Chen, W. Liu, H. Cui, and T. Yuan, "Triterpenoid saponin and lignan glycosides from the traditional medicine *Elaeagnus angustifolia* flowers and their cytotoxic activities," *Molecules*, vol. 25, no. 3, 2020.
- [10] N. P. Goneharova and A. I. Glushenkova, "Extract of *Elaeagnus angustifolia* flowers," *Chemistry of Natural Compounds*, vol. 33, no. 3, pp. 276–277, 1997.
- [11] A. I. Saleh, I. Mohamed, A. A. Mohamed et al., "*Elaeagnus angustifolia* plant extract inhibits angiogenesis and downgrades cell invasion of human oral cancer cells via Erk1/Erk2 inactivation," *Nutrition and Cancer*, vol. 70, no. 2, pp. 297–305, 2018.
- [12] A. Fonia, I. R. White, and J. M. L. White, "Allergic contact dermatitis to *Elaeagnus* plant (Oleaster)," *Contact Dermatitis*, vol. 60, no. 3, pp. 178–179, 2009.
- [13] T. I. Kiseleva and L. N. Chindyayeva, "Biology of oleaster (*Elaeagnus angustifolia* L.) at the northeastern limit of its range," *Contemporary Problems of Ecology*, vol. 4, no. 2, pp. 218–222, 2011.
- [14] Z. Amiri Tehranizadeh, A. Baratian, and H. Hosseinzadeh, "Russian olive (*Elaeagnus angustifolia*) as a herbal healer," *BioImpacts*, vol. 6, no. 3, pp. 155–167, 2016.
- [15] L. Jia, L. Zhang, Y.-H. Ye, J.-L. Li, M. Cong, and T. Yuan, "Effect and mechanism of *Elaeagnus angustifolia* flower and its major flavonoid tilirosin on inhibiting non-enzymatic glycosylation," *Journal of Agricultural and Food Chemistry*, vol. 67, no. 50, pp. 13960–13968, 2019.
- [16] X. Zhang, G. Li, and S. Du, "Simulating the potential distribution of *Elaeagnus angustifolia* L. based on climatic constraints in China," *Ecological Engineering*, vol. 113, pp. 27–34, 2018.
- [17] L. Bucur, G. Stanciu, and V. Istudor, "The GC-MS analysis of *Elaeagnus angustifolia* L. flowers essential oil," *Revista De Chimie*, vol. 58, no. 11, pp. 1027–1029, 2007.
- [18] X. Chen, Y. Liu, G. Chen et al., "Angustifolinoid A, a macrocyclic flavonoid glycoside from *Elaeagnus angustifolia* flowers," *Tetrahedron Letters*, vol. 59, no. 26, pp. 2610–2613, 2018.
- [19] Z.-G. Li, M.-R. Lee, and D.-L. Shen, "Analysis of volatile compounds emitted from fresh *Syringa oblata* flowers in different fluorescence by headspace solid-phase microextraction-gas chromatography-mass spectrometry," *Analytica Chimica Acta*, vol. 576, no. 1, pp. 43–49, 2006.
- [20] L. Zhang, X. Wang, J. Guo et al., "Metabolic profiling of Chinese tobacco leaf of different geographical origins by GC-MS," *Journal of Agricultural and Food Chemistry*, vol. 61, no. 11, pp. 2597–2605, 2013.

- [21] Y.-Y. Zhang, Q. Zhang, Y.-M. Zhang et al., "A comprehensive automatic data analysis strategy for gas chromatography-mass spectrometry based untargeted metabolomics," *Journal of Chromatography A*, vol. 1616, p. 460787, 2020.
- [22] L.-M. Wang, M.-T. Li, W.-W. Jin, S. Li, S.-Q. Zhang, and L.-J. Yu, "Variations in the components of *Osmanthus fragrans* lour. essential oil at different stages of flowering," *Food Chemistry*, vol. 114, no. 1, pp. 233–236, 2009.
- [23] L. Han, Y.-M. Zhang, J.-J. Song et al., "Automatic untargeted metabolic profiling analysis coupled with Chemometrics for improving metabolite identification quality to enhance geographical origin discrimination capability," *Journal of Chromatography A*, vol. 1541, pp. 12–20, 2018.
- [24] E. Ortiz-Villanueva, F. Benavente, B. Piña, V. Sanz-Nebot, R. Tauler, and J. Jaumot, "Knowledge integration strategies for untargeted metabolomics based on MCR-ALS analysis of CE-MS and LC-MS data," *Analytica Chimica Acta*, vol. 978, pp. 10–23, 2017.
- [25] J. Hou, L. Liang, and Y. Wang, "Volatile composition changes in navel orange at different growth stages by HS-SPME-GC-MS," *Food Research International*, vol. 136, Article ID 109333, 2020.